Technische Universität München

Lehrstuhl 2 für Technische Chemie

Surface chemistry and kinetics of the hydrolysis of isocyanic acid on TiO$_2$ anatase

Philipp Christian Dino Patrick Hauck

Vollständiger Abdruck der von der Fakultät für Chemie der Technischen Universität München zur Erlangung des akademischen Grades eines

Doktors der Naturwissenschaften (Dr.rer.nat.)

genehmigten Dissertation.

Vorsitzender: Univ.-Prof. Dr. Klaus Köhler

Prüfer der Dissertation:

1. Univ.-Prof. Dr. Johannes A. Lercher
2. Univ.-Prof. Dr. Kai-Olaf Hinrichsen

Die Dissertation wurde am 14.02.2007 bei der Technischen Universität München eingereicht und durch die Fakultät für Chemie am 16.04.2007 angenommen.

Gott sei Dank! Nun ist's vorbei mit der Übertäterei!

Meine Damen und Herren, vielleicht hat niemand mehr damit gerechnet.

Um so größer wird die Überraschung sein: Ich komme jetzt zum Ende.

Wilhelm Busch (1832-1908)

Acknowledgements

Finally the PhD time has drawn to its close and the tamer of the isocyanic acid would like to say a few words of thank to a bunch of people who made a substantial contribution to the ultimate thesis.

First of all I would like to thank Johannes (Prof. J.A. Lercher) for inviting me into his group and thus giving me the opportunity to work in a fairly international team on an adventurous project. Thank you for all the guidance, trust, fruitful, but also sharp-tongued discussions during the last three years three months and the sufficient freedom and independence with regard to structuring my work. The time at TC 2 has been an important and joyful part of my life for sure. Also thank you for giving me the many chances to go abroad to visit first-class conferences and discuss my results with scientific experts. Heidelberg, Weimar, Trondheim and Tokyo I will definitely keep in good memory as well as the one afternoon in the IR lab where you disclosed the secret of pressing thin titania wafers to me…

Thanks Andy (Dr. A Jentys) for the direct supervision of my work. You were really a great tutor at all times! Thank you for introducing me into IR and Raman spectroscopy, for the many profound and funny discussions, which were always productive and let me find the right solution, your readiness to discuss at any time and all the corrections and hints during many obstacles in the course of my PhD time. I really appreciated your honest and direct way when you hauled me over the coals sometimes! Thank you for accompanying me during the many project meetings and rallying behind me when the project partners disagreed about our taken approach. Memorable also the exiting and eventful "racing" ski seminars in Obertauern.

The heart of the Chair however are the fantastic colleagues, the technical staff, the secretaries, the software admin and last but not least the PhD students which keep the daily routine work and business moving:

Xaver and Andreas M., thank you for your great support in maintaining my set-up and Martin for the BET analyses.

Christian 'Elektronenwoltz', Josef. F. and Peter 'Raki' thank you for the congenial atmosphere during the task force 'Übungen', but also for the many discussions on our beloved topic 'kinetics'.

Benjamin, Florencia, Rahul, Mahdi and Williams, my lab mates, it was a funny and instructive time with you in the most dangerous lab of TC 2. Thanks for standing my chaotic and disordered benches and drawers!

Wolfgang, Kaufi 'Schlummifix', Jan-Olaf, Chintan, Xuebing, Alex 'Opa' and Andi S., it was a pleasure to share the office with you. You accompanied me in a good-humored manner during many ups and downs in the last three years. Thanks for helping me on many scientific and non-scientific questions.

Virginia 'Ginger' and Elvira, thanks for the many good times we have had at various events in Munich city. Biergarten rules!

Iker, thanks for the frequent runs alongside the Isar and the amazing conversations. I've learnt a lot about the Basque culture and traditions.

Hiroaki and Ayumu, my dear Japanese friends, I wish that we will keep up the contact. Toshi, thanks for my first experiment at the TPO where I killed the filaments.

Thank you Lucas, Hannes, Yuying, Marcus, Prado, Manu, Tobi and Richard, you were a great help with the many successful experiments you carried out.

Felix 'Chorkendorff' and 'Prof.' Rino, thanks for spreading high spirits at all times, without you there would not have been so many laughs!

Hendrik, special thanks to you for teaching me many practical tricks at the different set-ups, for pressing superb wafers and last but not least, for your help with formatting this thesis.

But also thanks to all the others which have not been mentioned so far: Helen, Heike, Wolfram, Lay-Hwa, Thomas, Roberta, Yongzhong, Anirban, Praveen, Chirag, Aon, Herui, Jürgen, Hitri, Frederik, Carsten, Josef M., Olga, Oriol, Manül, Krishna, Maria (Mary), Su, Reni, Dr. Kornatowski, Stevie, Adam and Andreas F. and maybe more which I've forgotten now.

Of course I would also like to thank the project partners for the excellent collaboration, Dr. Jacob, Mr. Döring, Dr. Spengler, Martin, Dr. Treiber and Dr. Held, Prof. Sattelmayer, Mr. Glückert, Oleg, Sebastian und Jürgen. You've had always stimulating comments during the project meetings and were very responsive on all my questions and inquiries.

arbauer, Soasch, Marcus und Artit, vielen Dank für die unvergessliche Studentenzeit in Erlangen! Ihr habt mir die lustige Seite der Wissenschaften eröffnet, wofür ich Euch nicht dankbar genug sein kann! Three cheers and a tiger for the ironman association!

Zum Schluß möchte ich mich bei meinen Eltern und meiner Schwester bedanken. Ich kann froh sein, so eine tolle Familie zu haben! Zu jeder Zeit in meinem Leben wart Ihr für mich da und habt mich nicht nur finanziell, sondern immer und bei allem unterstützt und an mich geglaubt. Vielen Dank dafür, Ihr seid die Größten!

Silke, Dir möchte ich für die letzten 7 ½ Jahre danken, die schöner nicht hätten sein können. Dein elfenhaftes Wesen, Deine Lebensenergie, Dein Lächeln und Deine Liebe sind für mich unverzichtbar! Ich wünsche mir, dass wir uns noch lange ‚riechen' können ;-)

Philipp

Januar 2007

TABLE OF CONTENTS

Nomenclature

Abbreviations

CD-CAT	Controlled Diesel catalyst
cpsi	cells per square inch
DPF	Diesel Particulate Filter
EEV	Enhanced environmentally friendly vehicle
EGR	exhaust gas recirculation
ELR	European Load Response
ESC	European Stationary Cycle
ETC	European Transient Cycle
HC	hydrocarbons
LPG	Liquefied Petroleum Gas
Nfz	Nutzfahrzeug *[German for commercial vehicle]*
NO_x	abbreviatory denotation for the nitrogen oxides NO and NO_2
NSR	NO_x storage-reduction
OBD	on-board diagnosis
PILC	pillared clay
PM	particulate matter
ppm	parts per million
SCR	selective catalytic reduction
TWC	three-way catalyst

Symbols

b_e specific fuel consumption; ratio between deployed fuel amount and effective power

$$b_e = \frac{\dot{m}_B}{P_e}$$

λ   relative air/fuel ratio: gives the amount of air which is λ-times the amount of air which is required for ideal combustion according to the reaction equation.

stoichiometric mixture: $\lambda = 1$

fuel-rich mixture: $\lambda < 1$

fuel-lean mixture: $\lambda > 1$

Chapter 1

1 INTRODUCTION

1.1 Emission of Pollutants from Motor Vehicles

Due to the increasing volume of traffic on all continents of the world, the motor vehicle comes to the fore of criticism through the emission of particulate matter (PM) as well as environmentally harmful components in the exhaust gas like the nitrogen oxides (NO and NO_2, short NO_x), the hydrocarbons (HC) and carbon monoxide (CO). The world's motor vehicle production has shown a nearly linear increase – from 8 million per year in 1950 to about 60 million per year in 2000, with a total number of over 500 million passenger cars on the road worldwide [1,2]. Approximately 20% of the global anthro-pogenic nitrogen oxide emissions originate from passenger cars and commercial vehicles [3]. In order to keep the statutory thresholds, contacts are approvedly used for the Otto engine for which the popular pseudonym three-way catalyst (TWC) has prevailed.

For the reduction of the nitrogen oxide emissions at the combustion engine, engine-side (primary) measures are in principle thinkable as well as methods for the after treatment of the exhaust gases (secondary measures, end-of-pipe technologies). Inner-motor measures for the NO_x emission abatement particularly affect the change of residence time, temperature and homogeneity of the fuel/air mixture in the combustion chamber as well as the direct or indirect use of reducing components. Also the exhaust gas recirculation (EGR) should be mentioned in this context. As such interventions are mostly connected with increased fuel consumption the main interest is directed to the consumption optimization of the available or future fuel. In consequence of the further aggravation of the thresholds for Diesel motor vehicles, it is indispensable that the development of additional effective secondary measures for emission abatement is supported [4].

Beyond dispute the Diesel engine has serious advantages compared to all other power engines regarding CO_2 emission. The disadvantages compared to the Otto engine with its controlled three-way catalyst are admittedly the higher particulate matter and nitrogen oxide emission. Unfortunately the exhaust gas after treatment proves to be considerably more difficult at the Diesel as well as the lean Otto engine than at the Otto engine. Due to the comparably high oxygen content in the exhaust gas (operating range

with relative air/fuel ratios λ clearly higher than 1) the potential of the reducing components present in the motor exhaust gas (CO, various hydrocarbons, H_2) is too low for effective removal of the nitrogen oxides (see Figure 1.1).
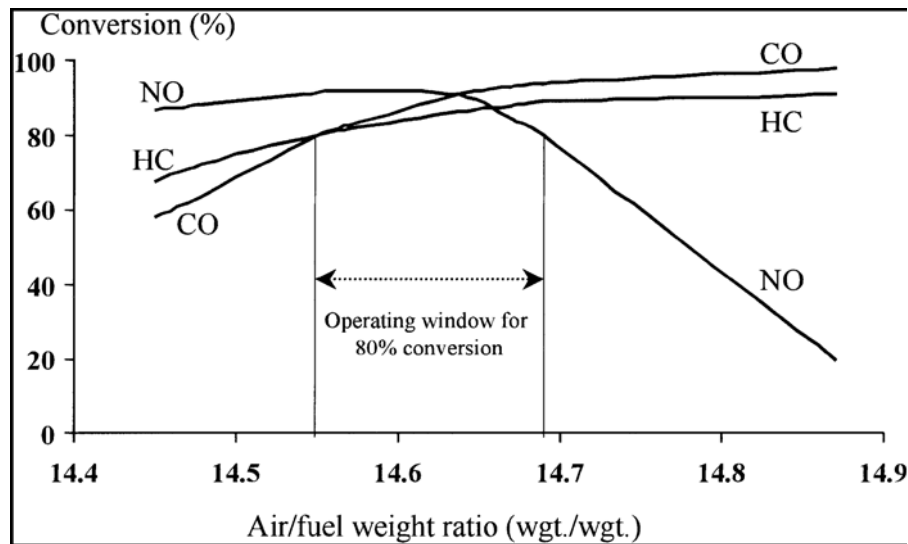
Figure 1.1 Three way catalyst performance determined by engine air to fuel ratio [2].

1.2 Formation of NO_x during Combustion

The nitrogen oxides NO and NO_2 are formed during combustion processes through the reaction of nitrogen and oxygen from the air (thermal NO) or through oxidation of nitrogenous compounds present in the fuel (fuel NO). Furthermore, the formation of NO_x is possibly boosted by the presence of reactive species being formed during the combustion [5]. At the motor combustion the formed NO_x is composed of over 90% NO. Concerning the formation of nitrogen oxides several formation mechanisms can be cited.

1.2.1 Thermal nitric oxide

The formation of thermal nitric oxide is today known to proceed via a sequence of elementary steps. Thereby atomic oxygen – not molecular oxygen - reacts with nitrogen. The reaction mechanism has been described by Zeldovich in 1946 for the first time [6]. The formation of atomic oxygen occurs via a collision partner M, e.g. N_2 or argon:

$$O_2 + M \rightarrow 2\,O + M \qquad\qquad \text{Equation 1.1}$$

$$O + N_2 \rightarrow NO + N \qquad\qquad \text{Equation 1.2}$$

$$N + O_2 \rightarrow NO + O \qquad\qquad \text{Equation 1.3}$$

$$N + OH \rightarrow NO + H \qquad\qquad \text{Equation 1.4}$$
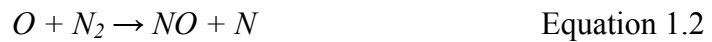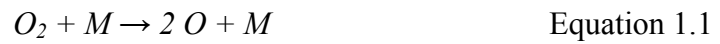
The slowest and thus the rate determining reaction for the NO formation is Equation 1.2. The activation energy is very high, E_A = 318 kJ/mol, in order to break the triple bond of the nitrogen molecule [7]. The thermal NO starts to form at a temperature of about 2000 K in the post-flame region [8].

1.2.2 Prompt nitric oxide

Prompt NO forms through oxidation of air-nitrogen with fuel radicals, whereat cyanides are produced.

$$N_2 + CH_2 \rightarrow HCN + NH \qquad\qquad \text{Equation 1.5}$$

$$N_2 + CH \rightarrow HCN + N \qquad\qquad \text{Equation 1.6}$$

$$HCN + H \rightarrow H_2 + CN \qquad\qquad \text{Equation 1.7}$$

$$CN + CO_2 \rightarrow NCO + CO \qquad\qquad \text{Equation 1.8}$$

$$NCO + O \rightarrow CO + NO \qquad\qquad \text{Equation 1.9}$$

The reaction mechanism is rather complex, however, radicals are necessary which are only built in the flame front. Prompt NO appears especially at fuel-rich combustions where the amount of hydrocarbon is relatively high, the formation starts already at moderate temperatures of around 700°C. The fraction of prompt NO in the total NO emission is often subordinate, however, it constitutes an unavoidable lower NO limit at low-NO$_x$ burners [9].

1.2.3 Fuel nitric oxide

Fuel NO is formed through oxidation of fuel-bound nitrogen. Its content in waste and coal is up to 2%, whereas the nitrogen concentration in today's Diesel fuels is only around 200 ppm. Although the mechansim is a complex radical one, it is easily calculable. The formation of fuel nitric oxide starts at T = 800°C. It can possibly be avoided or reduced by a fuel-rich combustion cycle, then the reaction path way is preferably towards N_2 [10].

1.2.4 Nitric oxide from N_2O

It is preferentially built at low combustion temperatures in zones with high air/fuel ratios, i.e. it plays an important role at very lean gas turbines at 16-30 bar, but also at Diesel engine combustion. As the mechanism contains a three partner reaction, it is rather seldom, but the reaction rate strongly increases with increasing pressure [11].

$$O + N_2 + M \rightarrow N_2O + M \qquad\qquad \text{Equation 1.10}$$

$$N_2O + H \rightarrow NO + NH \qquad\qquad \text{Equation 1.11}$$

$$N_2O + O \rightarrow NO + NO \qquad\qquad \text{Equation 1.12}$$
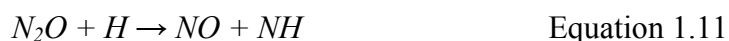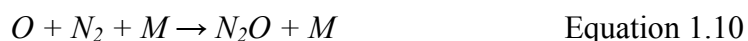
1.2.5 Nitrogen dioxide NO_2

Nitrogen dioxide is built through oxidation of NO with oxygen, but also the reaction of nitric oxide with HO_2 and OH radicals is known, described by the following representative reaction:

$$NO + HO_2 \rightarrow NO_2 + OH \qquad\qquad \text{Equation 1.13}$$

In a typical Diesel exhaust gas the NO_2 fraction of the nitrogen oxides is between 5 and 10%.

1.3 Impact of NO_x on Environment and Health

The emission of nitrogen oxides via the subsequent complex, partially photochemical processes at ground level leads to various effects on the environment (see Figure 1.2) [12]. NO reacts slowly with aerial oxygen in the atmosphere to NO_2 because the formation of the thermodynamically more stabile NO_2 is decelerated by the lower rate of reaction under atmospheric conditions. Formed NO_2 is photochemically reduced to NO when there is intense solar irradiation. Simultaneously ozone is formed which leads to damage of the respiratory organs in organisms. Vice versa during the night the ozone is decomposed through reoxidation of NO to NO_2. But the decomposition occurs mainly in the conurbations because only there the necessary NO is present in sufficient concentration in the atmosphere. Contrarily in the rural areas the damage of the vegetation by ozone can continue unabatedly.

Emitted NO can react to nitric acid through multi-step oxidation with ozone and further NO_2 in presence of air humidity, which even acidifies the rainfall of regions far away of the pollutor. The acid leads to the sustainable damage of flora, whereas especially the area-wide damage to forests in the 80s arrived at the awareness of the public. Furthermore, NO_2 together with emitted hydrocarbons can react to peroxyacetylnitrates which are made responsible for the irritant impact of the harmful gases emitted from motor vehicles on the human respiratory organs [13].
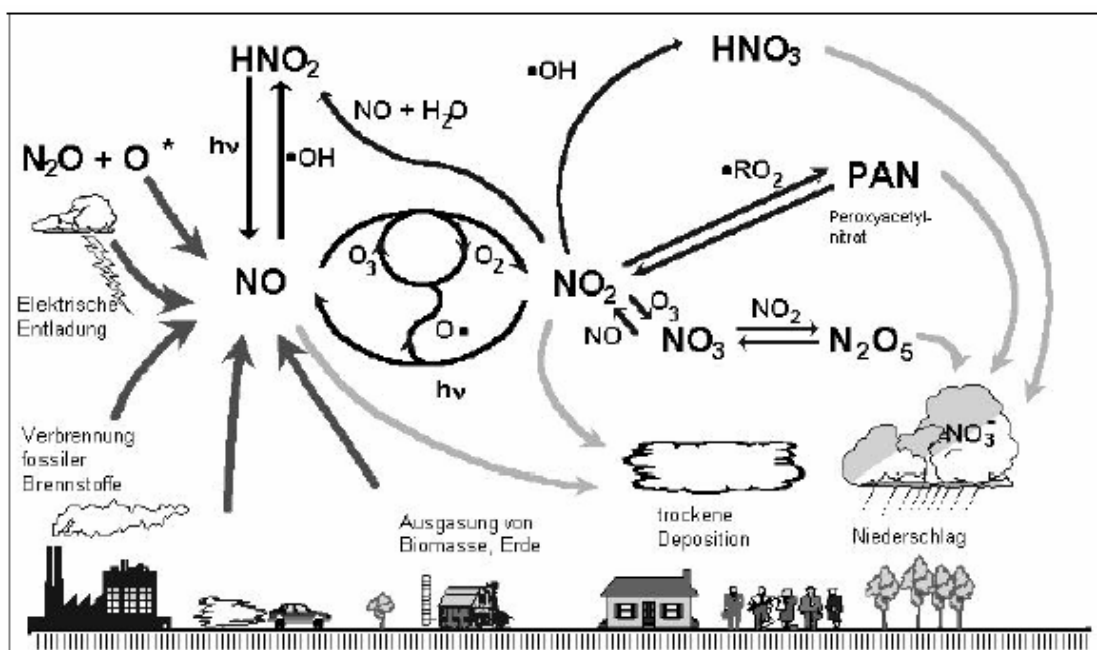

Figure 1.2 Simplified schematic on atmospheric chemistry of nitric oxides [14].

A summary of all possible emission compounds released by motor vehicles and their corresponding impacts on the local and global environment is given in Table 1.1.

Table 1.1 Summary of major pollutants from transportation sources [15].

Pollutants	Local Impacts	Global Impacts	Comments
CO	• Aggravates existing cardiovascular diseases, impairs visual perception and dexterity	• Indirect influence on warming through competition with methane for oxidation	• Transportation can be responsible for up to 95% of CO emissions in urban areas. • Globally distributed gas
HC	• Range of health impacts including respiratory, neurological & carcinogenic • Photochemical smog precursor	• Class of compounds includes methane, a potent greenhouse gas • Indirect warming influence through ozone formation	• A range of natural and anthropogenic sources ensures that HC species are generally available as ozone precursors
NO_x	• Respiratory irritant • Visibility impairment • Acid precursor • Photochemical smog precursor	• Indirect warming influence through ozone formation	• Acid and ozone production impacts of NO_x can be widely distributed through long-range transport of reservoir species
O_3	• Primary constituent of photochemical smog • Severe respiratory impacts • Material & crop damage	• Global warming impacts due to increasing background concentrations • Strong oxidation agent	• O_3 has no direct emissions sources—NO_x, HC, and sunlight are required for production
SO_x	• Respiratory irritant • Visibility impairment • Acid precursor	• Sulfate has some cooling impact due to light scattering	• SO_2 has a relatively long atmospheric lifetime leading to widespread acid impacts
PM (Particular Matter)	• Cardiovascular & respiratory impacts • Visibility impairment • Includes acid species	• Particles can influence warming or cooling, depending on carbon content & scattering abilities	• Atmospheric lifetime varies with particle size
GHG (Green house Gases)		• Leading to global warming through long-term atmospheric accumulation	• Transportation is a major source of CO_2 but less important for methane & N_2O

1.4 European Union Emission Standards [16]

The heavy-duty engine regulations were originally introduced by the Directive 88/77/EEC, followed by a number of amendments. In 2005, the regulations were re-cast and consolidated by the Directive 05/55/EC. The emission standards apply to all motor vehicles with a "technically permissible maximum laden mass" over 3,500 kg, equipped with compression ignition engines or positive ignition natural gas or LPG engines.

The following are some of the most important rulemaking steps in the heavy-duty engine regulations:

- Euro I standards were introduced in 1992, followed by the introduction of Euro II regulations in 1996. These standards applied to both truck engines and urban buses, the urban bus standards, however, were voluntary.

- In 1999, the EU adopted Directive 1999/96/EC, which introduced Euro III standards (2000), as well as Euro IV/V standards (2005/2008). This rule also set voluntary, stricter emission limits for extra low emission vehicles, known as "enhanced environmentally friendly vehicles" or EEV's.

- In 2001, the European Commission adopted Directive 2001/27/EC which prohibits the use of emission "defeat devices" and "irrational" emission control strategies, which would be reducing the efficiency of emission control systems when vehicles operate under normal driving conditions to levels below those determined during the emission testing procedure.

- Directive 2005/55/EC adopted by the EU Parliament in 2005 introduced durability and OBD requirements, as well as re-stated the emission limits for Euro IV and Euro V which were originally published in 1999/96/EC. In a "split-level" regulatory approach, the technical requirements pertaining to durability and on-board diagnosis (OBD) – including provisions for emission systems that use consumable reagents – have been described by the Commission in Directive 2005/78/EC.

The Commission is expected to publish a proposal for Euro VI emission standards in 2006. In addition to introducing more stringent emission limits, the Commission is required to review the need to introduce new standards for pollutants that are as yet unregulated, which may be related to the usage of alternative fuels and additive-based emission control systems, and to investigate whether setting an additional limit for particle levels and size is necessary, and, if so, to include it in the proposals.

The following table contains a summary of the emission standards and their implementation dates. Dates in the tables refer to new type approvals; the dates for all type approvals are in most cases one year later (EU type approvals are valid longer than one year).

Table 1.2 EU Emission Standards for HD Diesel Engines, g/kWh (smoke in m^{-1}) [16].

Tier	Date	Test	CO	HC	NO$_x$	PM	Smoke
Euro I	1992, < 85 kW	ECE R-49	4.5	1.1	8.0	0.612	
	1992, > 85 kW		4.5	1.1	8.0	0.36	
Euro II	1996.10		4.0	1.1	7.0	0.25	
	1998.10		4.0	1.1	7.0	0.15	
Euro III	*1999.10, EEVs only*	*ESC & ELR*	*1.5*	*0.25*	*2.0*	*0.02*	*0.15*
	2000.10	ESC & ELR	2.1	0.66	5.0	0.10 0.13*	0.8
Euro IV	2005.10		1.5	0.46	3.5	0.02	0.5
Euro V	2008.10		1.5	0.46	2.0	0.02	0.5
* for engines of less than 0.75 dm³ swept volume per cylinder and a rated power speed of more than 3000 min^{-1}							

Changes in the engine test cycle have been introduced in the Euro III standard (2000). The old steady-state engine test cycle ECE R-49 has been replaced by two cycles: the European Stationary Cycle (ESC) and the European Transient Cycle (ETC). Smoke opacity is measured on the European Load Response (ELR) test. The following testing requirements applied for type approval of new vehicles according to the Euro III standard (2000):

- Conventional diesel engines were tested over the ESC/ELR test.
- Diesel engines with "advanced aftertreatment" (NO$_x$ aftertreatment or Diesel Particulate Filters (DPF) were tested on both tests, ESC/ELR + ETC.
- Gas engines were tested over the ETC cycle.

For type approval according to the Euro IV (2005) and later limit values and for EEVs, emissions have to be determined on both the ETC and the ESC/ELR tests for all types of diesel engines.

1.5 *Methods of Exhaust Gas After-treatment to reduce NO$_x$*

Since the 1980s secondary measures for emissions control in Diesel engines have concentrated on the reduction of particulate matter (PM). The emissions of harmful compounds, e.g., CO, hydrocarbons and NO$_x$ were lower than the standards specified by legislation and their control was not necessary. Since 1991, oxidation catalysts have been implemented in passenger cars in the European Union and in some medium and heavy-duty trucks in the United States which convert CO, hydrocarbon and particulate emissions [17, 18]. Although oxidation catalysts are efficient for the control of particulate matter, carbon monoxide and hydrocarbons, the removal of NO$_x$ from engines working under lean-burn conditions still represents a challenge. Different methods for efficient removal of NO$_x$ in the presence of excess oxygen have been developed independently. Most of them have the joint characteristic that the reduction of the nitric oxides is therefore only possible in the presence of a selectively-acting reducing agent. In the following sections the major technologies herefore are summarized and described in detail.

1.5.1 Reduction of NO$_x$ with hydrocarbons

In 1990, the selective reduction of NO with hydrocarbons in an oxidizing atmosphere over CuMFI was first reported independently by Iwamoto and Held. In contrast to the direct NO decomposition where the presence of oxygen retards the process, when hydrocarbons are used as reducing agents, oxygen remarkably enhances the accomplishment of the reduction of NO [19]. Catalysts class in two categories, in high-temperature active ones based on zeolites which are exchanged with transition metals, for instance Cu-ZSM-5, Co- or Ni-exchanged zeolites, as well as in low-temperature active catalysts with Pt as basic active component. High-temperature type catalysts are metastable in water-containing environment and at high temperatures (hydrothermal synthesis conditions of zeolites) and thus are questionable in their application. On the other hand, the low-temperature types which are only active between 180 and 280°C favor the oxidation. Product selectivity is problematic due to formation of N$_2$O and NO$_2$,

respectively. The metal determines the preferred type of hydrocarbon used as reducing agent: Co-ZSM-5, Mn-ZSM-5, Ni-ZSM-5 and Rh-ZSM-5 effectively reduce NO to N_2 with methane as well as other alkanes [20]. Cu-ZSM-5 requires paraffins or olefins with at least three carbon atoms [21]. In general, the reaction mechanism for the reduction of NO appears to depend on the type of hydrocarbon used as reducing agent [21,22], as the breaking of the first C-H bond has been speculated to be the rate-limiting step in the reduction of NO with alkanes [23,24]. However, the carrying of an additional reducing agent on-board is generally disfavored by the car manufacturers. Therefore it is attempted to crack the (Diesel) fuel on-board by means of appropriate catalysts (e.g. Pt/H-ZSM-5 or HY zeolite) with the aim to obtain as high yields of C_2- to C_5-olefins as well as aromatics as possible, with which the hydrocarbon selective catalytic reduction (SCR) should then be operated more effectively. Unfortunately the yields in the oxygen rich exhaust gas turn out to be rather moderate at present. Coke formation is a problem, and secondly addional fuel must be applied in order to sustain the catalyst temperature [25].

Alternatively, a few research groups favor the SCR of NO by propene by means of Cu ion-exchanged titanium pillared clays (Cu-Ti-PILC) and claim that its catalytic performance is better than with Cu-ZSM-5 [26,27]. A disavantage seen here is the inhibting effect of water being present in the feed on the activity of the catalysts [27,28].

1.5.2 NO_x storage-reduction

A promising method for the reduction of NO_x under excess oxygen conditions from lean-burn and Diesel engines is based on the concept of NO_x storage-reduction (NSR), where the engine is operated in a mixed lean/rich operation mode [29,30]. In the year 1994 a press release from Toyota called a broad market's attention to the IP with regard to a novel concept of NO_x removal from exhaust gases of lean-mix engines. At the so-called NO_x storage-reduction principle both devices for conditioning of reducing agents (as at HC-SCR, see Section 1.5.1) and particularly the carrying of an additional reducing agent (compare urea or carbamate-SCR in Section 1.5.3) is forgone. With the NSR technique the necessary reducing agent is provided by active or passive motor-generated measures when required [31].

The mode of operation is as follows (see Figure 1.3): In the lean operating condition ($\lambda > 1$) the NSR contact functions as an oxidation catalyst. Unburnt hydrocarbons and carbon monoxide are oxidized to CO_2 and H_2O at the precious metal components (Pt). Furthermore it turns out that between 150 and 350°C HC and CO reduce a certain

fraction of the NO to N_2 and N_2O, respectively, comparable to the conditions at the HC-SCR. A larger fraction of the NO is oxidized at the platinum contact to NO_2 in order to be stored thereafter in the form of nitrates through the washcoat (γ-Al_2O_3) itself as well as through the preferably basic carbonates/oxides being massively inserted in the alumina. Those carbonates/oxides are typically alkali metals like potassium, basically heavy alkaline earth metals like barium, light rare earth metals like lanthanum or cerium or transition metals. At the latest when the NO_x storage capacity is depleted after a few minutes, a regeneration cycle must follow in which the exhaust gas is temporarily enriched to $\lambda = 0.98 - 0.8$ and the nitrates are decomposed. Thus the released NO_x, basically NO_2, is reduced to N_2 by the exhaust components HC, CO and H_2 being then present in excess. The N_2O formation here is not noteworthy. The enrichment of the mixture is effectuated by motor management if it is not already required by the operating condition (warm-up phase, acceleration, full load).
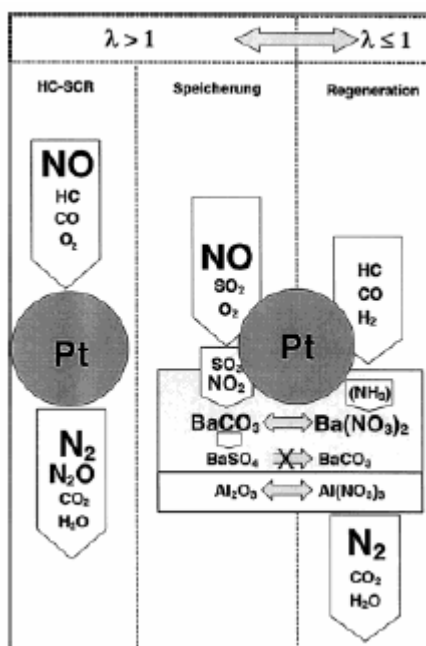
Figure 1.3 Functional diagram of a NSR catalyst based on NO_x storage and nitrate regeneration [4].

For the design of efficient NSR catalysts, storage components are required which temporarily store high concentrations of NO_x between 100 and 450°C in the presence of the typical gas components of motor exhaust gases and release the NO_x stored during the short regeneration cycles [32, 33]. In general a high basicity of the storage component increases the amount of adsorbed NO_x. A high surface area and, therefore, a

small particle size are additionally important for an efficient NO_x storage, as the NO_x is mainly stored as surface species [34,35].

Research on different zeolites exchanged with various metal cations for the removal of NO_x from engine exhaust gases is reported mainly on the fields of NH_3- and HC-SCR [36,37]. Monticelli *et al.* [38] as well as Sedlmair *et al.* [39] studied the NO_x storage of alkali and alkaline earth exchanged Y zeolites for the exhaust gas of lean burn engines. The problem at this process exists in the limited capacity for the storage of NO_x (Ce or Al_2O_3) or, in the case of usage of BaO, in the formation of thermodynamically stable $BaSO_4$. Attempts of a thermal regeneration led so far to vast loss of the catalytic activity.

1.5.3 NH₃-SCR and ammonia provision

Since the early 90s the so-called **selective catalytic reduction (SCR)** has emerged as the most promising technology for considerable reduction of the nitrogen oxides content in the Diesel exhaust gas. Serial applications that meet the Euro V standard were introduced in trucks in Europe at the beginning of 2005, but also in the US the system was introduced successfully. The abbreviated term SCR has to be understood as a synonym for NH_3-SCR since only the catalyzed reduction with ammon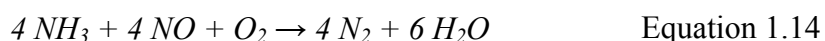ia as reducing agent meets the claim of a truly selective conversion of the nitrogen oxides towards N_2 and H_2O, appropriate non-precious metal containing catalysts preconditioned. The technology is well-known from power plant engineering, SCR systems were first installed in Japan in the late 1970s on both industrial and utility plants. More than 170 SCR commercial installations are nowadays in operation in the Japanese utility power companies for an estimated overall capacity close to 100,000 MW [40].

For the selective reduction of the nitrogen oxides an ammonia containing reducing agent is fed into the exhaust gas stream in front of the reduction catalyst. The nitrogen oxides react with ammonia to elemental nitrogen and water. Thereby, two reactions play an important role:

- Standard SCR reaction

$$4\ NH_3 + 4\ NO + O_2 \rightarrow 4\ N_2 + 6\ H_2O \qquad \text{Equation 1.14}$$

- Fast SCR reaction [41-43]

$$2\ NH_3 + NO + NO_2 \rightarrow 2\ N_2 + 3\ H_2O \qquad \text{Equation 1.15}$$
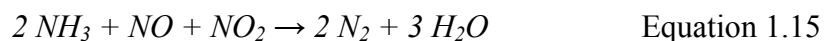
The fast SCR reaction, in which also NO_2 is involved beside NO, is crucial for the system activity in the low temperature range. An ideal NO/NO_2 ratio of 1 results from stoichiometry.

The SCR reaction necessitates ammonia being adsorbed on the catalytically active surface. The maximum of activity is achieved at approximately 400°C. At higher temperatures the ammonia desorbs, i.e. the activity decreases. Overall a temperature window of 150 – 500°C can be specified.

As gaseous ammonia is not appropriate for the mobile application due to safety issues, ammonia chipping substances are used instead. In this context the following methods of resolution are discussed:

- Urea-water-solution
- Solid urea
- Ammonium carbamate
- Ammonia-water-solution

The drawback of the technique is that an additional component has to be carried within the vehicle and that an additional dosing system for the reducing agent is required.

As catalysts titanium dioxide (stabilized anatase modification) supported V_2O_5-WO_3 contacts are predominantly applied. For the above mentioned, harsh power plant operation they are constructed as extrudate modules with coarse cell density in order to cope with the large exhaust gas amounts and the dust problem while investment and operational costs remain justifiable. The optimum range of working temperature is mostly specified between 280 – 400°C. NO_x conversions of 80% to even above 90% are achieved at which a conversion statement is only meaningful in connection with the statement of the NH_3 slip (usually smaller 5 ppm).

In recent years, Fe-ZSM-5 was extensively investigated as potential alternative to vanadia based SCR catalysts due to its lesser sensitivity to alkali and sulfur compounds [44,45]. The outcome was that Fe-ZSM-5 showed very good HNCO hydrolysis activity as well as SCR performance, especially after aging and in the presence of NO_2, which makes it a highly interesting catalyst for the practical application in urea-SCR systems in diesel vehicles.

1.5.4 Technology comparison

The reduction of NO_x with hydrocarbons has a couple of severe drawbacks, which make a robust application in mobile sources unfeasible. Product selectivity towards nitrogen is generally poor as the hydrocarbons are oxidized preferably by the excess oxygen present in the exhaust gas. If Pt-containing catalysts are used, the formation of N_2O plays a significant role also resulting in a low product selectivity. On the other hand, if zeolites are used, they show the characteristic of being unstable at high temperatures and in water-containing environment.

NO_x storage-reduction catalysts reveal their principal weakness in sulfur sensitivity. SO_2 present in the exhaust gas is oxidized to SO_3, which exhibits a high thermodynamic stability in the form of $BaSO_4$ for instance. A thermal regeneration necessitates temperatures above 650°C, which would lead to deactivation of the catalysts. Further disadvantages of the NO_x storage concept are the intermittent fuel-rich phases meaning an additional fuel consumption linked with the requirement of an advanced motor management. Some of the more robust catalysts do not exhibit sufficient NO_x storage capacity.

Therefore NH_3-SCR has emerged to be the most lucrative approach to reduce NO_x from Diesel exhaust gas in terms of efficiency and selectivity, at which the smart integration of an extra reducing agent is the only major challenge.

1.6 The Controlled Diesel Catalyst Concept (GD-KAT) [46]

The compliance with the Euro IV emission threshold values for commercial vehicle engines succeeds alternatively following two basic concepts:

- Inner-motor reduction of particulate matter at the b_e-optimized engine and NO_x reduction/oxidation of remainder particulate by means of GD-KAT systems [47]
- Inner-motor NO_x reduction and reduction of particulate matter by means of PM-KAT systems [48]

Compared to the GD-KAT system the PM-KAT system (see Figure 1.4) shows the characteristic of a higher fuel consumption due to the principle of inner-motor NO_x reduction, so that the decision upon the most economic Euro IV concept has to be made on the basis of the type of application and yearly mileage of the vehicle.
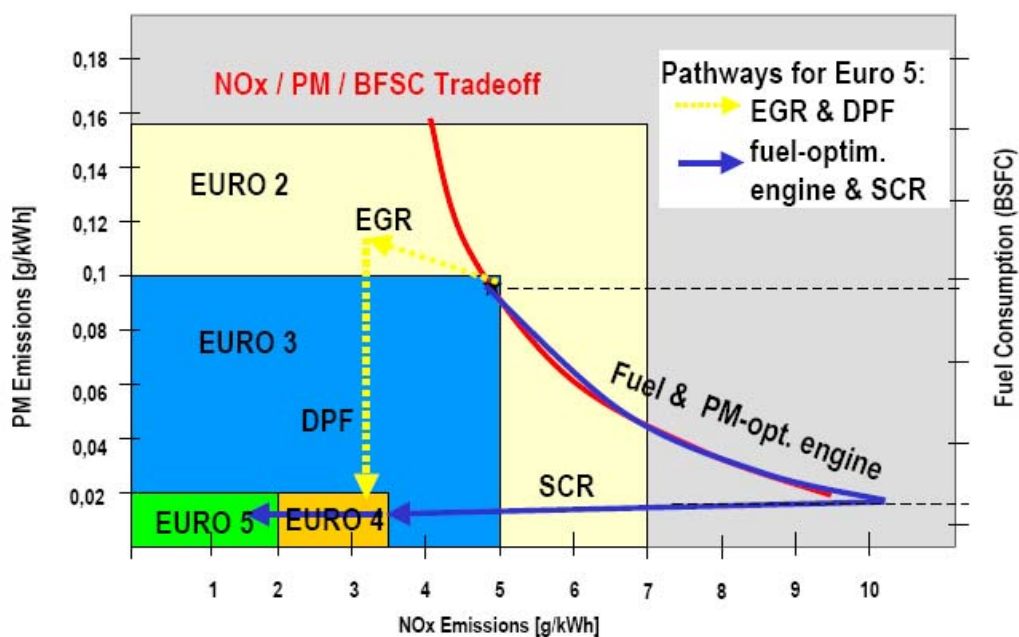
Figure 1.4 Strategies to reduce Diesel Emissions [49].

A GD-KAT system consists of two sub-systems:

- The dosing system of the reducing agent. AdBlue, an eutectic 32.5% urea solution of high purity is used as reducing agent.

- The catalyst system in the muffler region consisting of the reduction catalyst (SCR- or abbreviated R-cat) and various SCR auxiliary catalysts.

1.6.1 SCR catalysts (R-cats)

The reduction of NO_x in oxygen-containing exhaust gas is only successful with the reducing agent ammonia. We use the term selective reduction of the NO_x as the oxygen being present in excess does not react with ammonia over a broad temperature range up to 550°C in presence of appropriate catalysts. The most active and most selective known SCR catalysts are composed of 1.7-2.5% vanadium pentoxide (active component), 8-10% tungsten trioxide (promoter), carried by titanium dioxide in the anatase modification. They are available as full extrudates or coated catalysts.

Suitable SCR catalysts are honeycomb extrudates with fine cell density (300 cpsi or higher) or coated catalysts (400 cpsi), which are active and stable up to 550°C. Extrudated R-cats are integrated modularly as cylindrical monoliths (ø 143 mm) at lengths in the range of up to 250 mm in the main muffler while several monoliths are flown through in parallel.

At the application of SCR catalysts in the exhaust gas of commercial vehicle engines one has to consider the deactivation by engine oil ash. In order to reach the required long-term stability, the emission of ash must be limited to 0.5 mg/kWh by means of a corresponding measures package [50]. R-cats are particularly sensitive towards phosphorus. The active component di-vanadium pentoxide together with phosphoric acid forms vanadyl phosphate, which possesses a reduced high-temperature reduction activity.

The following sections introduce the so-called SCR auxiliary catalysts.

1.6.2 Hydrolysis catalysts (H-cats)

When an aqueous urea solution is sprayed into hot exhaust gas, contrary to the widespread opinion only a partial thermal decomposition of the urea (15/65% at 255/440°C, 3.5 m distance between injection nozzle and catalyst, corresponds to 0.1 s residence time) into an equimolar mixture of ammonia and isocyanic acid occurs [46]. The hydrolysis of the formed isocyanic acid to NH_3 by water vapor in the gas phase is not worth mentioning [51]. As there is by far less length of exhaust gas pipe available in the vehicles, this means that urea is significantly unconverted when reaching the front surface of the R-cat. Thus the reduction activity of the catalyst is considerably decreased. The task of an H-cat is to convert urea into ammonia as quantitatively as possible. The following single steps are part of this process:

- The completion of the water evaporation,
- The catalyzed thermal decomposition of the urea to ammonia and isocyanic acid and
- The catalyzed hydrolysis of the isocyanic acid to ammonia.

To its advantage an H-cat carrier consists of metal, has a mixing structure (see Figure 1.5) and is coated with titanium dioxide as most important active component. H-cats can be operated as external, separately heated or as internal, exhaust-gas-heated ammonia generators [52]. The hydrolysis activity of strong solid acids as TiO_2-carried tungsta or vanadia/tungsta (R-cats) is distinctly lower than the one of the much less acid TiO_2. Reason is the too short contact time of HNCO with superacidic surfaces.

Figure 1.5 Transmitted light photograph of a coated H-cat with special mixing structure [53].

1.6.3 Ammonia-oxidation catalysts (O-cats)

Positioned down-stream of the SCR catalysts, O-cats serve the avoidance of NH_3 emissions at short-time overdosing of the reducing agent. With platinum catalysts at very high space velocities NH_3 can be selectively oxidized to a great extent to nitrogen. A very elegant and low-priced process for the production of O-cats is the impregnation of the outlet side of the V_2O_5-WO_3/TiO_2 R-cat with approximately 0.2% platinum utilizing a length of 10-15 mm.

1.6.4 Pre-oxidation catalysts (V-cats)

At the pre-oxidation catalysts up to 50% of the motor-emitted NO is oxidized to NO_2. The NO_2 formed is extremely reactive and functions as key molecule at the R-cats for two simultaneously occurring reactions:

- Accelerated reduction of NO_x through NH_3 (fast SCR, see Equation 1.15). An equimolar mixture of NO and NO_2 is also very rapidly catalytically reduced through NH_3 in the range 200-330°C.

- Oxidation of the carbon-containing particulate matter, which is adsorbed on the subsequent R-cats.

At V-cats, to a minor degree also at O-cats, a sulfur content of the Diesel fuel leads to the production of sulfuric acid, which increases the particulate emission. Simultaneously the light-off temperatures for the NO- (V-cat) and ammonia oxidation (O-cat) are noteably increased. The application of V-cats therefore requires the use of sulfur-free fuel.

1.6.5 V/H-RO system (year 2000)

The complete decomposition and hydrolysis of the AdBlue, which is sprayed into the hot exhaust gas is of crucial importance with regard to the achievable conversions at the SCR catalyst. By means of an H-cat, which is positioned upstream in the full exhaust gas pipe a marked improvement in comparison with the decomposition in a thermolysis distance is succeeded. Admittedly, the necessary H-cat volume of 20-50% of the SCR catalyst volume is comparably high.

Therefore the system has been designed in such a configuration that the exhaust gas is split and that only around 20% of the total exhaust gas is directed over the H-cat. Thus, with improved activity, it can be reduced in volume to below 10% of the R-cat (see Figure 1.6).
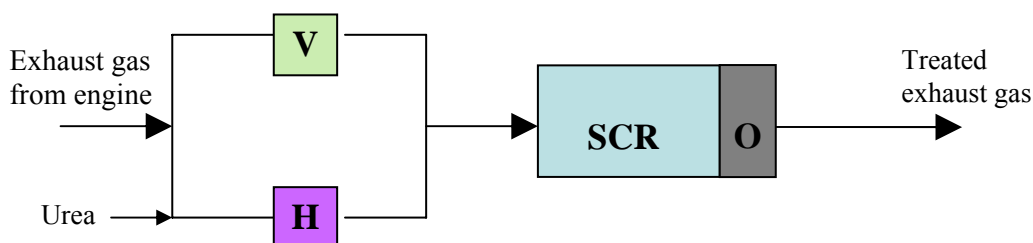
Figure 1.6 GD-KAT system [46].

Other strong arguments in favor of the parallel arrangement of V- and H-cat are

- Considerable reduction of the pressure drop
- Conversion improvement (factor 5) through increasing the contact time for the urea decomposition by reduction of the exhaust gas volumetric flow

This system has already been in development since the beginning of the 90s. For the future a further downsizing of the V/H-RO type of the GD-KAT system is aimed in order to improve further its application in the vehicle. There exists potential to reduce

the total volume of the catalytic system by maximum 40% from currently 27 to 18 liters (system 2005).

The target of this technology development to commercialize as soon as possible the latest development status (V/H-RO system) of the GD-KAT system for compliance with the EURO IV/V thresholds will not be possible before 2006 because of (i) the specific framework for commercial vehicles (emission stability for 500,000 km and on-board diagnosis (OBD), (ii) the Europe-wide availability of sulfur-free Diesel fuel and (iii) the required development and testing time of low-ash engine oils.

1.7 References

[1]   Automotive News, 1990 Market Data Book, May 30, 1990.

[2]   R.M. Heck, R.J. Farrauto, Appl. Catal. A: General 221 (2001) 443.

[3]   H.P. Lenz, S. Prüller, Emissionen und Immissionen von Abgaskomponenten, Fortschritt-Berichte VDI, Reihe 12, Nr. 528, VDI-Verlag, Düsseldorf, 2003, 16.

[4]   W. Weisweiler, Chemie Ingenieur Technik 72 (2000) 441.

[5]   C. Bowman, Pollutants from combustion: gas-phase reaction mechanisms for nitrogen oxide formation and removal in combustion. Kluwer Academic Press, Dordrecht, Norwell, New York, London (2000).

[6]   E. Zeldovich, Acta Physicochim. USSR 21 (1946) 577.

[7]   F. Dinkelacker, A. Leipertz, Lecture notes: Combustion engineering, Chair of Technical Thermodynamics, Friedrich-Alexander University Erlangen-Nuremberg, summer term 2000.

[8]   A. Herr, Thermische Zersetzung von Festharnstoff für mobile SCR-Katalysator-anwendungen, PhD Thesis, Technische Universität Kaiserslautern (2004).

[9]   C.P. Fenimore, Formation of nitric oxide in premixed hydrogen flames. In: Thirteenth Symposium (International) on combustion, The Combustion Institute, Pittsburgh, 1971, 373.

[10]   C.P. Fenimore, Combust. Flame 19 (1972) 289.

[11]   A.N. Hayhurst, H.A.G. McLean, Nature 251 (1974) 303.

[12]   G. Poulet, Pollutants from combustion: general description of atmospheric chemistry. Kluwer Academic Press, Dordrecht, Norwell, New York, London (2000).

[13]   W.J. Moxim, H. Levy, P.S. Kasibhatla, J. Geophys. Res. 101 D7 (1996) 12621.

[14]   R. Wunsch, Entwicklung eines Katalysator-Reduktionsmittel-Systems zur Stickoxid-Minderung in Abgasen aus Dieselmotoren, PhD Thesis, Universität Karlsruhe (2000).

[15]   K.O. Blumberg, M.P. Walsh, C. Pera, Low sulfur gasoline & Diesel: the key to lower vehicle emissions, Meeting of the international council on clean tranportation (ICCT), Napa, California, 2003.

[16]   http://www.dieselnet.com.

[17]   E.S.J. Lox, B.H. Engler, in Environmental Catalysis (Eds.: G. Ertl, H. Knözinger, J. Weitkamp), Wiley-VCH Verlag GmbH, Weinheim, 1999, 236.

[18]   A. König, G. Herding, B. Hupfeld, T. Richter, K. Weidmann, Topics in Catal. 16 (2001) 23.

[19]   H. Yahiro, M. Iwamoto, Appl. Catal. A 222 (2001) 163.

[20]   Y. Li, J.N. Armor, Appl. Catal. B 2 (1993) 239.

[21]   B.J. Adelman, T. Beutel, G.-D. Lei, W.M.H. Sachtler, J. Catal. 158 (1996) 327.

[22]   C. Gaudin, D. Duprez, G. Mabilon, M. Prigent, J. Catal. 160 (1996) 10.

[23]   F. Witzel, G.A. Still, W.K. Hall, J. Catal. 149 (1994) 229.

[24]   A.D. Cowan, R. Dumpelmann, N.W. Cant, J. Catal. 151 (1995) 356.

[25]   S. Kurze, W. Weisweiler, Chem. Eng. Technol. 22 (1999) 10, 855.

[26]   J.L. Valverde, A. de Lucas, F. Dorado, A. Romero, P.B. García, J. Mol. Catal. A 230 (2005) 23.

[27]   R.T. Yang, W. Li, J. Catal. 155 (1995) 414.

[28]   J.L. Valverde, A. de Lucas, P. Sanchez, F. Dorado, A. Romero, Appl. Catal. B 43 (2003) 43.

[29]   K. Katoh, T. Kihara, T. Asanuma, M. Gotoh, N. Shibagaki, Toyota Technol. Review 44 (1995) 27.

[30]   N. Miyoshi, S. Matsumoto, K. Katoh, T. Tanaka, J. Harada, N. Takahashi, K. Yokota, M. Sugiura, K. Kasahara, SAE Trans., 1995.

[31]   H. Lörch, W. Weisweiler, Chem.-Ing.-Tech. 70 (1998) 6, 749.

[32]   P. Zelenka, W. Cartellieri, P. Herzog, Appl. Catal. B 10 (2000) 3.

[33]   K.M. Adams, J.V. Cavataio, R.H. Hammerle, Appl. Catal. B 10 (1996) 157.

[34]   C. Sedlmair, K. Seshan, A. Jentys, J.A. Lercher, J. Catal. 214 (2003) 308.

[35]   B. Westerberg, E. Fridell, J. Mol. Catal. A: Chem. 165 (2001) 249.

[36]   Y. Traa, B. Burger, J. Weitkamp, Microporous Mesoporous Mater. 30 (1999) 3.

[37]   G. Busca, L. Lietti, G. Ramis, F. Berti, Appl. Catal. B 18 (1998) 1.

[38]   O. Monticelli, R. Loenders, P.A. Jacobs, J.A. Martens, Appl. Catal. B 21 (1999) 215.

[39]   C. Sedlmair, B. Gil, K. Seshan, A. Jentys, J.A. Lercher, Phys. Chem. Chem. Phys. 5 (2003) 1897.

[40]   P. Forzatti, Appl. Catal. A 222 (2001) 221.

[41]   A. Kato, S. Matsuda, T. Kamo, F. Nakajima, H. Kuroda, T. Narita, J. Phys. Chem. 85 (1981) 4099.

[42]   C. Ciardelli, I. Nova, E. Tronconi, D. Chatterjee, B. Bandl-Konrad, Chem. Commun. 23 (2004) 2718.

[43]   M. Koebel, G. Madia, F. Raimondi, A. Wokaun, J. Catal. 209 (2002) 159.

[44]   G. Piazzesi, M. Devadas, O. Kröcher, M. Elsener, A. Wokaun, Catal. Commun. 7 (2006) 600.

[45]   R.Q. Long, R.T. Yang, J. Catal. 198 (2001) 20.

[46]   E. Jacob, A. Döring, Vom SCR-Katalysator zum Gesteuerten Dieselkatalysator GD-KAT, in: Tagungsband VDA Technischer Kongress in Wolfsburg, April 2003, 163.

[47]   E. Jacob, A. Döring, GD-KAT: Abgasnachbehandlungssystem zur simultanen Kohlenstoffpartikel-Oxidation und NO_x-Reduktion für Euro IV/V-Nfz-Dieselmotoren, 21. Internationales Wiener Motorensymposium, H.P. Lenz (Hrsg.), Fortschritt-Berichte VDI, Reihe 12, Nr. 420, VDI-Verlag, Düsseldorf, 2000, 311.

[48]   E. Jacob, N. D'Alfonso, A. Döring, S. Reisch, D. Rothe, R. Brück, P. Treiber, PM-KAT: Nichtblockierende Lösung zur Minderung von Dieselruß für Euro IV-Nutzfahrzeugmotoren, 23. Internat. Wiener Motorensymp., H.P. Lenz, Fortschritt-Berichte VDI, Reihe 12, Nr. 490, VDI-Verlag, Düsseldorf, 2002, 196.

[49]   S. Fischer, K. Rusch, B. Amon, Presentation from SINOx Emissions Control, Argillon: SCR Technology to meet future Diesel Emission Regulations in Europe, Asian Vehicle Emission Control Conference (AVECC) in Bejing, China, April 2004.

[50]   E. Jacob, W. Gotre, D. Rothe, F. Rammer, K. Richter, Einfluß des Motorenöls auf die Emissionen von Dieselmotoren mit Abgasnachbehandlungssystem, 22. Internat. Wiener Motorensymp., H.P. Lenz, Fortschritt-Berichte VDI, Reihe 12, Nr. 490, VDI-Verlag, Düsseldorf, 2001, 286.

[51]   M. Koebel, M. Elsener, T. Marti, Combustion Science and Technology 121 (1996) 85.

[52]   E. Jacob (MAN Nutzfahrzeuge AG), EP a) 0487 886 (1990/4), b) 0 555 746 (1992/7).

[53]   E. Jacob, R. Müller, A. Scheeder, T. Cartus, R. Dreisbach, H.-P. Mai, M. Paulus, J. Spengler, Internationales Wiener Motorensymposium, H.P. Lenz (editor) Fortschritt-Berichte VDI, Reihe 12, Nr. 622, VDI-Verlag, Düsseldorf, 2006, 240.

Chapter 2

2 SCOPE AND OBJECTIVES OF THE THESIS

2.1 *Structuring of the Collaboration Project [1]*

Main parts of the experimental work of this thesis were carried out within the BFS-Project "Hochleistungs-GD-KAT – Katalytisches Hochleistungssystem zur NO_x-Verminderung für Fahrzeugdieselmotoren" which was divided into five thematically clearly separated sub-projects. Each sub-project is worked on by a partner. Two research centers make allowance for the scientific complexity of the assignment of tasks.

2.1.1 Sub-project V: Lehrstuhl für Thermodynamik, Technische Universität München (TUM)

The Lehrstuhl für Thermodynamik investigates the generation of aerosol as well as the thermo-fluiddynamic processes and performs a coordination function. Furthermore, the thermal urea decomposition is investigated on a global level in order to reveal important effects, which are due to the multiphase process. In the experimental part test units for the process as well as for single phenomena are constructed. Concurrently simulation tools for the ammonia generator are developed, into which the cognitions from the experimental work are introduced.

2.1.2 Sub-project A: MAN Nutzfahrzeuge

MAN Nutzfahrzeuge manufactures prototypes, carries out experiments under realistic conditions at highly dynamic engine test benches and provides the partners with the existing comprehensive knowledge with respect to the chemistry and to the process with aqueous urea solution.

2.1.3 Sub-project T: Emitec

Emitec advances in a custom-designed manner the technology with respect to the manufacture of metal, catalyst carrier substrates. The specific requirements of the individual catalyst types of the GD-KAT system, for instance the mixing function of the H-cat carrier as well as more efficient structures are in the center of interest. Emitec develops and delivers novel catalyst carriers with mixing function, internal flow compensation and improved mass transport for the sub-projects V, K and A.

2.1.4 Sub-project B: Süd-Chemie

Süd-Chemie develops optimized coatings and their production processes for the individual catalyst types of the GD-KAT system, in particular hydrolysis catalysts of the aerosol-ammonia generator (H-cat), and impregnates the catalyst carriers delivered from sub-project T for the sub-projects V, K and A.

2.1.5 Sub-project K: Lehrstuhl II für Technische Chemie, TUM

The Lehrstuhl II für Technische Chemie investigates activity and selectivity of the different catalyst types (V-, H-, R- and O-cat) of the GD-KAT system at a model gas test rig. Special attention is drawn to the conversion on catalytic surfaces during the multiphase catalytic process, i.e. at the time of the impact of the aerosol on the coated mixing structures of the hydrolysis catalyst. Furthermore, open questions about the gas phase kinetics are worked on at a model gas test rig with enhanced analytical instrumentation. Sub-project K also explores the prevention of undesired side products of the urea decomposition and in particular of the isocyanic acid HNCO.

Figure 2.1 below shows the collaboration of the partners schematically. The data and information exchange is not explicitly specified to simplify matters, but is represented globally through the gray connecting ring:
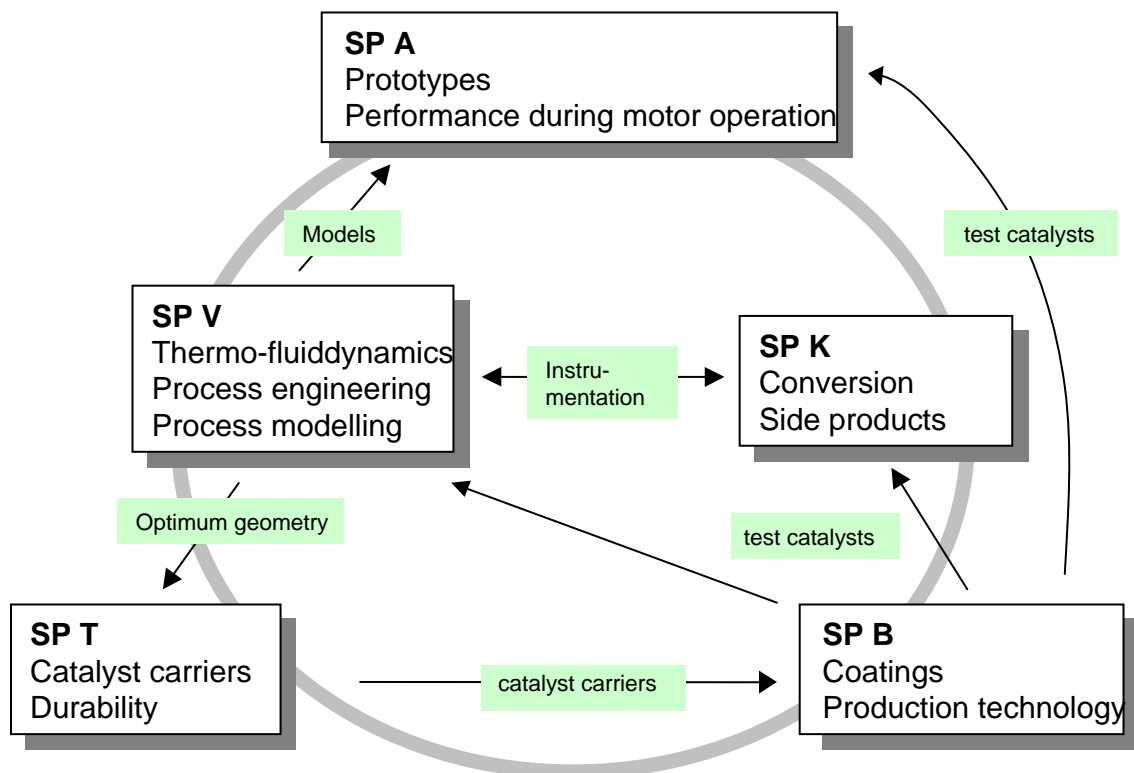

**Figure 2.1** Crosslinking of the sub-projects [1].

2.2 State-of-the-Art – Competitive Products or Processes

In stationary plants gaseous NH_3 is customarily used as reducing agent for the SCR (selective catalytic reduction) reaction [2]. Although NH_3 is the most suitable reducing agent on the part of the kinetics as well as of the reaction engineering, safety aspects are opposed to the use in mobile applications. The use of urea is an alternative, which can be employed both in aqueous solution and as solid [3-6]. The use of solid urea is advantageous due to the following reasons:

- Water has only a limited solubility for urea, therefore considerably more water than reducing agent has to be carried. Since relatively high mass flows of reducing agent are needed at a largely complete reduction also in the range of high loads, this is a substantial problem. The maximum for the binary system is the eutectic, which is 32.5 w% urea.

- Water supply is not required for reaction kinetic reasons and even deteriorates the low temperature performance of the process.

- Aqueous urea solution freezes at low ambient temperatures and requires a temperature-controlled storage and conveying system on-board.

- The need for an additional area-wide supply system with "filling stations" for urea solution is a serious logistic drawback.

Hence solid urea represents in the long term the most suitable reducing agent for the catalytic reduction of NO_x in mobile sources.

During heating up solid urea melts at 133°C and decomposes above 150°C via thermolysis to NH_3 and HNCO.

$$H_2N\text{-}CO\text{-}NH_2 \rightarrow NH_4^+ NCO^- \rightarrow NH_3 + HNCO \qquad \text{Equation 2.1}$$
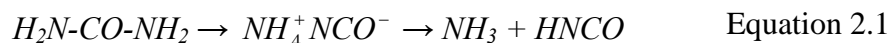
Over oxidic catalysts as e.g. TiO_2 and Al_2O_3 [3,4,7] the intermediately formed HNCO is hydrolyzed to NH_3 and CO_2.

$$HNCO + H_2O \rightarrow NH_3 + CO_2 \qquad \text{Equation 2.2}$$
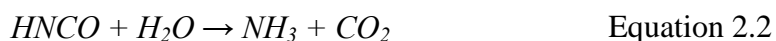
Since isocyanic acid is stable in the gas phase, solid polymerization products as cyanuric acid, ammelide, ammeline and melamine can be formed via a complex network of side reactions [8]:

$$3 \text{ HNCO} \longrightarrow$$

cyanuric acid

Equation 2.3

$$\text{HNCO} + \text{H}_2\text{N-CO-NH}_2 \longrightarrow$$

biuret

Equation 2.4

$$+ \text{ HNCO} \longrightarrow \quad + \text{ H}_2\text{O}$$

ammelide

Equation 2.5

$$+ \text{ HNCO} \longrightarrow \quad + 2 \text{ H}_2\text{O}$$

ammeline

Equation 2.6

melamine
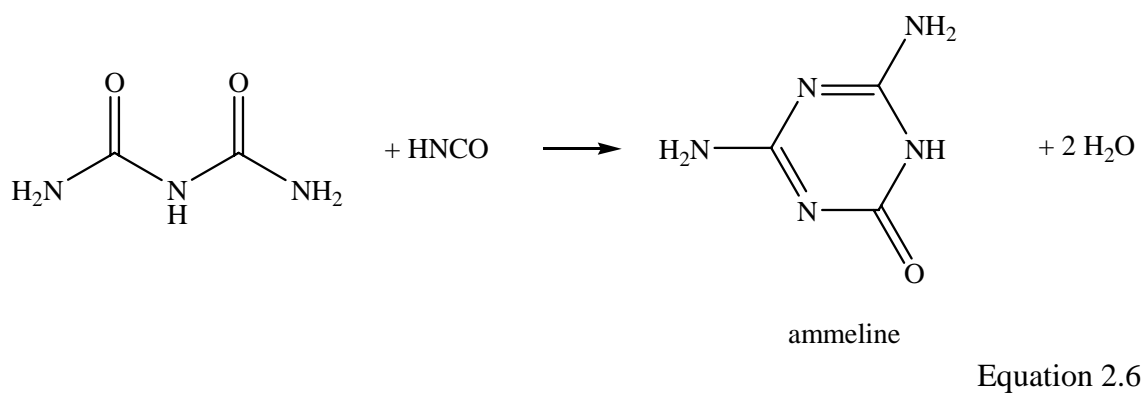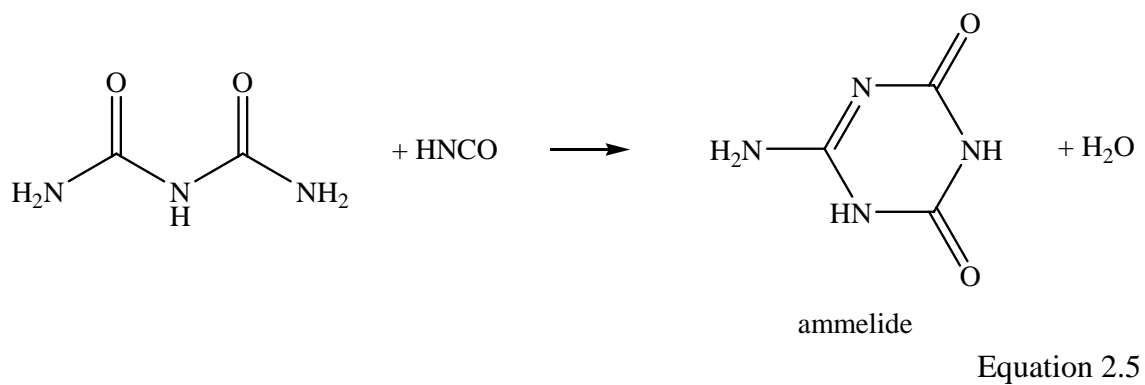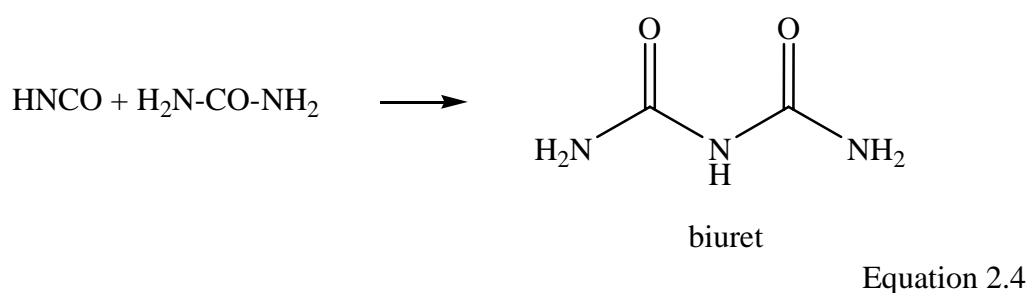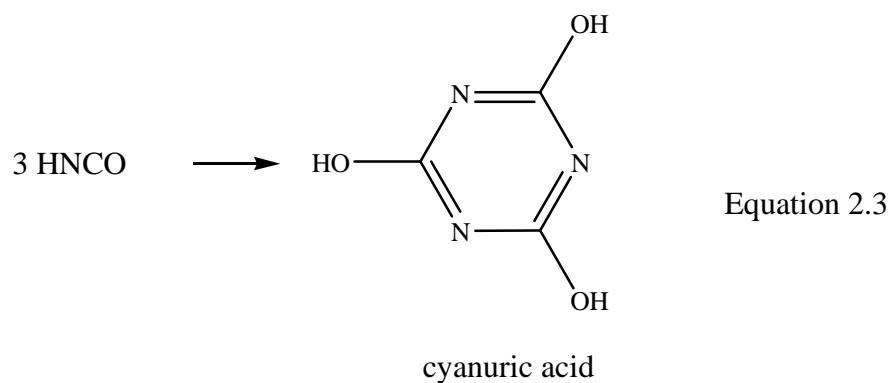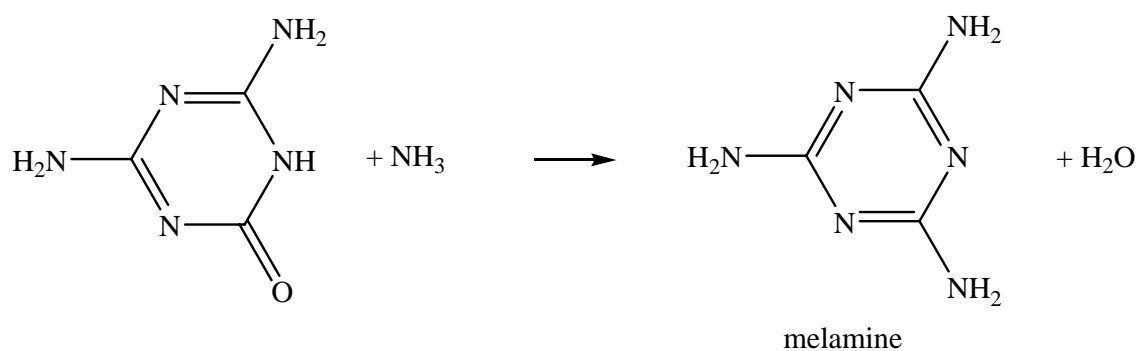
Equation 2.7

Although the polymerization products partially decompose to HNCO and NH_3 above 350°C, deactivation of the catalysts is expected through the formation of solid deposits. As the typical exhaust gas temperatures of Diesel engines are in the range of 150 to 450°C, it is of utmost importance for the SCR process with urea as reducing agent to employ highly active hydrolysis catalysts in order to avoid consecutive reactions of HNCO at the technical application, which can occur at a too long residence time of the reaction intermediates. Alternatively the utilization of carbamate as ammonia source has been proposed [9] since at usage of urea below 200°C the formation of solid deposits and the possible slip of HNCO was reported, while above 300°C direct oxidation of NH_3 to NO was observed [10]. Both observations however were proven wrong later through preliminary work of Koebel *et al.* [6] as well as through work of other groups [11,12]. Hence for a technical application of urea as reducing agent in the SCR process it is inevitably necessary to draw a comparison to other potential ammonia sources and to investigate the activity and space-time-yield as well as possible side reactions.

As hydrolysis catalysts both metal oxides as for instance Al_2O_3 [7,11] and the SCR catalyst composed of V_2O_5-WO_3/TiO_2 [12] and its single components can be used. TiO_2 (anatase) was identified as the most active catalyst [13]. In all cases the formation of equimolar proportions of NH_3 and CO_2 over the catalysts was determined. For V_2O_5-WO_3 (carried on TiO_2) a decrease of the hydrolysis activity was discovered with increasing V_2O_5 concentration [12]. Particularly at low reaction temperatures and high gas velocities the application of the SCR catalyst for the hydrolysis hence is not sufficient.

Vibrational spectroscopy is leveraged for the characterization of the surface sites on SCR catalysts [14-16] as well as their interaction with reactant molecules and non-reactive surface species [17-23]. Under reaction conditions (in presence of H_2O and O_2)

at the hydrolysis of HNCO over Al_2O_3 the formation of -NCO groups as reactive surface species as well as the accumulation of cyclic trimers of the isocyanic acid (cyanuric acid) and their products (ammelide, ammeline, melamine), respectively, on the surface of the catalysts were verified by *in situ* IR spectroscopy [11]. Both the presence of NH_3 and NO affects the rate of the HNCO hydrolysis. As NH_3 also adsorbs at the active sites of the catalysts, the surface concentration of HNCO and H_2O is reduced and the rate of reaction decreases.

Hence the characterization of the reactions at the contact surface between catalyst and solid, melting and liquid urea is a central problem area for the successful development of hydrolysis catalysts. In parallel to the urea conversion into NH_3 the investigation of the reaction of urea with NO_x on acidic catalyst surfaces is required to determine the influence of the partial reduction of NO_x and the competitive adsorption of reactants (NO_x) and intermediates (NH_3) at the hydrolysis catalyst on the HNCO hydrolysis activity.

2.3 Scientific and Technical Description of the Study

Sub-project K focuses on the investigation of the urea decomposition into NH_3 and HNCO, the catalyzed hydrolysis of HNCO into NH_3 and CO_2 as well as the investigation of the technical application of the coated catalysts developed in sub-project B.

2.3.1 Operation principles, novel methods of resolution, advantages, risks

The catalyzed hydrolysis of urea into NH_3 and CO_2 is a complex reaction, which proceeds via multiple intermediate stages and which can lead to solid deposits as side reaction. The solid deposits subsequently lead to catalyst deactivation and to blockage of the reactor system. Within the scope of the planned investigations, hence, the overall reaction should be split in single partial reactions on the one hand and those should be described on molecular level through the combination of *in situ* characterization and microkinetic reaction studies. On the other hand the complex physical and chemical interactions during the formation of NH_3 from solid or liquid urea particle on the catalyst surface should be explored, respectively.

It is planned to investigate the reactions of gaseous HNCO, of urea (as solid particle as well as in the form of droplets), NH_3 and NO/NO_2 on the catalyst surface by means of

laser-Raman and IR spectroscopy. There particularly the description of the sorption structure of intermediately formed HNCO on the catalyst surface in the presence of the other reaction partners is in the center of interest. From the knowledge of sorption structure, bond strength and concentration we should directly draw conclusions on the interactions between reactants and catalyst. Through the knowledge of the strength of the interaction of single species under reaction conditions in the case of competitive sorption of reactants and products on the active sites, the chemical characteristics of the catalysts can be correlated with their activity and selectivity.

In parallel to the spectroscopic studies of the reactions on the catalyst surface the influence of acidity and pore structure on the kinetics of the urea hydrolysis should be described at the model gas test rig. By comparison of the hydrolysis kinetics with the SCR kinetics the relative importance of both reaction pathways should be assessed. The potential of urea as reducing agent in the SCR process compared to other ammonia sources should be evaluated on the basis of achievable space-time-yields as well as formed side products. Additionally the activity and operability of the reduction catalysts (R-cats) and oxidation catalysts (V- and O-cats) produced via the coating technology developed in sub-project B should be compared with conventionally coated catalysts.

The comprehensive knowledge about the interrelation between structure and activity of the catalysts gained from the planned experiments represents the basis for the development and optimization of active catalysts as well as for the economical adaptation of the reaction conditions.

A set of pre-experiments with respect to the hydrolysis of HNCO over Al_2O_3 and TiO_2 catalysts was carried out in order to assess possible difficulties with the handling and dosing of liquid HNCO at the model gas test rig. Those proceeded successfully on the part of the reaction and dosing system, but showed that the analytical instrument used at that time (mass spectrometer with chemical ionization) was suitable to only a limited extent as uncontrolled side reactions in the intake systems falsified the determination of the gas concentrations. Hence the determination of the gas composition by means of FTIR with gas cell is suggested for the studies at the model gas test rig.

2.3.2 Objectives of the study

2.3.2.1   Setup and adaptation of the test facilities

At the outset of the work the gas supply system for the in situ measuring cells of the IR and Raman spectrometer has to be assembled as well as the measuring cells for the sorption of HNCO, NH_3 and NO under reaction conditions (in presence of H_2O and O_2) have to be adapted.

The model gas test rig has to be modified for adding HNCO (in liquid form via a saturator at temperatures between -40 and -10°C). The requested gas cuvette should be implemented in the gas flow of the model gas test rig. A calibration for the measurement of the concentrations of the reactants and products in the gas phase is generated by means of IR spectroscopy. Pre-studies have already shown that the calibration of the HNCO concentration and the prevention of potential oxidation or polymerization reactions of HNCO and NH_3 in the reactor system represent critical tasks at the validation of the reactor system.

2.3.2.2   Surface species and description of surface sites of hydrolysis catalysts

At the beginning of the vibrational spectroscopic studies the surface sites of the catalysts should be characterized by sorption of probe and reactant molecules. Next the interaction of reactant and product molecules with the surface sites under reaction conditions should be in the center of interest with respect to the spectroscopic studies. Starting from the investigation of the sorption of the single components over the temperature range between 150 and 450°C the stability of reactive surface species should be assessed.

At the model gas test rig the activity and selectivity of the catalyst provided by project partner B should be studied for the hydrolysis of HNCO and urea at steady state reaction conditions. Those measurements serve the determination of the most active and most selective coating for hydrolysis catalysts and the exploration of possible side reactions at the adhesion additives. They also provide a basis for the studies at transient reaction conditions and in presence of competitive reactions following in the second project year.

2.3.2.3 Stability, co-adsorption, kinetics and storage capacity of hydrolysis catalysts

In this part of the study the competitive adsorption of HNCO and NH_3, NO, NO_2 and H_2O should be investigated. For that purpose the catalyst surface should be first saturated with HNCO and the competitive adsorption of the reactants and possible product molecules of the SCR reaction should be studied. Subsequent the catalyst surface should be saturated with NH_3, NO, NO_2 or H_2O and the co-adsorption of HNCO should be explored.

At the same time as the spectroscopic investigations of the surface reactions, kinetic studies on the activity and selectivity of the HNCO and urea hydrolysis in presence of NH_3, NO/NO_2 and H_2O should be carried out. Under those conditions the SCR reaction can take place in parallel to the hydrolysis reaction. Reactions with time-variant HNCO concentration represent a further focal point with respect to the studies at the model gas test rig. Those should point out the storage capacity of the hydrolysis catalysts for the reactants and product molecules during load changes.

2.4 References

[1]   Förderantrag to the Bayerische Forschungsstiftung, *Hochleistungs-GD-KAT –*
        Katalytisches Hochleistungssystem zur NO$_x$-Verminderung für
        Fahrzeugdieselmotoren, 18.08.2002.

[2]   H. Bosch, F. Janssen, Catal. Today 2 (1988) 369.

[3]   E. Jacob, EP 0487 886 (1992).

[4]   E. Jacob, EP 0555 746 (1993).

[5]   E. Jacob, EP 0615 777 (1994).

[6]   M. Koebel, M. Elsener, M. Kleemann, Catal. Today 59 (2000) 335.

[7]   Z. Zhan, M. Müllner, J.A. Lercher, Catal. Today 27 (1996) 167.

[8]   P.M. Schaber, J. Colson, S. Higgins, E. Dietz, D. Thielen, B. Anspach, J. Brauer,
        Am. Lab. 13 (1999) 13.

[9]   W. Weissweiler, Chemie Ingenieur Technik 72 (2000) 946.

[10]   W. Weissweiler, F. Buchholz, Chemie Ingenieur Technik 73 (2001) 882.

[11]   N.W. Cant, D.C. Chambers, A.D. Cowan, I.O.Y. Liu, A. Satsuma, Top. Catal.
        10 (2000) 13.

[12]   M. Kleemann, M. Elsener, M. Koebel, A. Wokaun, Ind. Eng. Chem. Res. 39
        (2000) 4120.

[13]   S. Tong, I.G. Dalla Lana, K.T. Chuang, Canad. J. Chem. Eng. 71 (1993) 392.

[14]   N.Y. Topsoe, M. Anstrom, J.A. Dumesic, Catal. Lett. 76 (2001) 11.

[15]   M.D. Amirdis, R.V. Duevel, I.E. Wachs, Appl. Catal. B: Environ. 20 (1999) 111.

[16]   L. Lietti, G. Ramis, F. Berti, G. Toledo, D. Robba, G. Busca, P. Forzatti, Catal.
        Today 42 (1998) 101.

[17]   M.A. Larrubia, G. Ramis, G. Busca, Appl. Catal. B: Environ. 27 (2000) L145.

[18]   G. Busca, L. Lietti, G. Ramis, F. Berti, Appl. Catal. B: Environ. 18 (1998) 1.

[19]   M.A. Centeno, I. Carrizosa, J.A. Odriozola, Appl. Catal. B: Environ. 29 (2001)
        307.

[20]   S.M. Jung, P. Grange, Catal. Today 59 (2000) 305.

[21]   R.T. Yang, W.B. Li, N. Chen, Appl. Catal. A 215 (1998) 215.

[22]   A. Satsuma, A.D. Cowan, N.W. Cant, D.L. Trimm, J. Catal. 181 (1999) 165.

[23]   I. Nova, L. Lietti, E. Tronconi, P. Forzatti, Catal. Today 60 (2000) 73.

Chapter 3

3 SURFACE CHEMISTRY AND KINETICS OF THE HYDROLYSIS OF ISOCYANIC ACID ON ANATASE

3.1 Abstract

In order to meet the stricter NO_x and particulate emission limits for commercial vehicles, the selective catalytic reduction (SCR) with urea is currently seen having the highest potential. The conversion of urea into ammonia and carbon dioxide consists of two consecutive reactions, in which isocyanic acid is an intermediate that is hydrolyzed over TiO_2. The intrinsic kinetics and the surface chemistry for this reaction are explored. Up to a temperature of 132°C the reaction was in the intrinsic kinetic regime (E_A= 73 kJ/mol), while at higher temperatures the reaction was limited by pore and external diffusion constraints respectively. In the presence of NO, NH_3 and NO_2, the catalytic activity was negatively influenced, increasing in severity in the sequence mentioned indicating that nitrates formed from NO_2 were most effective in blocking cations and anions of TiO_2. IR spectroscopy indicates that dissociative adsorption of HNCO on TiO_2 forms Ti-N=C=O and hydrogen bonded OH species. In the presence of water, isocyanic acid was so rapidly hydrolyzed that only adsorbed ammonia was observed on the catalyst surface. The presence of NO, NH_3 and NO_2 retards hydrolysis leading to the appearance of isocyanate species on the surface.

3.2 Introduction

Approximately 20% of the global anthropogenic nitrogen oxide emissions originate from passenger cars and commercial vehicles [1]. In order to overcome these negative effects, increasingly rigid emission standards are being introduced, which require exhaust gas after-treatment of diesel engines. Today, the selective catalytic reduction (SCR) with ammonia is considered as the most promising technique for reducing NO_x emissions from heavy-duty diesel trucks and bus engines [2- 5]. In consequence, the European Automobile Manufacturers Association (ACEA for Association des Constructeurs Européens d'Automobiles, Brussels, Belgium) decided to recommend
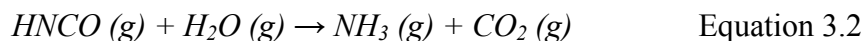
urea as the precursor for the reducing agent ammonia. In contrast to ammonia, urea is non-toxic and does not require elaborate safety precautions for handling and storage [5,6]. For most applications an aqueous urea solution (i.e., AdBlue® - 32.5% urea in H_2O) is injected into the hot exhaust gas stream. To be successful and robust, this approach requires detailed knowledge of the kinetics of the transformation of urea into ammonia [7].

Induced by the spatial constraints of the car, catalyst volume is aimed to be minimal. However, this is met with great difficulties, as the dynamically varying loads of the engine drastically affect the reaction conditions for the catalyst [8].

The practical conversion of the aqueous urea solution to ammonia consists of two steps. In the first the water of the aqueous urea solution sprayed into the flue gas stream evaporates and the remaining urea decomposes thermally into ammonia and isocyanic acid according to Equation 3.1.

$$H_2N\text{-}CO\text{-}NH_2 \ (s) \rightarrow NH_3 \ (g) + HNCO \ (g) \qquad \text{Equation 3.1}$$

In the second reaction step the isocyanic acid is hydrolyzed on an oxide catalyst yielding a second molecule of ammonia and carbon dioxide according to Equation 3.2.

$$HNCO \ (g) + H_2O \ (g) \rightarrow NH_3 \ (g) + CO_2 \ (g) \qquad \text{Equation 3.2}$$

Several engineering design variants have been proposed suggesting in essence reactors that are incorporated into the exhaust system or are built as separate units [7,9]. It should be noted, however, that isocyanic acid also undergoes a series of condensation reactions leading to a variety of solids ranging from cyanuric acid and biuret over ammelide and ammeline and melamine to polymeric forms of melamine [3,7,10]. These latter high molecular weight compounds have been reported to deposit on the walls of the exhaust pipe and inside the monolith channels and are only slowly decomposed under the typical reaction conditions. In order to minimize the formation of such polymeric species, the reaction conditions and the catalysts have to be adapted in order to maximize hydrolysis and to minimize condensation/ oligomerization of isocyanic acid.

The work presented here describes the kinetics and surface chemistry of the HNCO hydrolysis with water on TiO_2, a most promising material catalyzing hydrolysis, and the

influence of other molecules present in the reactant stream such as NH_3, NO and NO_2 on this catalytic chemistry.

3.3 Experimental

3.3.1 Catalysts

The hydrolysis catalyst (TiO_2 anatase from Süd-Chemie AG) was applied on a metal substrate (Emitec – Gesellschaft für Emissionstechnologie mbH) by impregnation. Textural promoters and/or binders (inorganic sol) were added to enhance the mechanical stability of the coating and to increase the adhesive strength to the metal foil, respectively. The specific surface area of the catalyst is 80 m^2/g (BET method).

3.3.2 Preparation of isocyanic acid

The synthesis of isocyanic acid was carried out by depolymerization of commercial cyanuric acid according to the method developed by Lercher and Zhan [11]. A heated quartz tubular reactor (18 mm ID) separated into three sections was used. The first section of the reactor was filled with quartz spheres to preheat the He carrier gas stream. The second part of the reactor contained 15 g of cyanuric acid (sublimation temperature 320 – 330°C) and the third section of the reactor held the Al_2O_3 catalyst bed used to depolymerize cyanuric acid. With the use of the catalyst, the decomposition temperature of cyanuric acid could be lowered to T = 370°C which results in superior product purity. Downstream of the reactor, the gaseous product was condensed in two serial cold traps at -80°C (isopropanol/dry ice). The method produced high purity HNCO with the final product containing less than 1 vol. % NH_3 without CO_2 being present. However, during start-up of the reaction hydrolysis on surface OH groups of the catalyst occurs, and it is essential to bypass the cold traps to avoid condensation of NH_3 and CO_2 into the product [12]. Depolymerization must be performed in the absence of water, as Al_2O_3 not only catalyzes the depolymerization but also the hydrolysis of HNCO.

3.3.3 Kinetic measurements

The experimental setup used for the kinetic experiments is shown in Figure 3.1. The composition of the feed gas was chosen to present a typical diesel exhaust gas, containing 4% H_2O and 10% O_2 with N_2 being the balancing gas [5,13]. The gas flow

rates were controlled using electronic mass flow controllers, and water was dosed through a fused silica capillary (0.1 mm ID) into the electrically heated heating block by means of a HPLC pump. HNCO was introduced into the system *via* an additional N_2 stream and a saturator, which was maintained at -30°C. The standard concentration of HNCO in all experiments was 500 ppm, for the reaction in presence of additional gas compounds, 500 ppm of NO, NO_2 or NH_3 were co-added.

The rate of the HNCO hydrolysis was determined using the active material coated onto a metal sheet to resemble the material in the technical application. The reactor was built from stainless steel with a rectangular cross section of the dimensions 3.5×2 mm (width $\times$ height). The catalyst was tested as a single coated metal sheet of 10 mm length and a thickness of 110 μm, simulating a two channel monolithic structure with a cell density of 185 cpsi. The mass of active material exposed to the gas stream was about 1.75 mg (calculated from the layer thickness and the packing density of the TiO_2 coating). The total flow rate was typically 3.6 l_N/min, and the geometric surface area of the catalyst was 70 mm^2. A thermocouple was incorporated in the reactor block for a direct measurement of the catalyst temperature. As the catalytic material employed was highly active, these very short residence times (areal velocity AV = volumetric flow rate/catalyst geometric surface area $\approx$ 3100 m_N/h) were necessary to reach differential reaction conditions (equivalent to conversion $X_{HNCO} \leq 10\%$).

The gas composition was continuously analyzed by a FTIR spectrometer (Thermo Electron Corporation Nexus, OMNIC QuantPad software) equipped with a heated, low volume multiple-path gas cell (2 m). The tubes connecting the reactor outlet and the gas cell in the IR spectrometer as well as the gas cell itself were heated to 185°C in order to prevent condensation/polymerization of HNCO at cold spots. The quantification method developed allowed to monitor concentrations in the ppm range of 25 compounds in total, including HNCO. Results were independent of the batch of synthesized HNCO and the mass balances based on carbon and nitrogen were better than 99%.
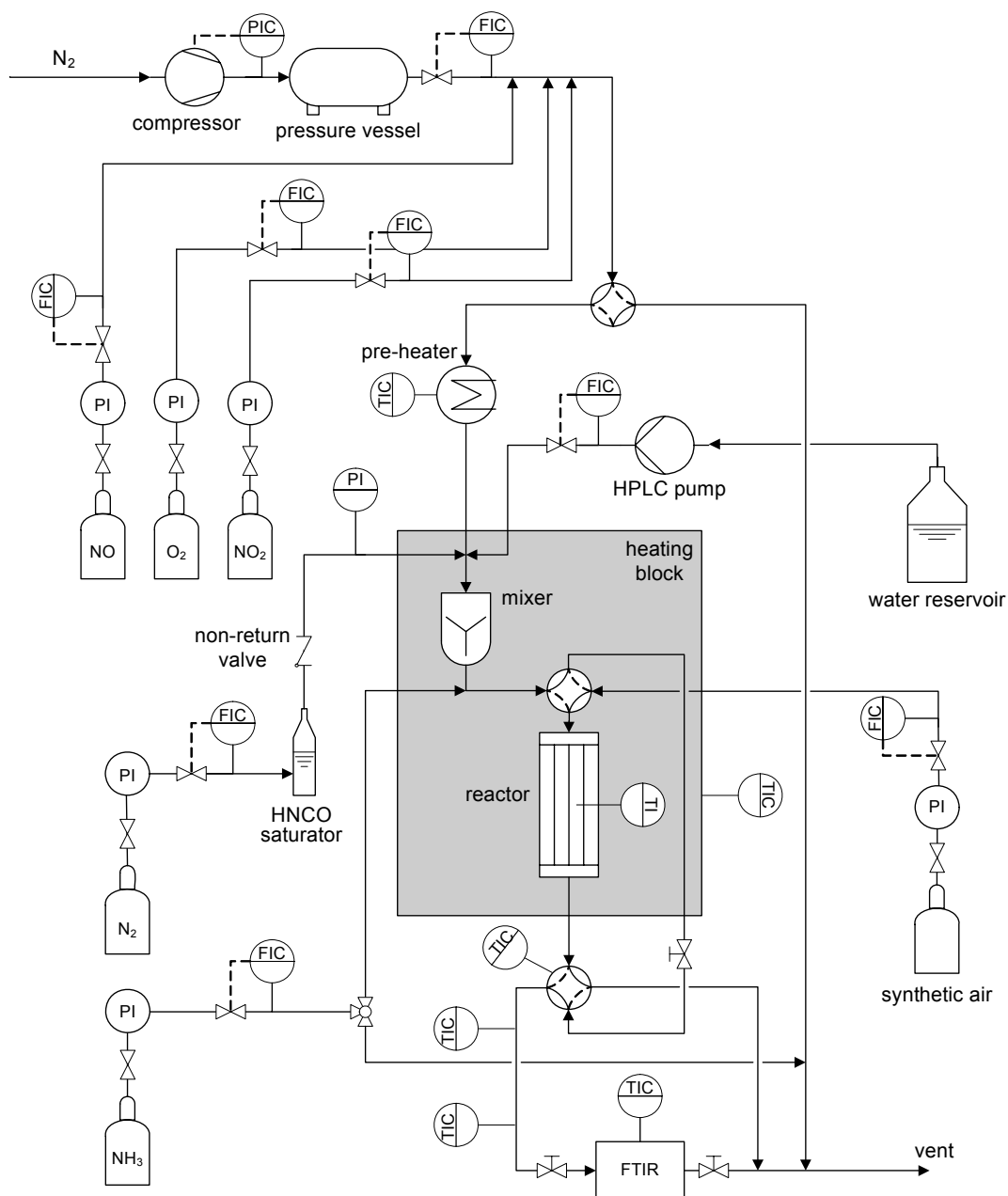
Figure 3.1 Flow scheme of the reaction system.

3.3.4 In situ infrared spectroscopy

In situ IR measurements were carried out with a Perkin-Elmer 2000 FTIR spectrometer equipped with a flow cell to collect IR spectra *in situ* during adsorption and reaction (for details see ref. [14]). The spectral resolution was 4 cm^{-1} and 40 interferograms were accumulated. Self-supporting wafers ($\approx$ 5 mg $\cdot$cm^{-2}) were prepared from TiO$_2$ (anatase). The samples were activated in helium at 150°C for 1 h. HNCO was fed into the system controlling the vapor pressure of the liquid phase in the

saturator which was kept at a constant temperature of -70°C in a dry ice/isopropanol bath. Concentrations of the reactants were around 800 ppm HNCO, 1000 ppm or 4% of water, 10% oxygen, the carrier gas was helium. For the coadsorption experiments, 500 ppm of NO, NO_2 or NH_3 were additionally fed into the gas stream. All experiments were carried out at 150°C. The flow of reactants (total 110 ml_N/min) was maintained over the sample for 1 h. NO and NO_2 in the gas mixture were quantified by a chemiluminescence analyzer (TEI 42C). Before each experiment, spectra of the activated sample were recorded and subtracted from the spectra during the exposure to the reactants to enhance the spectral changes.

3.4 Results

3.4.1 Kinetics of the HNCO hydrolysis

Figure 3.2 shows the HNCO conversion and the NH_3 yield as functions of the temperature. From 120°C to 165°C the catalytic activity increased sharply, while above 180°C this increase was very weak. At 428°C a minor concentration of 6 ppm NO was detected, at all other temperatures the selectivity to NH_3 was 100%.
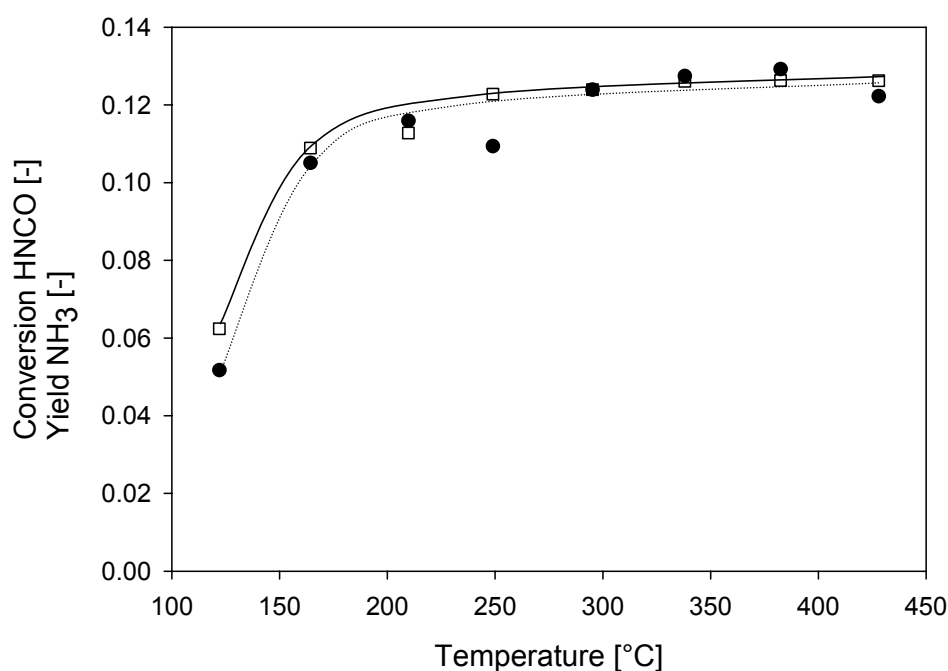

Figure 3.2 HNCO conversion (□) and NH_3 yield (●) as a function of temperature for TiO_2 anatase, c_{HNCO} = 500 ppm.

Pseudo-first order rate constants of the HNCO hydrolysis were calculated according to the rate equation for reactions under differential conditions in a plug flow reactor (Equation 3.3)

$$k_{hyd} = \frac{\dot{V}_{total}}{V_{cat}} X_{HNCO} \qquad \text{Equation 3.3}$$

$\dot{V}_{total}$ denotes the total flow rate, V_{cat} the catalyst volume and X_{HNCO} the conversion of HNCO. Table 3.1 summarizes the HNCO conversions and the pseudo-first order rate constants for the TiO_2 catalyst.

Table 3.1 Conversion of HNCO and rate constants over TiO_2 anatase.

T [°C]	X_{HNCO} [%]	k_{hyd} [s^{-1}]
428	12.6	11 786
382	12.6	11 016
338	12.6	10 244
295	12.4	9 361
249	12.3	8 501
209	11.3	7 233
163.5	10.2	5 916
154	9.4	5 301
143	9.2	5 071
132.5	6.8	3 656
121.5	4.1	2 143
110.5	2.1	1 067

For temperatures higher than 154°C, the apparent activation energy of HNCO hydrolysis was approximately 7 kJ/mol (see Figure 3.3). However, the temperature dependence in the low temperature region (110°C < T < 132°C) led to an apparent energy of activation of approximately 73 kJ/mol. The first value suggests that external diffusion controls the overall rate, while the second would suggest that one of the surface steps is being rate determining. In the temperature region 132 – 154°C a transition regime is assumed mainly controlled by internal mass transfer within the

catalyst pores (E_A = 25 kJ/mol). Note that the regime of the external transport control is in agreement with prior reports [5,15], while the apparent energy of activation in the kinetic regime is noted here for the first time.
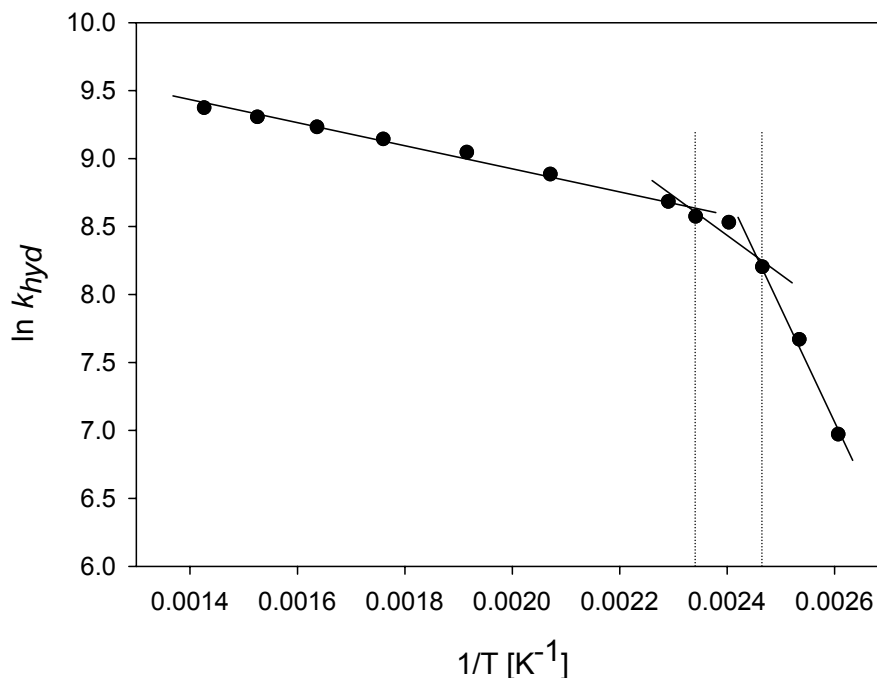

Figure 3.3 Arrhenius plot for hydrolysis catalyst TiO_2, measured with the two channel monolithic structure, AV = 3100 m_N/h.

3.4.2 Influence of reactants and products on the HNCO hydrolysis

The influence of additional gas components typically present in the feed gas on the kinetics of the HNCO hydrolysis was investigated by adding 500 ppm of NO, NO_2, or NH_3 into the gas stream containing 500 ppm HNCO, 4 % H_2O and 10 %O_2. The comparisons of the hydrolysis reaction with and without the respective co-reactant are shown in Figure 3.4. Significant effects of co-reacting molecules were only observed in the kinetic regime, while in the regime of mass transfer the impact was marginal.

The presence of NO showed the weakest effect on the activity of the catalyst for HNCO hydrolysis, i.e., the difference caused by the presence of NO was only 7%. The presence of 500 ppm NH_3 led to a somewhat stronger decrease of the activity. At 120°C the conversion of HNCO dropped from 6.2 % to 2.9%. The strongest influence on the activity, however, was observed in presence of 500 ppm NO_2. At temperatures below 220°C the conversion was significantly suppressed and decreased, e.g., at 120°C from 6.2 % to 1.1%.

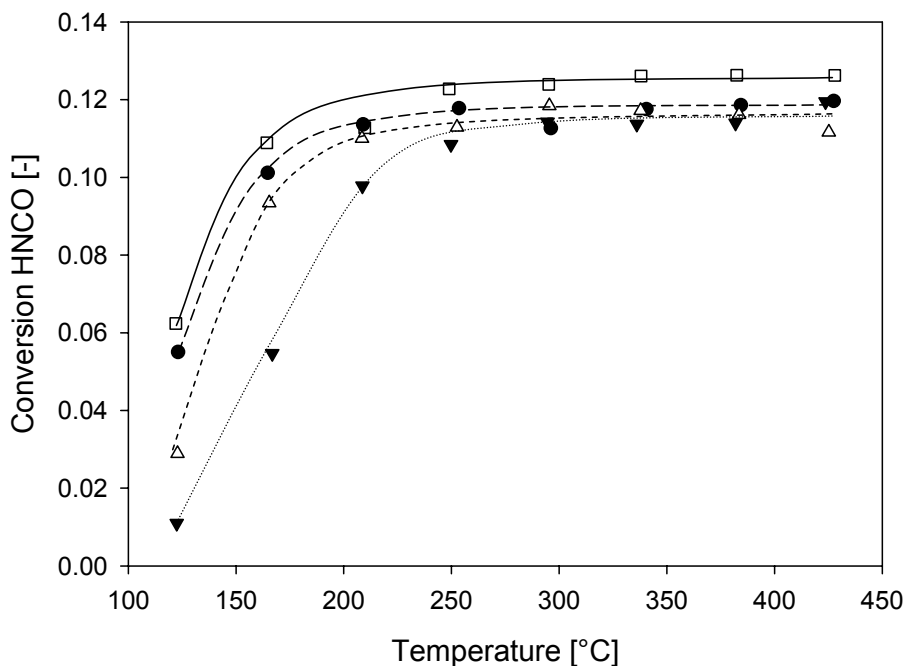**Figure 3.4** Influence of NO ($-\bullet-$), NH$_3$ ($- \cdot \triangle - \cdot$) and NO$_2$ ($\cdots\blacktriangledown\cdots$) on the HNCO conversion
(Catalyst = TiO$_2$ anatase, AV = 3100 m$_N$/h). Hydrolysis reaction without co-
reactant ($-\square-$).

3.4.3 Surface chemistry of HNCO studied by infrared spectroscopy

For the *in situ* IR spectroscopic measurements, the single metal sheet catalyst used for the kinetic experiments was replaced by a pressed self-supporting wafer of the catalyst coating, i.e., TiO$_2$. Limited by the experimental capabilities, the total flow rate of the reaction gas mixture was 110 ml$_N$/min and, thus, much lower than in the kinetic experiments leading in return to a higher contact time. The areal velocity was approximately 20 m$_N$/h compared to 3100 m$_N$/h in the kinetic experiments. The concentration of water necessary for the hydrolysis was reduced from 4% to 1000 ppm of H$_2$O in order to improve the spectral quality. However, the impact of 4% H$_2$O has been studied separately.

3.4.3.1 Adsorption and reaction of isocyanic acid

For the measurements TiO_2 (anatase) was contacted with 790 ppm HNCO in He at 150°C. The IR spectra after 5, 30 and 60 minutes are shown in Figure 3.5. The contact with HNCO led to the decrease of the intensity of the band of the hydroxyl groups (3667 cm^{-1}) [16] and to the simultaneous formation of bands at 3510, 3375, 3265 and 3163 cm^{-1}. The first two are assigned to hydrogen bonded OH groups which are perturbed by interaction with surface NCO$^-$ groups and which may be partly generated by the dissociation of HNCO [12]. The other two bands result from NH stretching modes. The most intense band at 2230 cm^{-1} is assigned to surface isocyanate (M-NCO) species bound to accessible Ti^{4+} cations [17]. At short time on stream (t.o.s.) the band appeared at 2210 cm^{-1} and shifted with increasing coverage to 2230 cm^{-1}. The shoulder at 2189 cm^{-1} is tentatively assigned to CO adsorbed on TiO_2 [18]. The bands at 1647, 1562 and 1496 cm^{-1} are attributed to the asymmetric and symmetric stretching vibration of the [N=C=O]$^-$ anion [19]. The weak band at 2066 cm^{-1} is attributed to cyanuric acid, the trimer of HNCO, because a band at the same wavenumber was observed in the spectrum of cyanuric acid in KBr. Its formation is explained by trimerization induced by the relatively long residence time of HNCO in the backmixed reactor used for the IR studies. The negative band at 1360 cm^{-1} is attributed to the characteristic ν(S=O) vibration of sulfate species [20,21]. These sulfates are impurities of the synthesis procedure of the particular TiO_2 sample. The IR spectra during the first 5 min of adsorption of HNCO (including the spectrum after 30 min) are shown in Figure 3.6. The sulfate groups strongly interact with HNCO which leads to a shift of the band at 1360 cm^{-1} to 1315 cm^{-1} (accompanied with a strong broadening of the band).
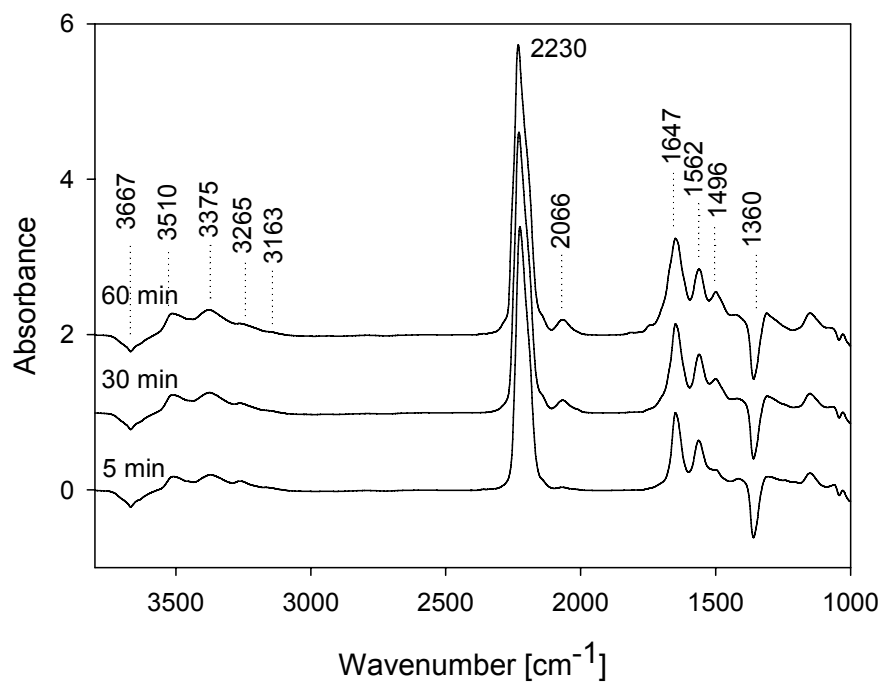
Figure 3.5 IR spectra of 790 ppm HNCO in contact with TiO_2 anatase, T_{Ads} = 150°C.
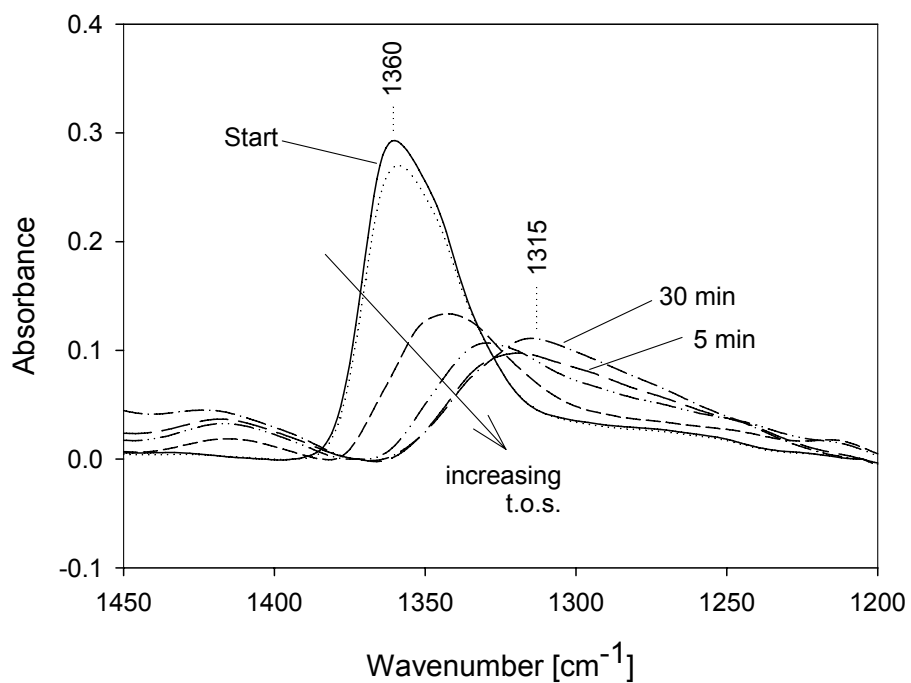

Figure 3.6 IR spectra between 1450 and 1200 cm^{-1} during adsorption of 790 ppm HNCO
(T = 150°C). The figure is a magnification of the respective wavenumber range of
Figure 3.5.

3.4.3.2   Sorption and reaction of HNCO in the presence of water

The surface species during the HNCO hydrolysis in presence of 4% H_2O and 10% O_2 after 5, 30 and 60 min reaction time are shown in Figure 3.7. The adsorption of H_2O on TiO_2 led to a broad band around 3240 cm^{-1}, while the band of the N=C=O stretching vibration of isocyanic acid at 2210 cm^{-1} was hardly detected. The bands at 3397, 3353, 3268 and 3169 cm^{-1} can be assigned to NH_3 formed in the reaction [22]. With increasing t.o.s., bands at 1620 and 1608 cm^{-1} appeared, the first one assigned to adsorbed water, the second one to the asymmetric deformation vibration of NH_3. The sharp (negative) band at 1357 cm^{-1} is attributed to the disappearance of the sulfate S=O band after interacting with H_2O. The band at 1197 cm^{-1} is assigned to the symmetric deformation of NH_3 and hence is also indicative of the HNCO hydrolysis. The absence of the intense band of adsorbed HNCO indicates that the hydrolysis is fast compared to adsorption, leading to a very low surface coverage of the reactant.

To study the effect of H_2O on the reactive surface species, experiments with 1000 ppm H_2O were also carried out (see Figure 3.8). At the ratio of $HNCO/H_2O = 830/1000$, small bands of isocyanates (2199 cm^{-1}) were observed. Additionally, multiple overlapping bands in the region around 1600 cm^{-1} were observed: 1643 and 1568 cm^{-1} for the [N=C=O]$^-$ anion, 1620 cm^{-1} for water and 1599 cm^{-1} for ammonia.
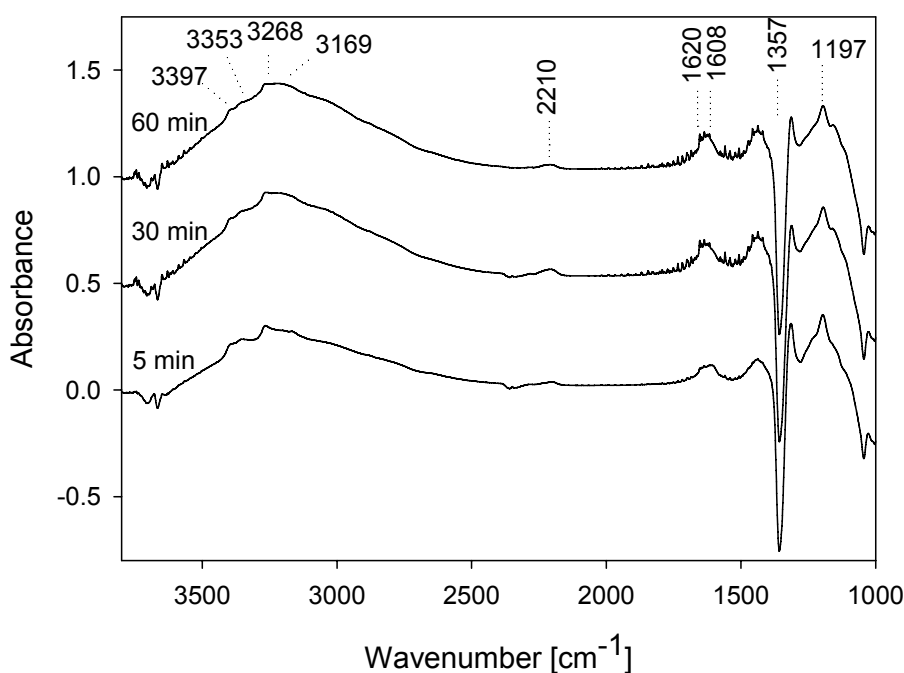
Figure 3.7 IR spectra during hydrolysis of HNCO (c_{HNCO} = 790 ppm, c_{H2O} = 4%, T = 150°C).
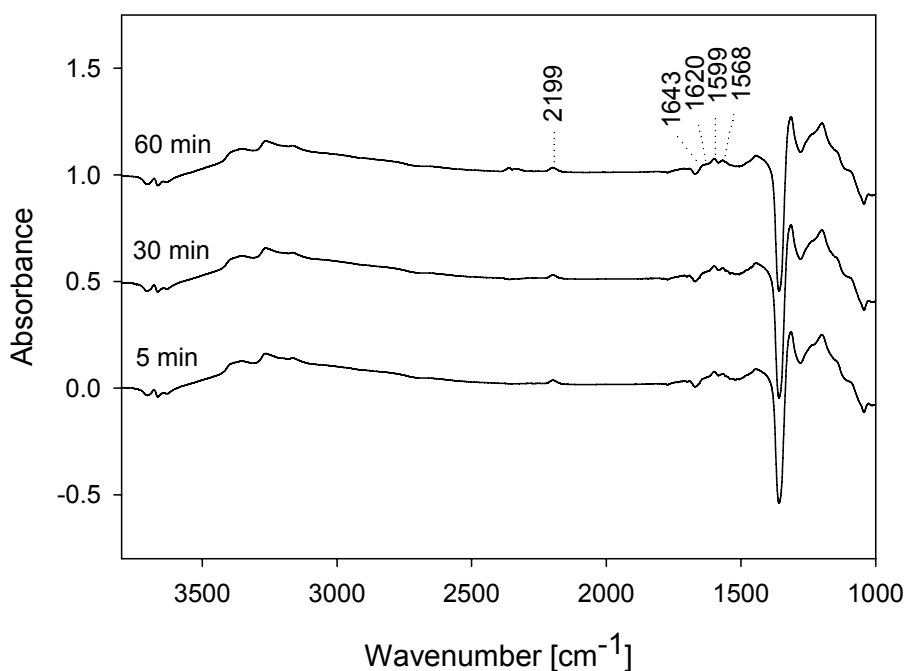
Figure 3.8 IR spectra during hydrolysis of HNCO (c_{HNCO} = 830 ppm, c_{H2O} = 1000 ppm, T = 150°C).

3.4.3.3   Reactions of HNCO in the presence of reactant/product molecules

The surface species during HNCO hydrolysis in presence of 500 ppm of NO, NH_3 and NO_2 after 5, 30 and 60 min t.o.s. are shown in Figure 3.9-Figure 3.11. During the HNCO hydrolysis in presence of NO (Figure 3.9) bands at 2206 cm^{-1} ([N=C=O]$^-$ stretching vibration) as well as 1648, 1563 and 1497 cm^{-1} (asymmetric and symmetric stretching vibrations of [N=C=O]$^-$) and in the region 1330-1200 cm^{-1} (surface nitrites) were observed [23]. The formation of NH_3 and its accumulation on the surface was revealed by the appearance of NH stretching bands (3263 and 3163 cm^{-1}). Hydrogen bonded OH groups were observed at 3508 and 3371 cm^{-1}. The small band at 2064 cm^{-1} is tentatively assigned to cyanuric acid formed by trimerization of HNCO. Characteristic bands of adsorbed NO were not observed. It is important to note that in parallel experiments, the adsorption of 10 mbar NO led to weak bands at 1650-1600 cm^{-1} assigned to nitrates, nitrites, nitro compounds and adsorbed NO_2 [24].

In contrast, when 500 ppm NH_3 were added to the reaction gas mixture, only bands assigned to the asymmetric and symmetric deformation vibration of NH_3 (1600 and

1196 cm^{-1}) were observed, while the typical bands of isocyanate species were absent (Figure 3.10).

During the HNCO hydrolysis in the presence of 500 ppm of NO$_2$, surface M-NCO species (2213 cm^{-1}) and cyanuric acid (2065 cm^{-1}) were detected (Figure 3.11). The region 1750-1450 cm^{-1} is enlarged in Figure 3.12 (spectra during the first 10 min of reaction including the last spectrum after 60 min). Bands of adsorbed isocyanic acid (1648 and 1561 cm^{-1}) strongly overlapped with bands assigned to nitrate ions (1637, 1606 and 1581 cm^{-1}) [22]. The bands at 1648 and 1561 cm^{-1} ([N=C=O]$^-$ anion) started to develop after 10 min when the nitrates were already present on the surface. This is consistent with the delayed appearance of the isocyanate band at 2213cm^{-1}. With increasing t.o.s., the band developing at 1617 cm^{-1} is assumed to shift to 1637 cm^{-1}. This phenomenon has been seen earlier during adsorption of 237 ppm NO$_2$ on TiO$_2$. In ref. [22] three doublets of bands at 1586 and 1291 cm^{-1}, 1608 and 1250 cm^{-1}, and 1630 and 1195 cm^{-1} were observed during adsorption of NO$_2$ on TiO$_2$. Note that Mosqueda-Jiménez *et al.* [25] assigned a band at 1602 cm^{-1} to v_{as}(NO$_2$) of nitro compounds. The bands at 1561 and 1495 cm^{-1}, attributed to the [N=C=O]$^-$ anion, were clearly resolved after peak separation.

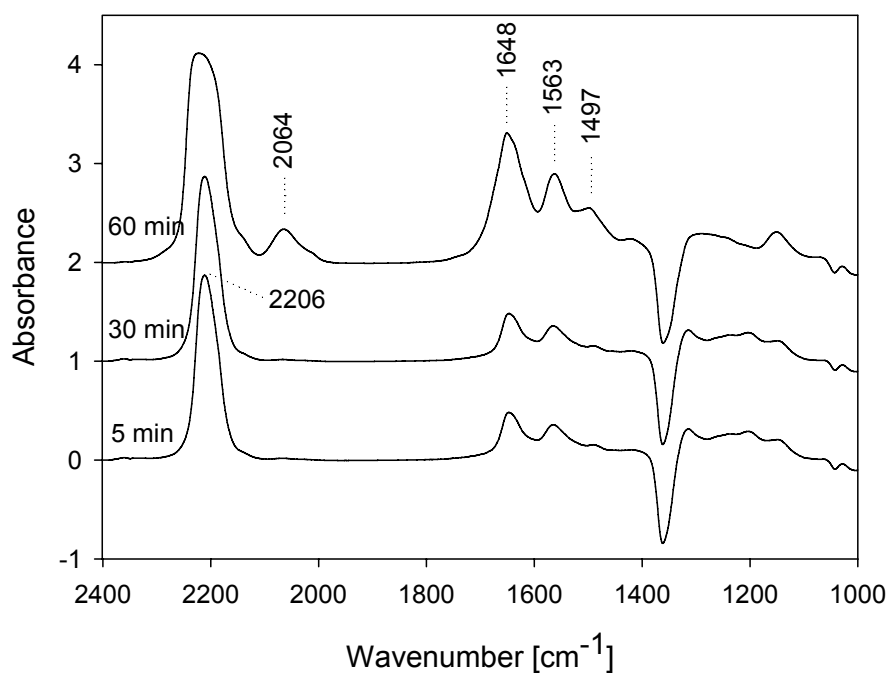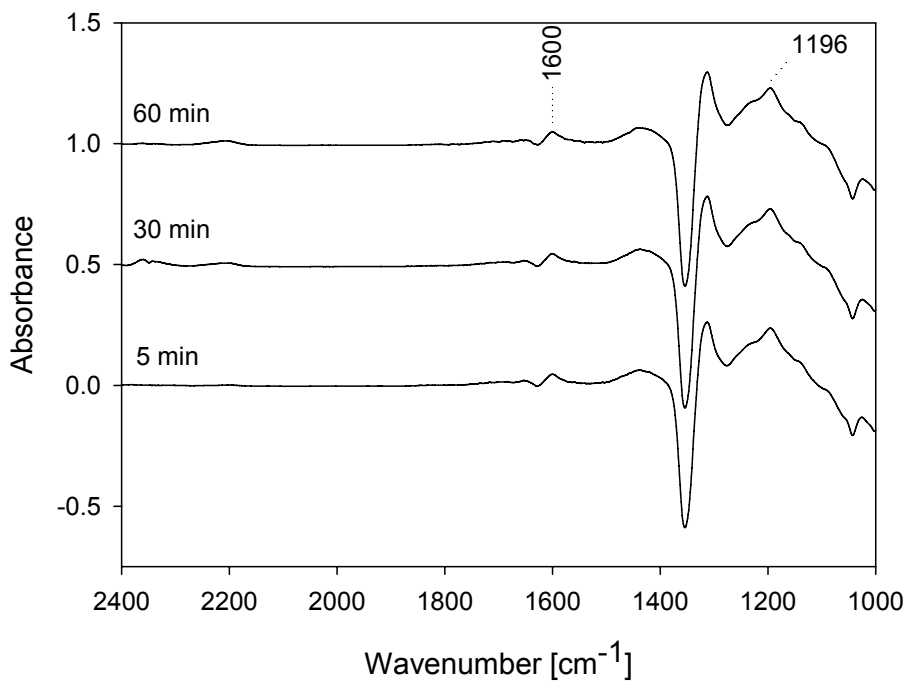**Figure 3.9** IR spectra during hydrolysis of HNCO in the presence of 500 ppm NO (T = 150°C).

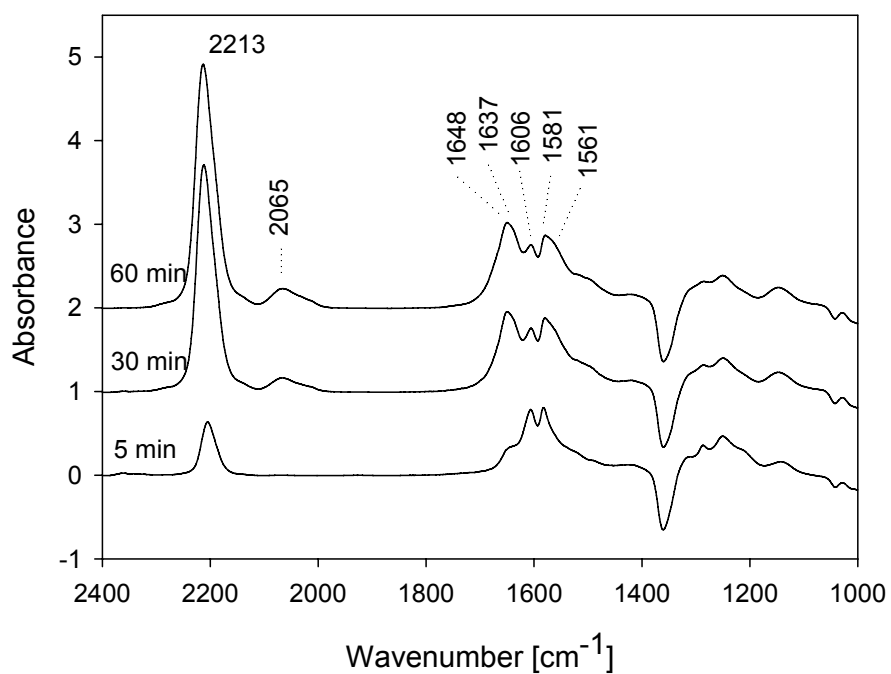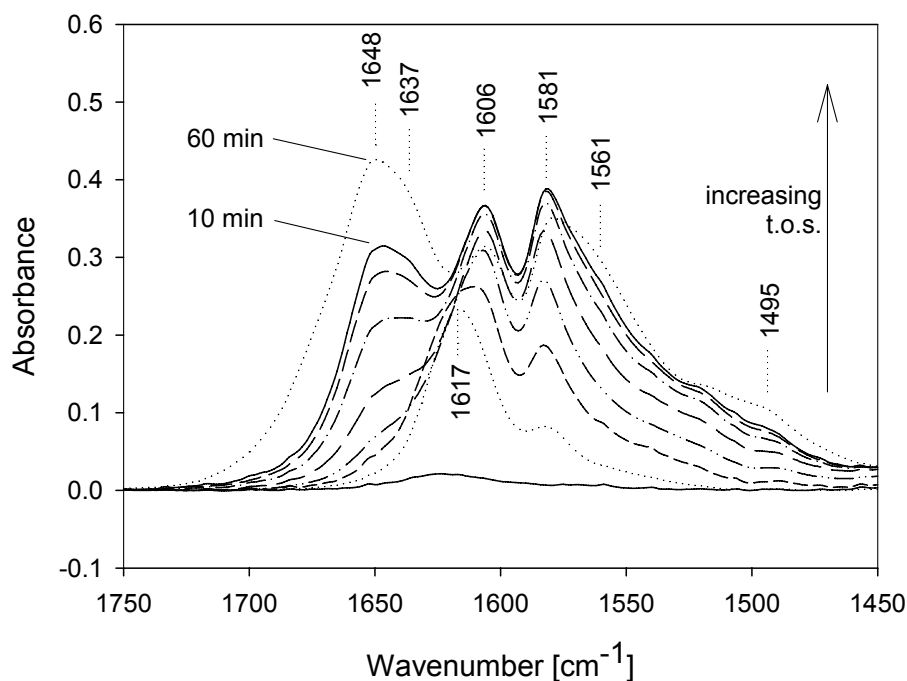**Figure 3.10** IR spectra during hydrolysis of HNCO in the presence of 500 ppm NH_3 (T = 150°C).

Figure 3.11 IR spectra during hydrolysis of HNCO in the presence of 500 ppm NO_2 (T = 150°C).

Figure 3.12 IR spectra between 1750 and 1450 cm^{-1} during hydrolysis of HNCO in the presence of 500 ppm NO$_2$ (T = 150°C). The figure is a magnification of the respective wavenumber range of Figure 3.11.

3.5 Discussion

3.5.1 Conversion of isocyanic acid with water

The conversion of HNCO over TiO$_2$ at temperatures between 110 and 428°C passes through three different kinetic regimes. Above 150°C the rate (and with it the conversion) increased only slightly. In agreement with Kleemann *et al.* [5] and Tronconi and Beretta [15] we attribute this to gas-phase mass transfer limitations of the reaction. The apparent energy of activation in all three papers is approximately 10 ± 5 kJ/mol. This strongly suggests that the reaction rate is controlled by external transport constraints. Even when a high gas hourly space velocity in combination with a packed fixed bed reactor was used [5], i.e., when the diffusion path length was drastically reduced compared to the monolith, the apparent activation energy was 12.7 kJ/mol. This indicates that the hydrolysis reaction is very fast under the conditions tested.

When we used a lower reaction temperature than those in the mentioned reports, the apparent energy of activation increased. Below 132°C, the apparent energy of activation was 73 kJ/mol. This indicates a quite substantial energetic barrier for the reaction and in turn a high preexponential factor, i.e., that the reaction proceeds on a relatively large number of sites.

IR spectra recorded at 150°C, i.e., under conditions at which the hydrolysis reaction begins to be controlled by diffusional constraints, show that in the absence of water HNCO adsorbs on TiO_2 dissociatively and most likely also associatively. The relatively broad free OH band of TiO_2 disappeared completely after contact with 750 ppm HNCO indicating that all OH groups of the oxide interact with HNCO, i.e., that a nearly full coverage exists. The interaction with the surface produced four hydrogen bonded OH and NH groups at 3510, 3375, 3265 and 3163 cm^{-1}. While it is clear that the first two bands are due to hydrogen bonded OH groups, the latter two are attributed to NH groups.

The perturbed OH groups are concluded to originate from TiOH groups or OH groups generated by dissociation of HNCO laterally interacting with NCO^- groups. However, we cannot exclude direct interaction of undissociated HNCO with OH groups. The NH groups are concluded to have formed from the hydrolysis of HNCO by surface OH groups. Again, contributions of a small fraction of weakly adsorbed, but not dissociated HNCO cannot be fully excluded.

The majority of HNCO is, however, dissociatively adsorbed forming Ti-NCO groups at accessible Ti^{4+} cations (2210-2230 cm^{-1}) and an OH group or a water molecule in case a Ti-OH group is present. Also the (symmetric and asymmetric) stretching vibrations at 1647, 1562 and 1496 cm^{-1} point to the presence of larger concentrations of strongly bound NCO^- anions. It should be noted that water molecules formed would react with NCO^- anions under the experimental conditions forming NH_3 and CO_2.

The presence of water changes the concentration of surface species dramatically. The NCO^- groups (2230 cm^{-1}) bound to the Ti^{4+} cations disappeared completely in the presence of 4 vol. % water, while in the presence of 1000 ppm H_2O traces of these groups were observed. Instead, the bands of (hydrogen bonded) molecular water and of ammonia are observed. The deformation vibrations of water (1620 cm^{-1}) and of ammonia (1608 cm^{-1}) indicate that both molecules coexist. This indicates that the surface reaction is so fast that only the products and spectator molecules (excess water)

are observed. It should, however, also be mentioned that the reaction is pore diffusion limited under the experimental conditions and, hence, the concentration of sorbed reactants has to be minimal. Additionally, it should be noted that the IR spectra under reaction conditions have been recorded in a backmixed reactor at relatively high conversions. Thus, in the reactor the HNCO concentrations are minimal. It is interesting to see, however, how subtly the surface chemistry is influenced by the presence of other molecules present in the real exhaust gas stream as discussed below.

3.5.2 Conversion of isocyanic acid with water in the presence of NO, NH_3 and NO_2

The presence of three additional compounds present in the exhaust gas stream (NO, NO_2) or being formed on the catalyst (NH_3) has a pronounced effect on the kinetics and the surface chemistry observed. All three molecules decrease the reaction rate in the kinetically relevant regime. The retardation increases in the sequence NO < NH_3 < NO_2 suggesting that the formation of nitrates has the most profound impact, as it involves both acidic and basic sites of the TiO_2 surface. In contrast, the sorption of NO on exposed Ti^{4+} cations is relatively weak, especially in the presence of 1000 ppm water, but also in this case acid and base sites are involved leading to nitrites rather than nitrates [26]. However, the weaker interaction of NO with TiO_2 and the lower thermal stability of the nitrites are in accordance with the lower impact of NO on the overall chemistry. The minor decrease in activity for the reaction in presence of NH_3 is explained by a product inhibition effect suppressing adsorption of HNCO.

The surface chemistry revealed by the IR spectra recorded under operating conditions suggests, however, a marked qualitative difference between the effects of NH_3 and the nitrogen oxides. With ammonia present, the bands of NCO^- stretching vibrations were hardly observed. At large, the IR spectra resemble those recorded during the hydrolysis without ammonia being present, i.e., only bands of water (to a minor extent) and ammonia appear in the IR spectra. This is in line with the high conversion of isocyanic acid in both experiments and the backmixed reactor used for the IR spectroscopic measurements. In both cases hardly any HNCO is present in the reactor with the only difference being that the partial pressure of NH_3 is more than twice as high when NH_3 is being co-fed.

This situation is drastically different in the presence of NO and NO_2 as both molecules undergo a reversible surface reaction, which leads to appreciable concentrations of nitrites and nitrates. Of course, the latter is present in much higher concentration than the nitrites. The formation of nitrates has been directly concluded from the bands at 1637, 1606 and 1581 cm^{-1}. The corresponding bands of the surface nitrites are typically observed in the region 1260 to 1330 cm^{-1}, however, due to the strong overlap with the sulfate bands in this region an unambiguous assignment of the bands is not possible. The formation of nitrites and nitrates is a formal oxidation and correspondingly should lead to the reduction of the metal cation. However, at solid surfaces, the base strength of the oxygen suffices to form the salts without the formal change in the oxidation state. Evidence for such well defined surface reactions can for example be seen in the adsorption of NO_2 on alkali cation exchanged zeolites [26]. None of the elements involved is able to change the oxidation state under the conditions studied while NO_2 is bound exclusively in the form of nitrates. Nitrates can also be formed from NO, but require stronger acid-base pairs such as Lewis sites formed by highly coordinatively unsaturated Ti^{4+} at defect sites. Own IR adsorption experiments with NO (10 mbar) and NO_2 (237 ppm) on the TiO_2 studied show that the nitrate deformation bands generated by NO have only 5% of the intensity of those formed from NO_2.

The presence of NO and NO_2 leads to the accumulation of isocyanates and/or isocyanic acid on the TiO_2 surface, which increase in concentration under the experimental conditions used to the extent that also the formation of smaller quantities of cyanuric acid is possible (band at 2065 cm^{-1}). This indicates that accessible Ti^{4+} cations and or Ti-OH groups (blocked and removed by nitrate formation) are indispensable for hydrolysis. Blocking these sites, however, seems to leave still sufficient sites for HNCO to adsorb molecularly or weakly bound. Alternatively, we would like to suggest that the chemisorption of nitrogen oxides makes the surface less basic and may impede the interaction of the carbon atom in the NCO^- group with neighboring lattice oxygen. This would retard the N-C bond cleavage and could allow the reactive addition of further HNCO molecules to surface NCO^- groups.

3.6 Conclusions

TiO$_2$ is a very efficient catalyst for the hydrolysis of HNCO to NH$_3$ and CO$_2$.Over a broad temperature range, i.e., above 150°C, the hydrolysis of HNCO on TiO$_2$ is controlled by external mass-transfer under the experimental conditions used in this study as well as in all other reports in the literature [5,15]. This is evidenced by the low temperature dependence expressed by the apparent activation energy of 10 ± 5 kJ/mol. However, at low temperatures, i.e., 110 − 130°C the evaluation of the surface reaction controlled kinetics was possible using a two channel monolithic structure at high areal velocities. The apparent energy of activation of 73 kJ/mol determined indicates a substantial barrier in the rate determining step. In the absence of water isocyanic acid adsorbs preferentially in dissociative form generating OH groups or water and Ti-NCO groups. At longer time of exposure the formation of cyanuric acid occurs indicating that some of the isocyanic acid molecules do not dissociate and are able to be added to NCO$^-$ groups. In the presence of water the hydrolysis dominates the surface chemistry so that only the more basic product, ammonia, and the reactant, water, are directly observed by IR spectroscopy.

In the presence of additional NO, NH$_3$ and NO$_2$ in the reactant gas stream the reaction rate decreases, when the catalyst is in the surface reaction rate controlled regime. While the overall impact increased in the sequence NO < NH$_3$ < NO$_2$, the impact on the surface chemistry differs markedly between the presence of the product ammonia and the nitrogen oxides. While ammonia had little impact on the surface concentrations measured during hydrolysis (note that under the experimental conditions chosen the conversions were high), the presence of NO and NO$_2$ led to the accumulation of NCO$^-$ on TiO$_2$. Notably with NO$_2$ the surface is quickly covered with nitrates, while the accumulation of NCO$^-$ and the eventual formation of cyanuric acid are much slower. This suggests that nitrates block the sites catalytically active for hydrolysis and retard so the conversion of isocyanic acid. The present data do not allow concluding whether or not HNCO is converted *via* an alternative reaction pathway under such conditions.

3.7 Acknowledgements

3.8 References

[1]   H.P. Lenz, S. Prüller, Emissionen und Immissionen von Abgaskomponenten, Fortschritt-Berichte VDI, Reihe 12, Nr. 528, VDI-Verlag, Düsseldorf, 2003, 16.

[2]   P. Forzatti, Appl. Catal. A 222 (2001) 221.

[3]   H.L. Fang, H.F.M. DaCosta, Appl. Catal. B: Environmental 46 (2003) 18.

[4]   G. Busca, L. Lietti, G. Ramis, F. Berti, Appl. Catal. B: Environmental 18 (1998) 1.

[5]   M. Kleemann, M. Elsener, M. Koebel, A. Wokaun, Ind. Eng. Chem. Res. 39 (2000) 4120.

[6]   http://www.acea.be, Position Papers, 30/06/2003.

[7]   M. Koebel, E.O. Strutz, Ind. Eng. Chem. Res. 42 (2003) 2093.

[8]   M. Koebel, M. Elsener, O. Kröcher, C. Schär, R. Röthlisberger, F. Jaussi, M. Mangold, Top. Catal. 30/31 (2004) 43.

[9]   E. Jacob, A. Döring, From the SCR catalyst to the Controlled Diesel Catalyst (GD-KAT), Tagungsband VDA Technischer Kongress in Wolfsburg, April 2003, 163.

[10]   P.M. Schaber, J. Colson, S. Higgins, E. Dietz, D. Thielen, B. Anspach, J. Brauer, Am. Lab. 13 (1999) 13.

[11]   J.A. Lercher, Z. Zhan, Eur. Pat. Appl. 94113599 (1995).

[12]   Z. Zhan, Catalytic synthesis and conversion of melamine and its analogues, PhD Thesis, University of Twente, Netherlands (1995).

[13]   P.L.T. Gabrielsson, Top. Catal. 28 (2004) 177.

[14]   G. Mirth, F. Eder, J.A. Lercher, Appl. Spectrosc. 48 (1994) 194.

[15]   E. Tronconi, A. Beretta, Catal. Today 52 (1999) 249.

[16]   J.A. Lercher, Z. Phys. Chem. Neue Folge 118 (1979) 209.

[17]   F. Solymosi, T. Bánsági, J. Phys. Chem. 83 (1979) 552.

[18]   G. Busca, H. Saussey, O. Saur, J.C. Lavalley, V. Lorenzelli, Appl. Catal. 14 (1985) 245.

[19]   M.A. Larrubia, G. Ramis, G. Busca, Appl. Catal. B: Environmental 30 (2001) 101.

[20]   M. Waqif, J. Bachelier, O. Saur, J.C. Lavalley, J. Mol. Catal. 72 (1992) 127.

[21]   O. Saur, M. Bensitel, A.B. Mohammed Saad, J.C. Lavalley, C.P. Tripp, B.A. Morrow, J. Catal. 99 (1986) 104.

[22]   G. Ramis, G. Busca, V. Lorenzelli, P. Forzatti, Appl. Catal. 64 (1990) 243.

[23]   K. Hadjiivanov, Catal. Rev. Sci. Eng. 42 (2000) 71.

[24]   K. Hadjiivanov, H. Knözinger, Phys. Chem. Chem. Phys. 2 (2000) 2803.

[25]   B.I. Mosqueda-Jiménez, A. Jentys, K. Seshan, J.A. Lercher, Appl. Catal. B: Environmental 46 (2003) 189.

[26]   C. Sedlmair, B. Gil, K. Seshan, A. Jentys, J.A. Lercher, Phys. Chem. Chem. Phys. 5 (2003) 1897.

Chapter 4

4   KINETICS AND TRANSPORT PHENOMENA OF THE HYDROLYSIS OF ISOCYANIC ACID ON ANATASE

4.1 Abstract

More stringent NO_x and particulate emission limits for commercial vehicles have revived the so-called **selective catalytic reduction (SCR)** for application in mobile sources. The technology with urea as reducing agent constitutes the most promising strategy up to now and closest to start of production in order to reduce considerably the content of nitrogen oxides in Diesel exhaust gas. The conversion of urea into ammonia and carbon dioxide consists of two consecutive reactions, in which isocyanic acid is an intermediate that is hydrolyzed over TiO_2 anatase. With a novel design of flat bed reactor simulating a two channel monolithic structure, differential reaction conditions were achieved. The orders of reaction with respect to both reactants and products were explored experimentally. The isocyanic acid shows a pseudo first-order behavior within a limited concentration range, the partial order with respect to water was 0.33. Concerning the hydrolysis products, ammonia has an inhibiting effect, the determined order was -0.70. In contrast carbon dioxide did not influence the rate of reaction. Under the given experimental conditions, i.e. at relatively high volumetric gas flows in the first instance, the rate of hydrolysis is not limited by gas to solid diffusive transport, but limited by intraporous diffusion. Thus, for automotive exhaust gas after-treatment the increase of the coating thickness is limited by the diffusional resistence.

4.2 Introduction

Approximately 20% of the global anthropogenic nitrogen oxide emissions originate from passenger cars and commercial vehicles [1]. In order to reduce the emissions, increasingly rigid emission standards are introduced, which require exhaust gas after-treatment of diesel engines. Today, the selective catalytic reduction (SCR) with ammonia is the most promising technique for reducing NO_x emissions from heavy-duty diesel trucks and bus engines [2- 5]. In consequence, the European Automobile
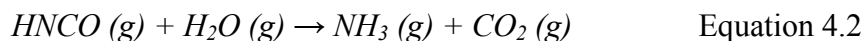
Manufacturers Association decided to recommend urea as the precursor for the reducing agent ammonia. In contrast to ammonia, urea is non-toxic and does not require sophisticated safety precautions for handling and storage [5,6]. For most applications an aqueous urea solution (AdBlue®, i.e. a solution of 32.5% urea in H_2O) is injected into the hot exhaust gas stream. To be successful and robust, this approach requires detailed knowledge of the kinetics of the transformation of urea into ammonia [7].

Induced by the spatial constraints of the car, catalyst volume is aimed to be minimal. However, this is met with great difficulties, as the dynamically varying loads of the engine drastically affect the reaction conditions for the catalyst [8].

The practical conversion of the aqueous urea solution to ammonia consists of two steps. In the first step, the aqueous urea solution is sprayed into the flue gas stream. After evaporation of H_2O, the remaining urea melts and decomposes thermally into ammonia and isocyanic acid according to Equation 4.1.

$$H_2N\text{-}CO\text{-}NH_2 \ (s) \rightarrow NH_3 \ (g) + HNCO \ (g) \qquad \text{Equation 4.1}$$

In the second step, the isocyanic acid is hydrolyzed on an oxide catalyst yielding a second molecule of ammonia and carbon dioxide according to Equation 4.2.

$$HNCO \ (g) + H_2O \ (g) \rightarrow NH_3 \ (g) + CO_2 \ (g) \qquad \text{Equation 4.2}$$

Several engineering design variants have been proposed suggesting in essence reactors that are incorporated into the exhaust system or are built as separate units [7,9]. It should be noted, however, that isocyanic acid also undergoes a series of condensation reactions leading to a variety of solids ranging from cyanuric acid and biuret over ammelide and ammeline and melamine to polymeric forms of melamine [3,7,10]. These latter high molecular weight compounds have been reported to deposit on the walls of the exhaust pipe and inside the monolith channels and are only slowly decomposed under the typical reaction conditions. In order to minimize the formation of such polymeric species, the reaction conditions and the catalysts have to be adapted in order to maximize hydrolysis and to minimize condensation/ oligomerization of isocyanic acid.

The work presented here focuses on the HNCO hydrolysis with water on TiO_2 anatase, a most promising material catalyzing hydrolysis reactions. The individual

orders of reaction with respect to the reactants and products are determined in a novel type of flat bed reactor under differential conditions. Furthermore, we address external and internal mass transport processes at a two-channel monolithic structure.

4.3 Experimental

4.3.1 Catalysts

The hydrolysis catalyst (TiO_2 anatase from Süd-Chemie AG) was applied on a metal substrate by impregnation. Rheology modifiers and binders (inorganic sols) were added to enhance the mechanical stability of the coating and to increase the adhesive strength to the metal foil, respectively. The specific surface area of the catalyst is 80 m^2/g (BET method).

4.3.2 Preparation of isocyanic acid

The synthesis of isocyanic acid was carried out by depolymerization of commercial cyanuric acid according to the method developed by Lercher and Zhan [11]. A heated quartz tubular reactor (18 mm ID) separated into three sections was used. The first section of the reactor was filled with quartz spheres to preheat the He carrier gas stream. The second part of the reactor contained 15 g of cyanuric acid (sublimation temperature 320 – 330°C) and the third section of the reactor held the Al_2O_3 catalyst bed used to depolymerize cyanuric acid. With the use of the catalyst, the decomposition temperature of cyanuric acid could be lowered to T = 370°C which results in superior product purity. Downstream of the reactor, the gaseous product was condensed in two serial cold traps at -80°C (isopropanol/dry ice). The method produced high purity HNCO with the final product containing less than 1 vol.% NH_3 without CO_2 being present. However, during start-up of the reaction hydrolysis on surface OH groups of the catalyst occurs, and it is essential to bypass the cold traps to avoid condensation of NH_3 and CO_2 into the product [12]. Depolymerization must be performed in the absence of water, as Al_2O_3 not only catalyzes the depolymerization but also the hydrolysis of HNCO.

4.3.3 Kinetic measurements

The experimental setup used for the kinetic experiments is shown in Figure 4.1. The composition of the feed gas was chosen to present a typical diesel exhaust gas, containing 4% H_2O and 10% O_2 with N_2 being the balancing gas [5,13]. The gas flow rates were controlled using electronic mass flow controllers, and water was dosed through a fused silica capillary (0.1 mm ID) into the electrically heated heating block by means of a HPLC pump. HNCO was introduced into the system *via* an additional N_2 stream and a saturator, which was maintained at -30°C; the standard concentration of HNCO was 500 ppm.
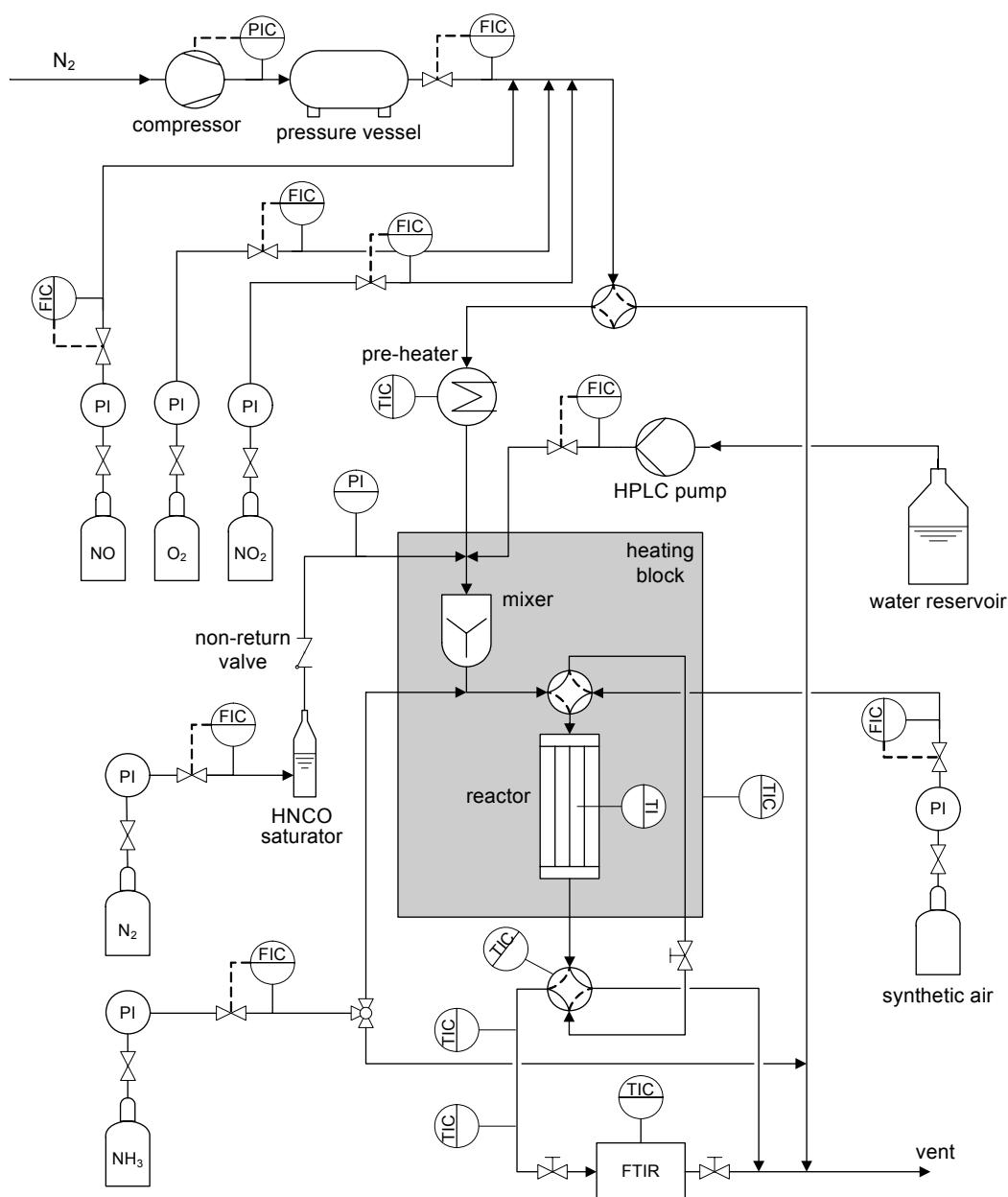
Figure 4.1 Flow scheme of the reaction system.

The rate of the HNCO hydrolysis was determined using the active material coated onto a metal sheet to resemble the material in the technical application. The reactor was built from stainless steel with a rectangular cross section of dimensions 3.5×2 mm (width $\times$ height) or 7.5×2 mm in the case of experiments addressed to film diffusion (Figure 4.2), respectively. The catalyst was tested as a single coated metal sheet of 10 or 20 mm length and a thickness of 110 μm, simulating a two channel monolithic structure with a cell density of 185 cpsi (86 cpsi for experiments addressed to film diffusion). The mass of active material exposed to the gas stream was between 1.75 and 7.5 mg (calculated from the layer thickness and the packing density of the TiO_2 coating) dependent on the applied metal sheet. The total flow rate was typically 3.6 l_N/min, and the geometric surface area of the catalyst was between 70 and 300 mm^2. A thermocouple was incorporated in the reactor block for a direct measurement of the catalyst temperature. As the catalytic material employed was highly active, these very short residence times (areal velocity AV = volumetric flow rate/catalyst geometric surface area $\approx$ 3100 m_N/h) were necessary to reach differential reaction conditions (equivalent to conversion $X_{HNCO} \leq 10\%$).
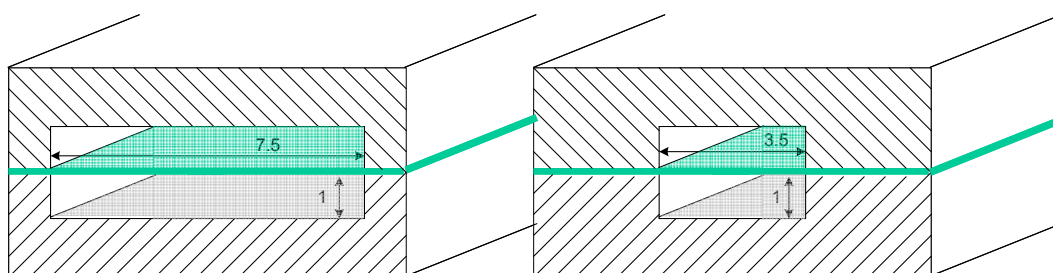

Figure 4.2 Design of flat bed reactor with two different internals simulating a two channel monolithic structure.

The gas composition was continuously analyzed by a FTIR spectrometer (Thermo Electron Corporation Nexus, OMNIC QuantPad software) equipped with a heated, low volume multiple-path gas cell (2 m). The tubes connecting the reactor outlet and the gas cell in the IR spectrometer as well as the gas cell itself were heated to 185°C in order to prevent condensation/polymerization of HNCO at cold spots. The quantification method developed allowed to monitor concentrations in the ppm range of 25 compounds in total, including HNCO. Results were independent of the batch of synthesized HNCO and the mass balances based on carbon and nitrogen were better than 99%.

4.4 Results and Discussion

4.4.1 Orders of reaction

Provided that the reaction of interest is irreversible and that its rate equation can be expressed by a simple power law rate expression

$$r = k \cdot c_i^m,$$

Equation 4.3

the logarithmic plot of the rate of reaction over the concentration typically yields a straight line of which the slope equals the exponent m, i.e. the order of reaction with respect to the reactant i, and of which the intersection with the ordinate equals the logarithm of the rate constant.

Applying the above given fundamentals on the hydrolysis reaction, we start from the following power law expression including the products NH_3 and CO_2

$$r = k \cdot [HNCO]^m [H_2O]^n [NH_3]^p [CO_2]^q$$

Equation 4.4

or

$$\ln r = \ln k + m \cdot \ln[HNCO] + n \cdot \ln[H_2O] + p \cdot \ln[NH_3] + q \cdot \ln[CO_2]$$

Equation 4.5

in logarithmic form, respectively. In order to experimentally determine the order of reaction with respect to HNCO, we vary its concentration while keeping all other concentrations constant. Equation 4.5 simplifies to give

$$\ln r = \ln k' + m \cdot \ln[HNCO]$$

Equation 4.6

The HNCO concentration was varied between 0 and 1000 ppm, the calculated rate was based on NH_3 formation

66

$$r = \frac{dc_i}{dt} = \frac{[NH_3] - [NH_3]_0}{\tau}.$$ Equation 4.7

The reaction temperature was 393 K in all experiments shown here in order to stay in the kinetically controlled regime, while at higher temperatures mass transfer starts to limit the reaction rate. In the temperature regime between 383 and 403 K an apparent activation energy of 73 kJ/mol was observed [14]. The rate-concentration plot is shown in Figure 4.3. Two regimes are observed, both exhibit linear dependence of the rate on the concentration. At low concentrations of HNCO the increase of the rate is more pronounced than at high concentrations. The transition appears between 200 and 250 ppm. This change in the concentration dependence is tentatively attributed to polymeric species, most probably trimer-adsorbed HNCO - cyanuric acid, on the titania surface at high concentrations suppressing the hydrolysis [15].
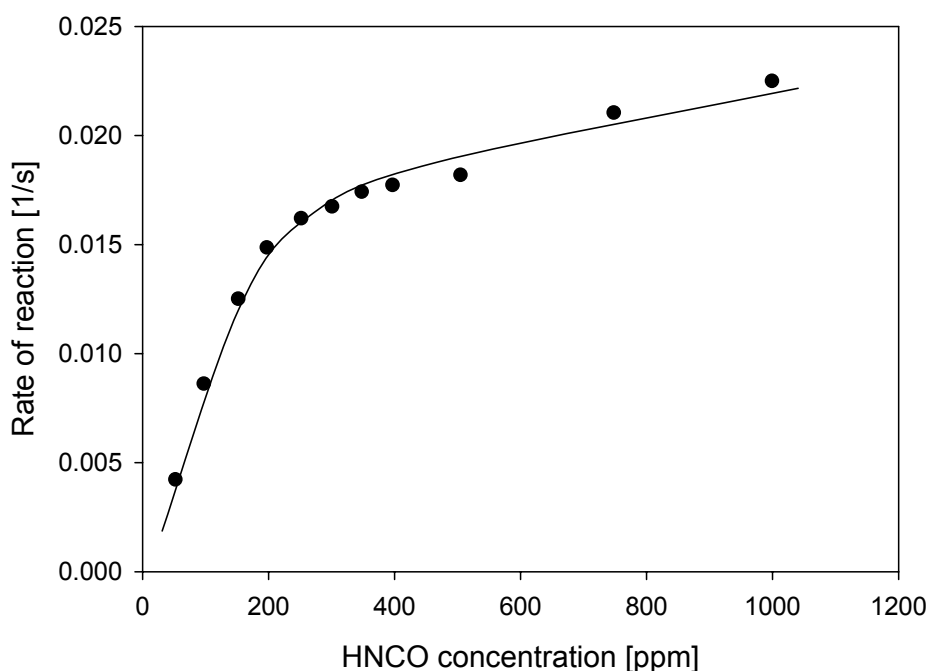

Figure 4.3 Effect of variation of HNCO concentration on rate of hydrolysis, T = 393 K, $[H_2O]_0$ = 4 vol.%.

The logarithmic plot (Figure 4.4) yields the order of reaction with respect to HNCO. In the low concentration range $[HNCO]_0 \leq$ 200 ppm the determined order of reaction is 0.95, for $[HNCO]_0 >$ 200 ppm a value of 0.24 is obtained. We ascribe this lower reaction order to the transition range to 0 order, i.e. full coverage of the titania surface

with isocyanate species, rather than to the existence of two different sites, as own IR adsorption studies confirm this theory. Often in literature in conjunction with kinetic parameter evaluation, a first order with respect to HNCO is assumed, e.g. Kleemann *et al.* [5], but has not been experimentally confirmed in an adequate manner yet.
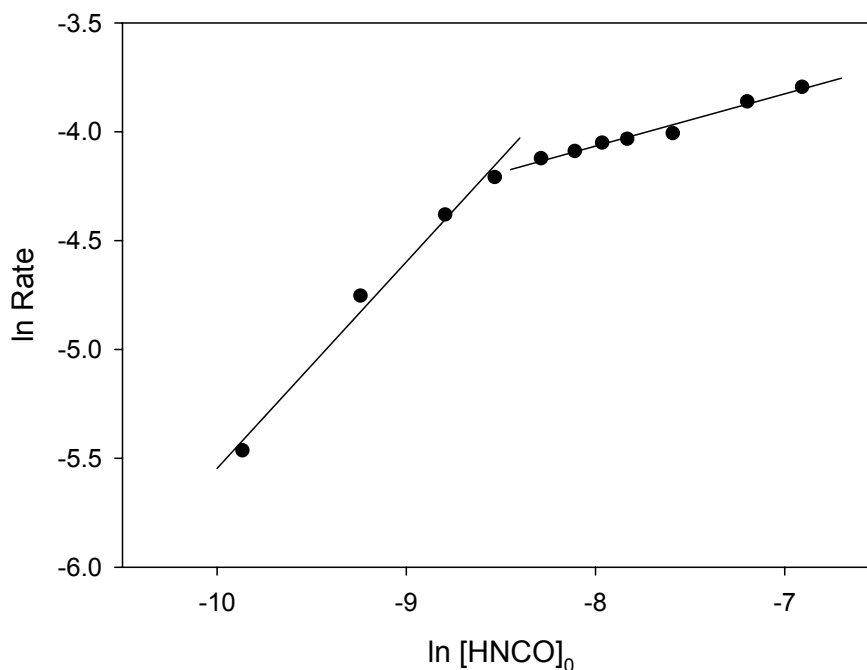

Figure 4.4 Determination of the order of reaction with respect to HNCO.

In order to determine analogously the order of reaction with respect to H_2O, the concentration of $[HNCO]_0 = 500$ ppm was kept constant while the H_2O concentration was varied between 0.2 and 10 vol.%. The hydrolysis rate increases with increasing H_2O content (see Figure 4.5). The logarithmic dependence shown in Figure 4.6 suggests an apparent reaction order in water of 0.33.
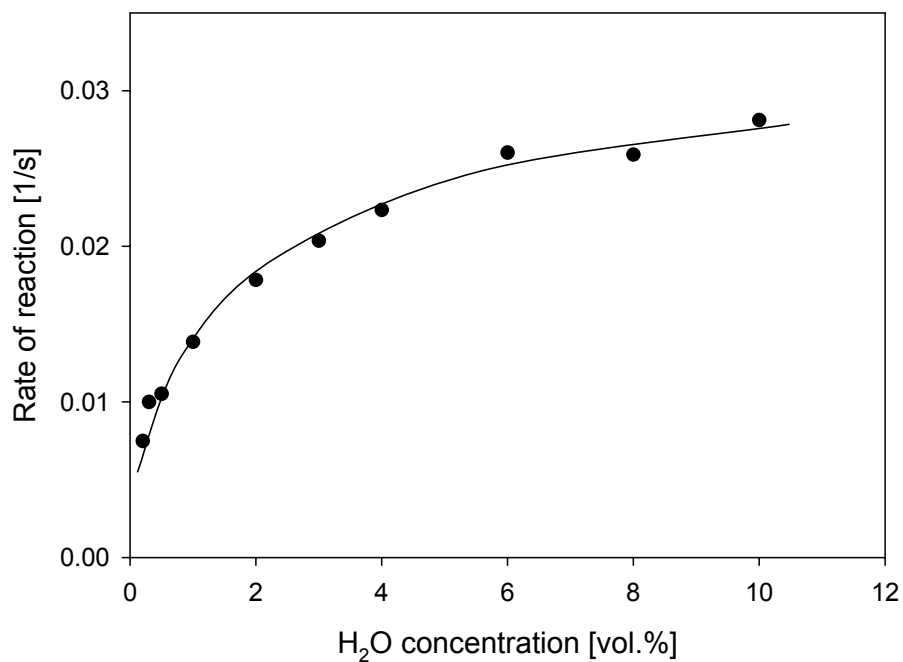
Figure 4.5 Effect of variation of H_2O concentration on rate of hydrolysis, T = 393 K, $[HNCO]_0$ = 500 ppm.
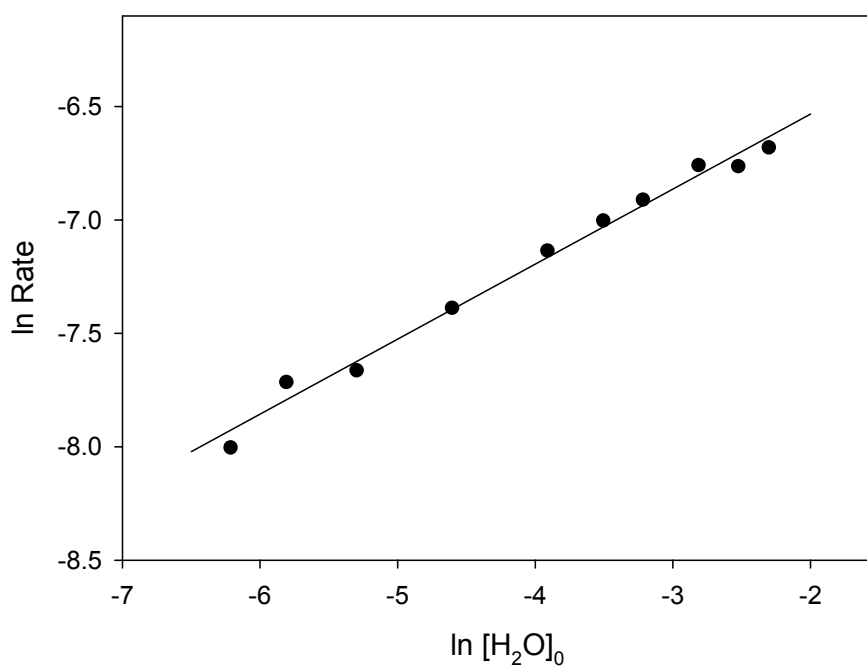

Figure 4.6 Determination of the order of reaction with respect to H_2O.

For the determination of the reaction order with respect to NH_3, its concentration was varied between 0 and 1300 ppm while keeping both the HNCO and H_2O concentration constant: $[HNCO]_0 = 500$ ppm, $[H_2O]_0 = 4$ vol.% and assuming differential reaction conditions $X_{HNCO} \leq 10\%$. The rate-concentration plot is shown in Figure 4.7. It is observed that the hydrolysis rate decreases with increasing NH_3 concentration.
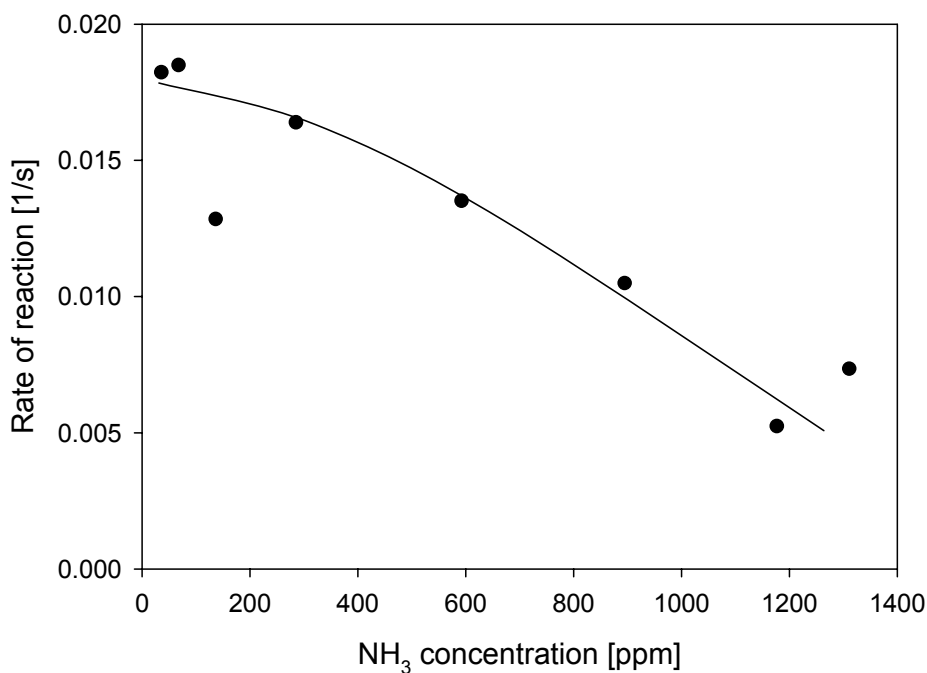

Figure 4.7 Effect of variation of NH_3 concentration on rate of hydrolysis, T = 393 K, $[HNCO]_0 = 500$ ppm, $[H_2O]_0 = 4$ vol.%.

The logarithmic plot of the data is shown in Figure 4.8. While at low partial pressures of NH_3 the reaction rate is influenced only to a minor degree by the presence of NH_3, the reaction order was -0.70 at higher pressures. The order of reaction was determined in the restricted concentration range 300 – 1200 ppm since the product inhibiting effect was most pronounced here. For $[NH_3]_0 < 300$ ppm an order of reaction of -0.057 was obtained under consideration of the measuring error.
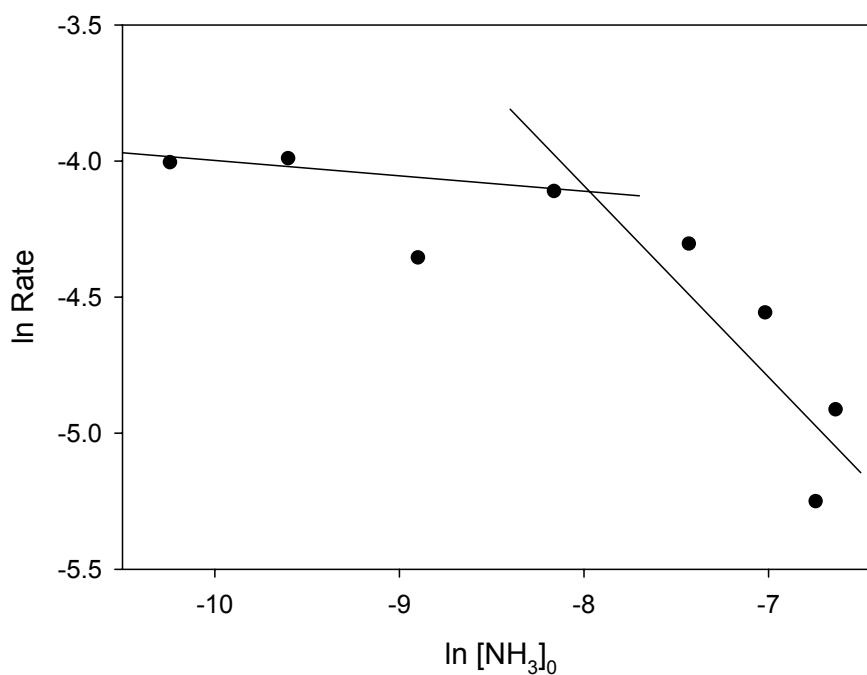
Figure 4.8 Determination of the order of reaction with respect to NH_3.

The CO_2 concentration was variied between 0 and 3 vol.% in the feed gas stream to determine the reaction order with respect to CO_2. The corresponding rate-concentration plot in Figure 4.9 shows that the rate stays constant over the entire concentration range within the limits of accuracy. Thus carbon dioxide does not influence the sorption of other molecules. A reaction order in CO_2 of 0.011 was obtained.
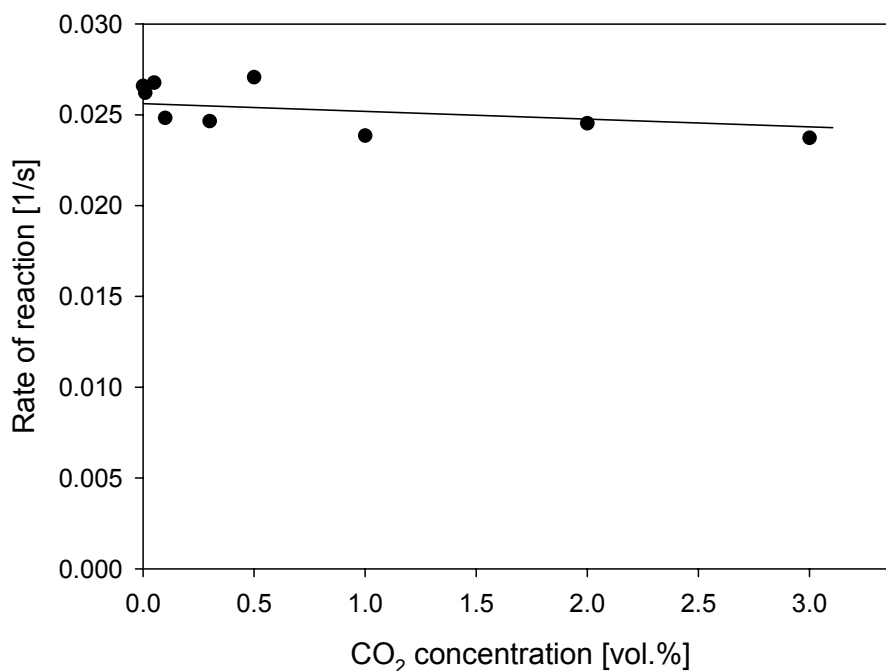
Figure 4.9 Effect of variation of CO_2 concentration on rate of hydrolysis, $T = 393$ K,
$[HNCO]_0 = 500$ ppm, $[H_2O]_0 = 4$ vol.%.

4.4.2 External mass transport

The influence of film diffusion in the vicinity of the catalyst surface was investigated experimentally by means of wash-coated metal substrates of different lengths. In these experiments it was the aim to keep the areal velocity constant while applying different catalyst lengths, i.e. the total volumetric flow was increased at the same time with the longer metal substrate.

$$AV = \frac{\dot{V}_{total}}{GSA}$$

Equation 4.8

Thus an increased linear velocity axial to the flow channel is achieved. If external diffusion limitation existed, the conversion would increase with the longer plate as the laminar boundary layer at the catalyst wall gets thinnner. Two different lengths of catalyst plates were tested, viz 1 and 2 cm. The corresponding geometric surface areas were 1.5 and 3 cm^2, respectively. The total flow range was between 0.6 and 3.7 l_N/min. The results are summarized for three different temperatures in Figure 4.10 - Figure 4.12.
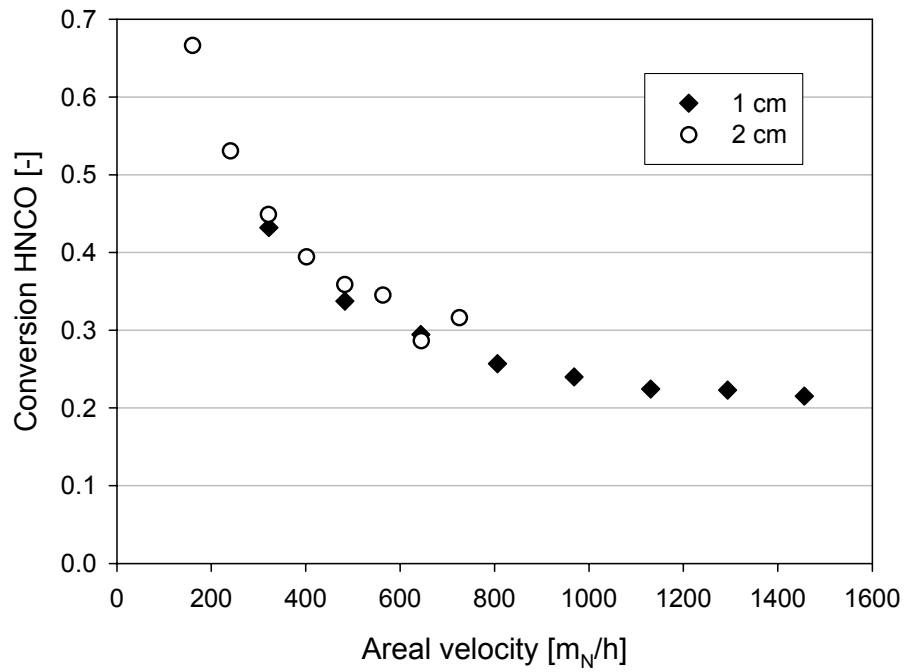
Figure 4.10 Effect of catalyst bed length and areal velocity, T = 200°C.

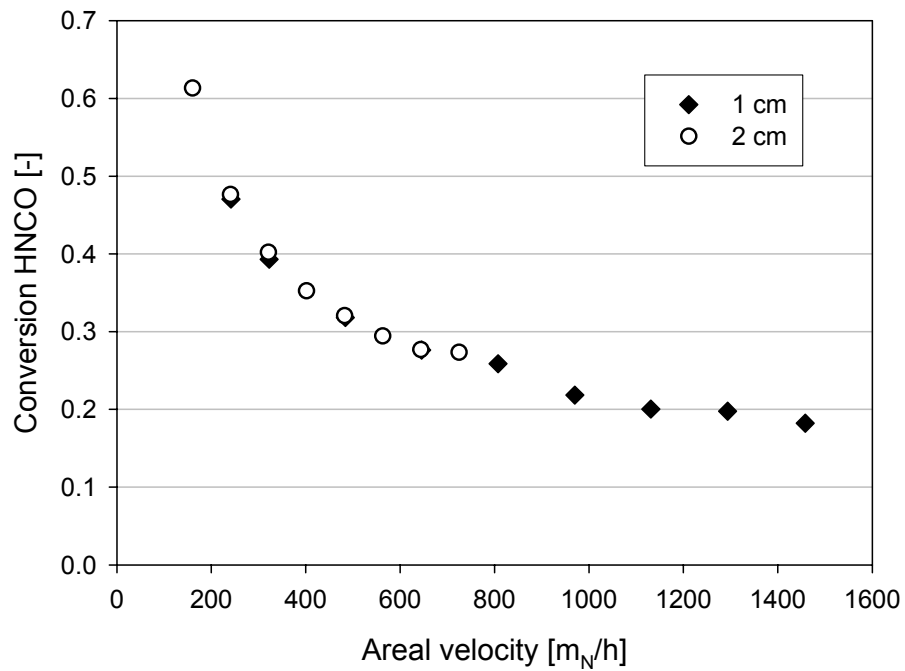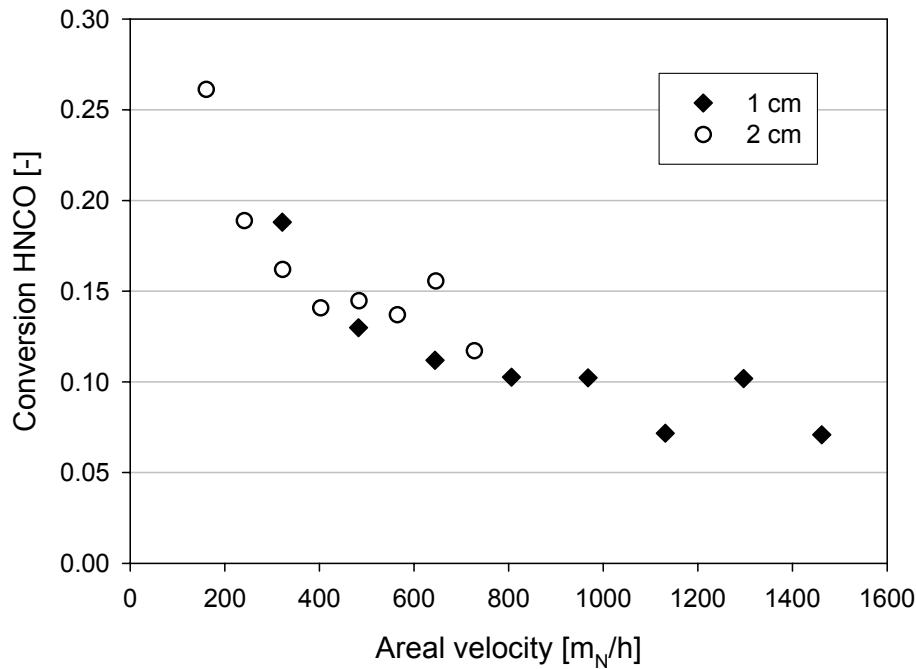**Figure 4.11** Effect of catalyst bed length and areal velocity, T = 160°C.

Figure 4.12 Effect of catalyst bed length and areal velocity, T = 120°C.

For the investigated temperatures it is observed that the achievable conversions are similar with the long and the short catalyst plate (in the range of the measuring error). The results clearly suggest that under the given reaction conditions, i.e. at relatively high areal velocity and within the temperature range 120 – 200°C, diffusion of the reactant molecules to and from the catalytic surface does not play a role and therefore the rate of external diffusion must be higher than the intrinsic reaction rate. The non-appearance of mass transport limitation here is tentatively attributed to the disordered non-laminar flow at the catalyst inlet, which originates from displacement of the streamlines at the edge of the coated metal plate (compare Figure 4.2).

Tronconi *et al.* [16-18] have stated that monolithic catalysts in industrial SCR-DeNO$_x$ applications typically run both under internal and external mass transport limitation. Data confirming the existence of film diffusion limitation is available as well as the contrary, the critical parameters in this regard are the magnitude of the applied areal velocity and the channel hydraulic diameter.

4.4.3 Internal mass transport

In the following results are shown, which demonstrate the influence of internal diffusion within the pore structure of the applied catalysts. For determining the intrinsic kinetics of the hydrolysis reaction this influence has to be eliminated. In case of a fixed bed of catalyst typically particles with sufficiently small diameter d_p are used as the first measure to achieve this. In the application described herein where a planar coated metal plate is clamped in a type of enclosing cassette simulating a two channel monolithic structure, the smaller particle diameter corresponds to a lower coating thickness.

The catalyst samples were prepared as described in Section 4.3.1 - by impregnation of the TiO_2-based wash-coat suspension on the metal substrates. Different coating thicknesses were realized on purpose. The ratio of active component to binder was kept constant irrespective of the coating thickness.

It was the objective of this set of experiments to determine the threshold from which further increase of the coating thickness would no longer result in higher HNCO conversions.

The prepared catalyst plates were analyzed by scanning electron microscopy (SEM) in order to (i) determine the coating thickness and to (ii) assess the homogeneity of the impregnation procedure. Figure 4.13 and Figure 4.14 show the metal plate with the least amount of wash-coat applied. The coating thickness here is approximately 13 μm (average value calculated over different positions), and a planar and highly homogeneous surface is found from Figure 4.14.
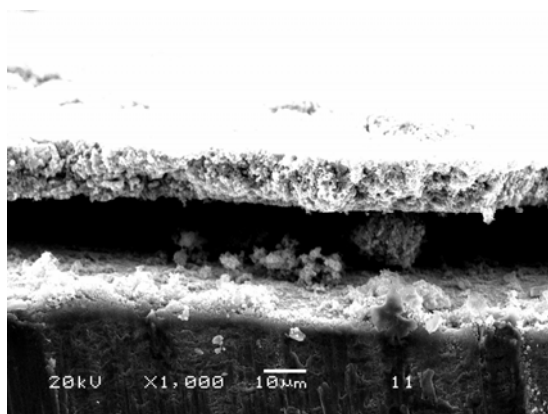

Figure 4.13 SEM picture 1 of catalyst #1 with thin coating thickness.

Figure 4.14 SEM picture 2 of catalyst #1 with thin coating thickness.

Figure 4.15 and Figure 4.16 both show catalyst #2, where the amount of TiO_2 wash-coat has been increased yielding an averaged coating thickness of 35 μm.
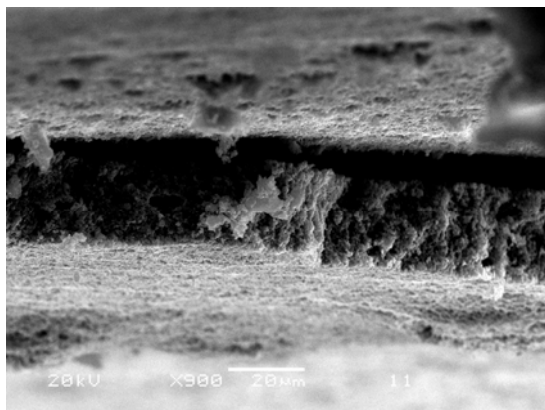

Figure 4.15 SEM picture 1 of catalyst #2 with middle coating thickness.
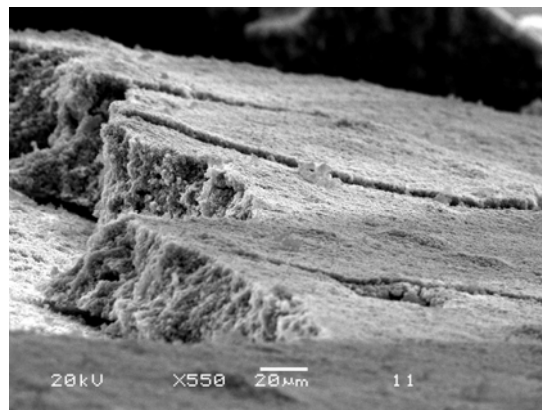
Figure 4.16 SEM picture 2 of catalyst #2 with middle coating thickness.

At catalyst #3 the applied wash-coat was maximized, further increase of the coating thickness resulted in flaking of the coating. Figure 4.17 and Figure 4.18 are evidence for the fact that the surface has become rougher and strongly fissured in comparison with catalysts #1 and #2, respectively. The coating thickness determined was 53 μm.
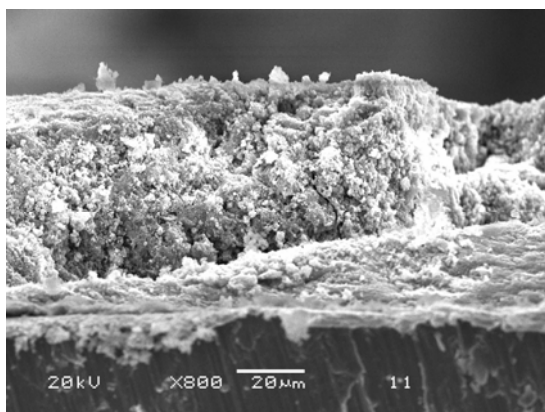
Figure 4.17 SEM picture 1 of catalyst #3 with thick coating thickness.

Figure 4.18 SEM picture 2 of catalyst #3 with thick coating thickness.

The performances of the different catalyst samples #1 - 3 are illustrated in Figure 4.19. It should be pointed out that the reaction conditions were identical in all experiments: $[HNCO]_0$ = 500 ppm, $[H_2O]_0$ = 4 vol.%, $[O_2]$ = 10 vol.%, temperature range 120 – 380°C, areal velocity 3100 m_N/h.
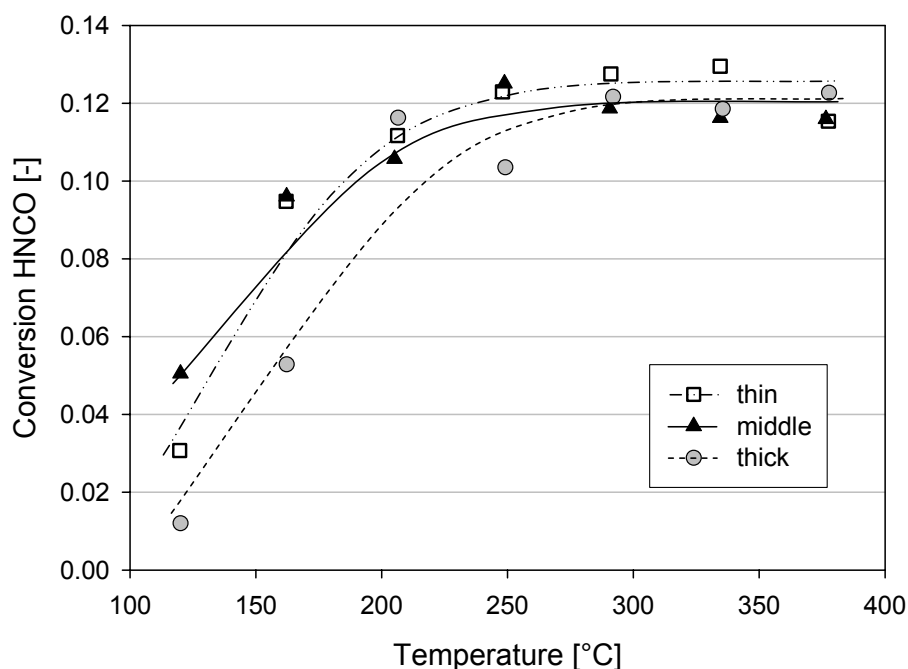
Figure 4.19 Influence of coating thickness on HNCO conversion.

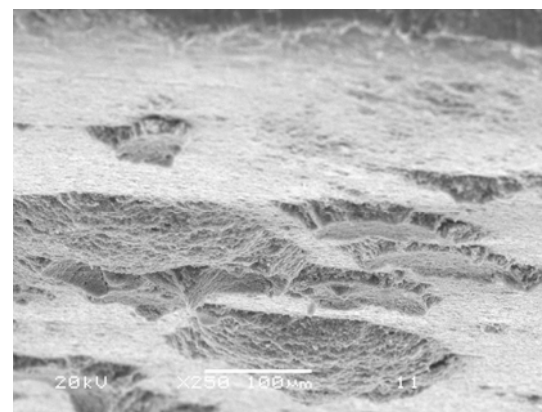The conversion is similar at the thin and the middle coated catalyst sample, it is between 3.5 and 12.7% in the investigated temperature range. The catalyst plate with the thick coating surprisingly shows a marginally lower activity, here only 1.7 to 12.0% of the HNCO feed are converted. Actually one would expect that the three plates should show the same activity if mass transfer limitation was present. We tentatively attribute the observed behavior to the increased probability of consecutive reactions of HNCO to polymeric products at the thick-coated plate due to the increased residence time. Because of the higher mass of active material applied here, the HNCO adsorption capacity and consequently also the storage capacity is increased. Especially at low temperatures where the hydrolysis activity is low the increased residence time of HNCO molecules in the catalyst pores is a byword for longer diffusion pathways. Those lead to the occurrence of undesired side reactions – predominantly the trimerization of HNCO to form solid cyanuric acid – and thus to blockage of the catalytically active sites for hydrolysis.

Moreover, an interesting observation when comparing the thin- with the middle-coated plate is that the middle coating shows higher conversion at low temperatures (T < 165°C) while for temperatures above 165°C this effect levels off. This is according to expectations as here mass transport limitation obviously kicks off at a certain

temperature level. The difference in the low temperature range is primarily due to the different amounts of catalytically active material present.

Efforts with respect to catalyst development could be more profitable if they are aimed at optimization of the monolith pore size distribution. Thus the catalyst utilization can be enhanced, rather than increasing the intrinsic activity, which is not the limiting factor under industrial conditions.

4.5 Conclusions

The kinetics of the HNCO hydrolysis were investigated by means of a novel type of flat bed reactor simulating a two-channel monolithic structure, which afforded differential reaction conditions. Educt as well as product partial pressures were varied individually in the feed gas mixture in order to determine the respective orders of reaction. Variation of the HNCO concentration confirmed a first order dependence while water showed an order of reaction of 0.33. NH_3 revealed a product inhibiting effect proven by the partial order of -0.70. Excess CO_2 in the feed gas up to 3 vol.% did not show any impact on the reaction rate.

It has been demonstrated by standard reaction engineering experimentation that under the investigated conditions – i.e. at relatively high areal velocity and within the investigated temperature range - the hydrolysis of HNCO is not limited by external mass transport.

In contrast, studies on the internal mass transport within the oxidic coating showed that in case of wash-coated metal substrates the coating thickness will be only rewarding up to a defined maximum value. If the coating thickness exceeds this threshold the enhanced adsorption capacity is not beneficial to activity anymore, but leads to a sub-optimal residence time of the HNCO in the pore structure. The result is the formation of undesired polymeric species blocking the active sites for hydrolysis.

4.6 Acknowledgements

4.7 References

[1]   H.P. Lenz, S. Prüller, Emissionen und Immissionen von Abgaskomponenten, Fortschritt-Berichte VDI, Reihe 12, Nr. 528, VDI-Verlag, Düsseldorf, 2003, 16.

[2]   P. Forzatti, Appl. Catal. A 222 (2001) 221.

[3]   H.L. Fang, H.F.M. DaCosta, Appl. Catal. B: Environmental 46 (2003) 18.

[4]   G. Busca, L. Lietti, G. Ramis, F. Berti, Appl. Catal. B: Environmental 18 (1998) 1.

[5]   M. Kleemann, M. Elsener, M. Koebel, A. Wokaun, Ind. Eng. Chem. Res. 39 (2000) 4120.

[6]   http://www.acea.be, Position Papers, 30/06/2003.

[7]   M. Koebel, E.O. Strutz, Ind. Eng. Chem. Res. 42 (2003) 2093.

[8]   M. Koebel, M. Elsener, O. Kröcher, C. Schär, R. Röthlisberger, F. Jaussi, M. Mangold, Top. Catal. 30/31 (2004) 43.

[9]   E. Jacob, A. Döring, From the SCR catalyst to the Controlled Diesel Catalyst (GD-KAT), Tagungsband VDA Technischer Kongress in Wolfsburg, April 2003, 163.

[10]   P.M. Schaber, J. Colson, S. Higgins, E. Dietz, D. Thielen, B. Anspach, J. Brauer, Am. Lab. 13 (1999) 13.

[11]   J.A. Lercher, Z. Zhan, Eur. Pat. Appl. 94113599 (1995).

[12]   Z. Zhan, Catalytic synthesis and conversion of melamine and its analogues, PhD Thesis, University of Twente, Netherlands (1995).

[13]   P.L.T. Gabrielsson, Top. Catal. 28 (2004) 177.

[14]   P. Hauck, A. Jentys, J.A. Lercher, Appl. Catal. B: Environmental 70 (2007) 91.

[15]   P. Hauck, A. Jentys, J.A. Lercher, Catal. Today, submitted for publication.

[16]   E. Tronconi, P. Forzatti, J.P. Gomez Martin, S. Malloggi, Chem. Eng. Sci. 47 (1992) 2401.

[17]   E. Tronconi, Catal. Today 34 (1997) 421.

[18]   E. Tronconi, A. Beretta, Catal. Today 52 (1999) 249.

Chapter 5

5 ON THE QUANTITATIVE ASPECTS OF HYDROLYSIS OF ISOCYANIC ACID ON TIO$_2$

5.1 Abstract

The selective catalytic reduction with aqueous solutions of urea is currently seen having the highest potential to reduce NO$_x$ and particulate emissions for commercial diesel powered vehicles. Ammonia as the actual reduction medium is formed from urea in two consecutive reactions, i.e., *via* the thermolysis of urea to isocyanic acid and NH$_3$ and the catalyzed hydrolysis of HNCO over TiO$_2$ to NH$_3$ and CO$_2$. A kinetic model for the hydrolysis reaction was derived for a reaction scheme comprising a set of elementary steps. To minimize the number of unknown variables in the kinetic model for the overall rate, the equilibrium constants for both reactants (HNCO and H$_2$O) and products (NH$_3$ and CO$_2$) were determined from adsorption isotherms using Langmuir and multilayer adsorption models. A data set consisting of 49 data points for the rate determined at varying reactant concentrations was fitted with the kinetic model using a non-linear least mean squares regression analysis.

5.2 Introduction

Approximately 20% of the current global anthropogenic nitrogen oxide emissions originate from passenger cars and commercial vehicles [1], and it is foreseen that the increasingly rigid emission standards for NO$_x$ being introduced by European and US legislation over the next years can only be fulfilled by exhaust gas after-treatment technology. Today, the selective catalytic reduction (SCR) with ammonia is considered as the most promising technique for reducing NO$_x$ emissions from heavy-duty diesel engines [2-5]. However, the use of gaseous NH$_3$ requires elaborate safety precautions for handling and storage. Therefore, the European Automobile Manufacturers Association decided to recommend urea for the on-board production of the reducing agent NH$_3$ [6]. At present in most applications an aqueous urea solution (AdBlue®, i.e. a solution of 32.5% urea in H$_2$O) is injected into the exhaust gas stream.

Resulting from the typical spatial constraints of cars, the catalyst volume is aimed to be minimal. However, this is met with difficulties, as the dynamically varying loads of the engine drastically affect the reaction conditions for the catalyst [7]. To avoid overdosing and consequently the release of NH_3 under dynamic conditions a complex strategy is required. Several engineering design variants have been proposed suggesting urea decomposition reactors that are incorporated into the exhaust system or are built as separate units [8,9]. The most effective design introduced so far is an external monolithic hydrolysis catalyst heated by a partial stream of the exhaust gas. For a further optimization of the hydrolysis process a detailed knowledge of the kinetics of the (thermal and catalytic) transformation of urea into ammonia is essential [8].

The conversion of the aqueous urea solution to ammonia consists of two steps. In the first step, the aqueous urea solution is sprayed into the flue gas stream. After evaporation of H_2O, the remaining urea decomposes thermally into ammonia and isocyanic acid according to Equation 5.1.

$$H_2N\text{-}CO\text{-}NH_2 \; (s) \rightarrow NH_3 \; (g) + HNCO \; (g) \qquad \text{Equation 5.1}$$

In the second step, the isocyanic acid is hydrolyzed over an oxide catalyst yielding ammonia and carbon dioxide according to Equation 5.2.

$$HNCO \; (g) + H_2O \; (g) \rightarrow NH_3 \; (g) + CO_2 \; (g) \qquad \text{Equation 5.2}$$
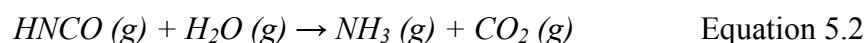
It should be noted, however, that isocyanic acid can also undergo a series of condensation reactions leading to solid products ranging from cyanuric acid and biuret over ammelide and ammeline and melamine to polymeric forms of melamine [3, 8,10]. These high molecular weight compounds have been reported [3] to deposit on the walls of the exhaust pipe and inside the monolith channels and are only slowly decomposed under the typical reaction conditions, which leads to severe catalyst deactivation. In order to minimize the formation of these polymeric species, the reaction conditions and the catalysts have to be optimized to maximize the rate of hydrolysis and to minimize condensation/oligomerization reactions of isocyanic acid.

The present chapter introduces a kinetic model for the overall rate of the HNCO hydrolysis on TiO_2 anatase, which is the well-established catalyst for hydrolysis reactions. Values for the adsorption equilibrium constants of the reactants HNCO and

water as well as of the products ammonia and carbon dioxide were determined experimentally from sorption isotherms (by IR spectroscopy and gravimetry) and implemented into the kinetic model. Thus, the sensitivity of the model was enhanced by reducing the number of unknown variables being determined.

5.3 Experimental

5.3.1 Catalyst

The hydrolysis catalyst was TiO_2 in anatase form obtained from Süd-Chemie AG and coated onto a metal substrate obtained from Emitec. Textural promoters and/or binders (inorganic sol) were added to enhance the mechanical stability of the coating and to increase the adhesive strength to the metal foil, respectively. This catalyst is a typical formulation used in heavy-duty diesel trucks in the technical application. For studying the sorption of reactants and products by IR spectroscopy TiO_2 from the same source was used in powder form. TiO_2 was synthesized following the sulfate process in which titanium slag obtained by reduction of ilmenite $FeTiO_3$ with coke at around 1200°C is treated with concentrated sulfuric acid at $100 - 180$°C [11]. The preparation process of TiO_2 is the origin of sulfate impurities observed by IR spectroscopy, which are discussed in the paper.

The specific surface area of the TiO_2 determined by the BET method was 80 m^2/g.

5.3.2 Preparation of isocyanic acid

The synthesis of isocyanic acid was carried out by the depolymerization of commercial cyanuric acid catalyzed by Al_2O_3 according to the method developed by Lercher and Zhan [12]. A heated quartz tubular reactor (18 mm ID) separated into three sections was used. The first section of the reactor was filled with quartz spheres to preheat the He carrier gas stream. The second section of the reactor contained 15 g of cyanuric acid (sublimation temperature $593 - 603$ K), and the third section of the reactor held the Al_2O_3 catalyst used to depolymerize cyanuric acid. By using a catalyst, the decomposition temperature of the cyanuric acid could be lowered to $T = 643$ K compared to 753 K for thermal decomposition, which leads to a high purity of the product (less than 1 vol.% NH_3 and less than 1000 ppm CO_2). Downstream of the reactor, the gaseous HNCO was condensed in two serial cold traps at 193 K

(isopropanol/dry ice). To obtain a CO_2 and NH_3 free product it is essential to bypass the cold traps during start-up of the reaction [13]. The depolymerization has to be performed in the absence of water, as Al_2O_3 not only catalyzes the depolymerization but also the hydrolysis of HNCO.

5.3.3 *In situ* infrared spectroscopy

Infrared spectra were measured with a Bruker IFS 88 FTIR spectrometer in a vacuum cell that allows to collect IR spectra *in situ* during activation and adsorption [14]. The spectra were recorded with a resolution of 4 cm^{-1} using a MCT detector. The catalyst samples were pressed into thin, self-supporting wafers ($\sim$ 5 $mg \cdot cm^{-2}$) and placed in a heatable sample-holder in the center of the IR cell equipped with CaF_2 windows. The samples were heated in vacuum (p < 10^{-6} mbar) to 673 K (10 $K \cdot min^{-1}$ increment). After reaching the activation temperature, O_2 with 1 mbar equilibrium pressure was introduced into the cell for 60 min in order to saturate the oxygen vacancies on the surface. The samples were subsequently cooled to 393 K in the O_2 atmosphere and evacuated. With this procedure the white color of the titania sample could be restored indicating the saturation of defect sites of TiO_2.

Ammonia, water, isocyanic acid and carbon dioxide were adsorbed at 393 K at equilibrium pressures between 10^{-4} and 10^{-1} mbar. For isocyanic acid the desorption was investigated by heating the sample from 393 K to 673 K in vacuum (10 $K \cdot min^{-1}$ increment). The surface coverage of the adsorbate was determined form the integral intensity of the characteristic IR bands.

5.3.4 Thermogravimetry

The sorption isotherm for water was additionally measured on a Setaram TG–DSC 111 thermoanalyzer. The sample ($\sim$ 20 mg) was activated at 673 K for 1 h (heating rate 10 $K \cdot min^{-1}$) under vacuum (p < 10^{-7} mbar). Water was adsorbed at 393 K using stepwise pressure increments from $3 \cdot 10^{-3}$ mbar up to 16.1 mbar, and the weight increase was measured.

5.3.5 Kinetic measurements

The experimental setup used for the kinetic experiments is shown in Figure 5.1. The composition of the feed gas was chosen to present a typical diesel exhaust gas, containing 4% H_2O and 10% O_2 with N_2 being the balancing gas [5,15]. The gas flow rates were controlled using electronic mass flow controllers, and water was dosed

through a fused silica capillary (0.1 mm ID) into the electrically heated heating block by means of a HPLC pump. HNCO was introduced into the system *via* an additional N_2 stream and a saturator, which was maintained at -30°C; the standard concentration of HNCO was 500 ppm.
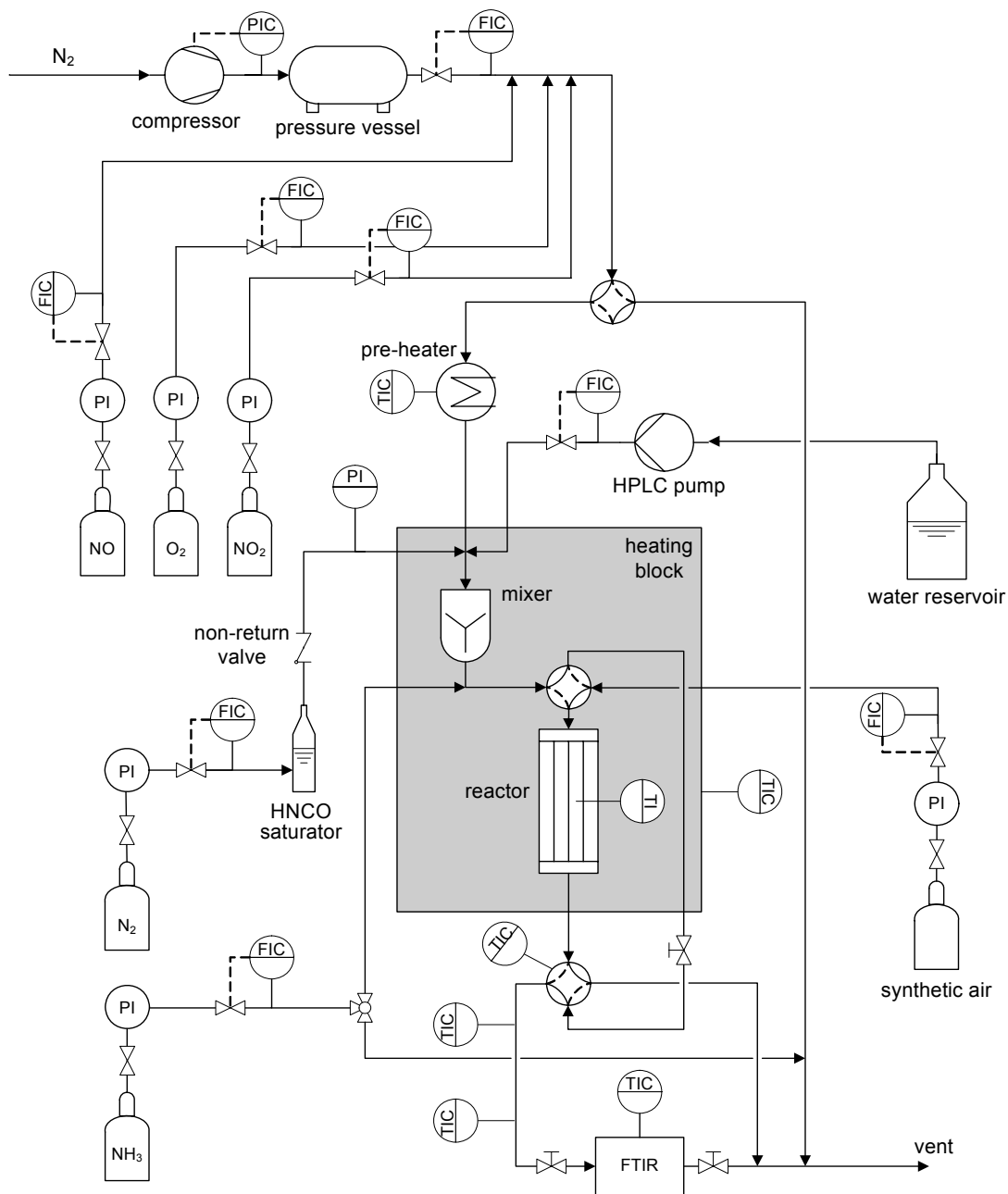

Figure 5.1 Flow scheme of the reaction system.

For the kinetic experiments aiming at the individual order of reaction, the concentration of the corresponding reactant or product, respectively, was varied over a reasonable range, and the rate was calculated.

The rate of the HNCO hydrolysis was determined using the active material coated onto a metal sheet to resemble the material in the technical application. The reactor was built from stainless steel with a rectangular cross section of dimensions 3.5×2 mm (width $\times$ height) (Figure 5.2). The catalyst was tested as a single coated metal sheet of 10 mm length and a thickness of 110 μm, simulating a two channel monolithic structure with a cell density of 185 cpsi. The mass of active material exposed to the gas stream was 1.75 mg (calculated from the layer thickness and the packing density of the TiO_2 coating). The total flow rate was typically 3.6 l_N/min, and the geometric surface area of the catalyst was 70 mm^2. A thermocouple was incorporated in the reactor block for a direct measurement of the catalyst temperature. As the catalytic material employed was highly active, these very short residence times (areal velocity AV = volumetric flow rate/catalyst geometric surface area $\approx$ 3100 m_N/h) were necessary to reach differential reaction conditions (equivalent to conversion $X_{HNCO} \leq 10\%$).
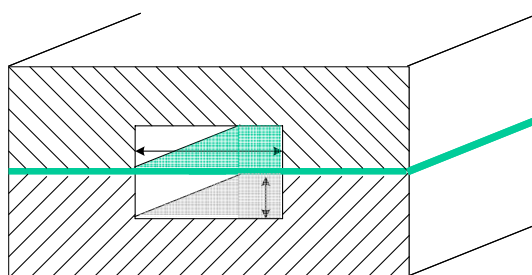
Figure 5.2 Design of flat bed reactor with internal simulating a two channel monolithic structure.

The gas composition was continuously analyzed by a FTIR spectrometer (Thermo Electron Corporation Nexus, OMNIC QuantPad software) equipped with a heated, low volume multiple-path gas cell (2 m). The tubes connecting the reactor outlet and the gas cell in the IR spectrometer as well as the gas cell itself were heated to 185°C in order to prevent condensation/polymerization of HNCO at cold spots. The quantification method developed allowed to monitor concentrations in the ppm range of 25 compounds in total, including HNCO. Results were independent of the batch of synthesized HNCO and the mass balances based on carbon and nitrogen were better than 99%.

5.4 Results and Discussion

5.4.1 Adsorption isotherms derived from IR spectroscopy

The IR spectra of the activated sample and after adsorption of NH_3 at partial pressures of $1 \cdot 10^{-3}$, $1 \cdot 10^{-2}$ and $1 \cdot 10^{-1}$ mbar are shown in Figure 5.3. Sorption of NH_3 led to a decrease of the intensity of the bands assigned to the hydroxyl groups of TiO_2 (3714 and 3666 cm^{-1}) [16,17] and to the simultaneous formation of bands at 3388, 3352, 3260, 3199 and 3160 cm^{-1}. The observed multiplet in the NH stretching region can be assigned to the asymmetric and symmetric stretching vibrations (ν_{NH}) as well as to the first overtone of the asymmetric deformation band of two chemisorbed NH_3 species [18]. An evidence for the presence of two types of Lewis sites for the sorption of NH_3 on the surface of anatase is the splitting of the symmetric deformation band (1211 and 1169 cm^{-1}) [19,20]. The asymmetric deformation band at 1605 cm^{-1} is known to be less sensitive to the strength of the coordination band and thus appears unsplit. The band at 1371 cm^{-1}, present in the activated sample (spectrum (a) in Figure 5.3) is attributed to the characteristic $\nu_{S=O}$ vibration of sulfate species [21,22], which resulted from impurities during the synthesis of the particular TiO_2 sample. Upon adsorption of NH_3 two new bands were observed at 1338 and 1314 cm^{-1} while the band at 1371 cm^{-1} disappeared, which indicates the breaking of the Ti-O-S bonds upon interaction of NH_3 with the sulfate groups and the formation of Ti-NH_2 species (similar to the adsorption of water described in the following paragraph).

Figure 5.3 IR spectra during NH_3 adsorption on TiO_2 anatase, T_{Ads} = 393 K. (a) activated sample, (b) $1 \cdot 10^{-3}$ mbar, (c) $1 \cdot 10^{-2}$ mbar and (d) $1 \cdot 10^{-1}$ mbar NH_3.

The surface coverage was calculated from the intensity of the symmetric deformation band of NH_3 at 1605 cm^{-1}, and the sorption isotherm was described with the Langmuir model (Figure 5.4):

$$\Theta_i = \frac{K_i p_i^*}{1 + K_i p_i^*}$$

Equation 5.3

in which $K_i = \dfrac{k_{i,ads}}{k_{i,des}}$ is the equilibrium constant and p_i^* the pressure normalized to standard conditions (p* = p/p$_0$ with p$_0$ = 1013.25 mbar). From the fit of the experimental data to a Langmuir isotherm K_{NH3} = $9.73 \cdot 10^5$ was determined.

Figure 5.4 Adsorption isotherm of NH_3 on TiO_2 anatase, T_{Ads} = 393 K.

The IR spectra during H_2O adsorption at pressure between $3 \cdot 10^{-4}$ and $6 \cdot 10^{-1}$ mbar are shown in Figure 5.5. In presence of water, the intensity of the hydroxyl bands (3668 and 3650 cm^{-1}) strongly increased, accompanied with the appearance of a broad band between 3500 and 3000 cm^{-1}. According to Knözinger [23], water molecules adsorb dissociatively on five-coordinate Ti^{4+} cations with the O^{2-} ions bridging two cations and form two types of surface OH groups – a monodentate terminal and another bidentate bridged hydroxyl. The band at 1616 cm^{-1} can be clearly assigned to the deformation vibrations of water *molecules* [24]. The band of the sulfate groups at 1371 cm^{-1} decreased in intensity and shifted gradually to 1348 cm^{-1}, which indicates a strong interaction with the water molecules adsorbed. Simultaneously a new band was observed at 1338 cm^{-1} as a shoulder in spectrum (d) in Figure 5.5. At the highest H_2O concentration applied ($p_{equ} = 6 \cdot 10^{-1}$ mbar) the latter band was predominant, while the band at 1348 cm^{-1} has disappeared. Saur *et al.* [22] studied this effect and postulated a change from structure II into III:
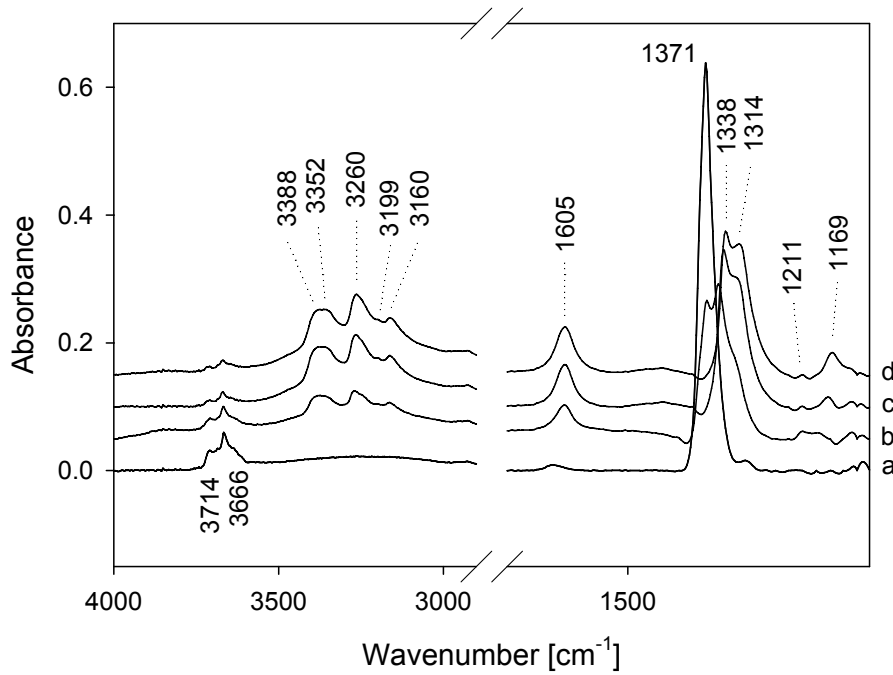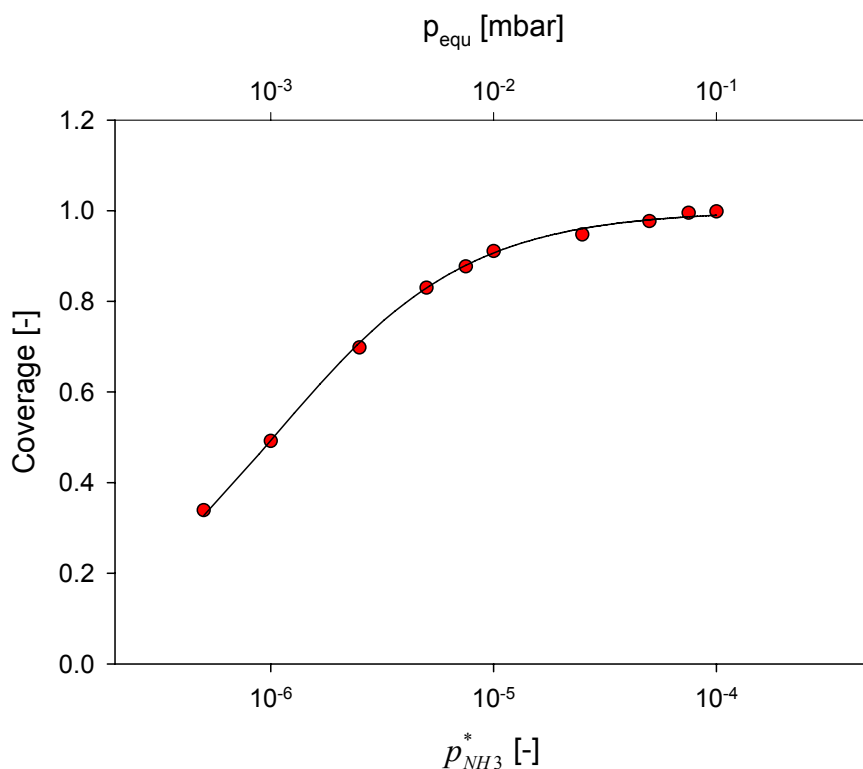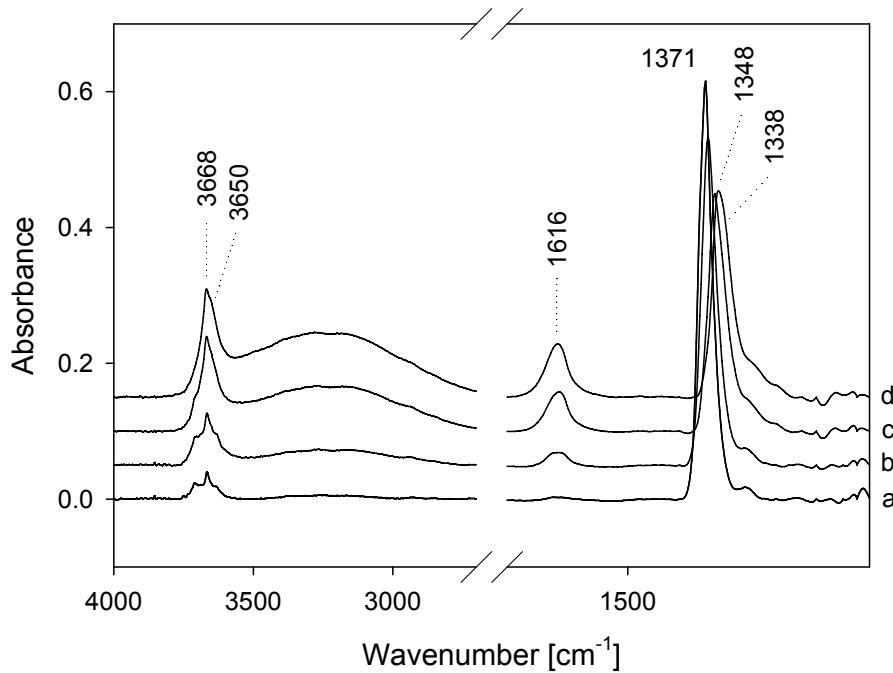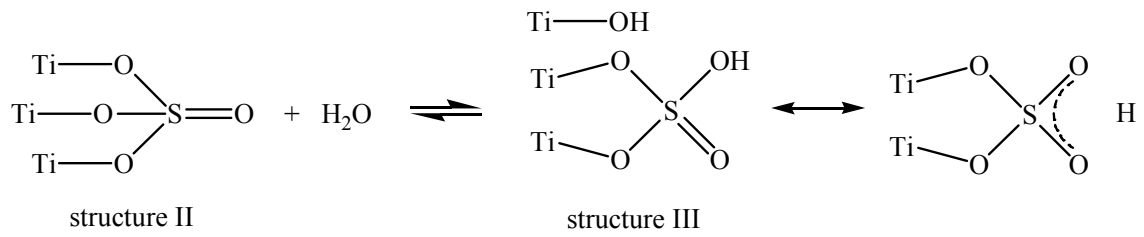
Figure 5.5 IR spectra during H_2O adsorption on TiO_2 anatase, $T_{Ads} = 393$ K. (a) activated sample, (b) $1 \cdot 10^{-3}$ mbar, (c) $1 \cdot 10^{-2}$ mbar and (d) $1 \cdot 10^{-1}$ mbar H_2O.

The sorption isotherm of H_2O was determined from the intensity of the band at $1616 \, \text{cm}^{-1}$ and described with the BET isotherm Type II [25], which is the most commonly used isotherm for multilayer adsorption:

$$\frac{V}{V_{Mono}} = \frac{cz}{(1-z)[1-(1-c)z]}$$

Equation 5.4

with $z = \dfrac{p}{p'}$.

In this expression p' denotes the vapor pressure above an adsorbate layer of more than one molecule thickness (similar to a normal liquid), which is 1.81 bar at 393 K [26].

V_{Mono} is the adsorbed gas volume corresponding to the monolayer and c is a constant that can be considered as an equilibrium constant for the first layer.

Equation 5.4 can be written as

$$\frac{z}{(1-z)V} = \frac{1}{cV_{Mono}} + \frac{(c-1)z}{cV_{Mono}}$$

Equation 5.5

When plotting the left hand side of Equation 5.5 vs. z (see Figure 5.6), V_{Mono} and c can be calculated from the slope and ordinate intercept of the resulting straight line. Thus, $V_{Mono} = 5.432$ and $c = 1.24 \cdot 10^5$ were obtained. Note that the value retrieved here for V_{Mono} has arbitrary units as the underlying quantitative measure was peak area.
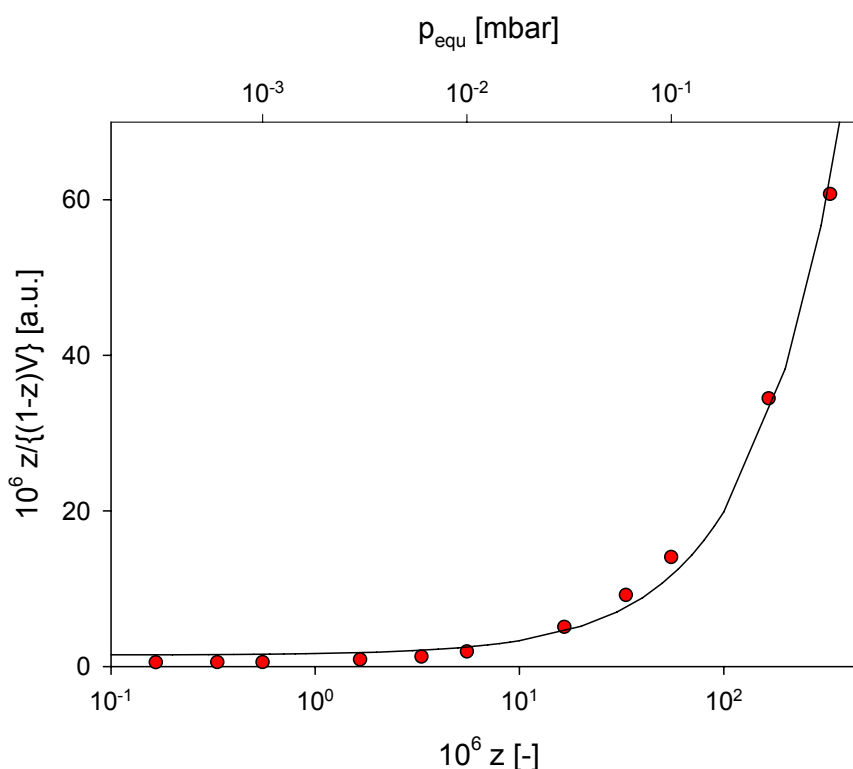
Figure 5.6 Adsorption isotherm of H_2O on TiO_2 anatase, $T_{Ads} = 393$ K.

During adsorption of HNCO on the TiO_2 sample at 393 K the intensity of the surface species suddenly increased, when the equilibrium pressure was raised from $6 \cdot 10^{-3}$ to $1 \cdot 10^{-2}$ mbar (see Figure 5.8). Most of the IR bands observed are already discussed in detail in the literature - a few still with controversy. The most intense band at 2206 cm^{-1} starts to evolve at $3 \cdot 10^{-3}$ mbar and shifts gradually to 2230 cm^{-1} with increasing partial pressure. Two shoulders at 2189 and 2255 cm^{-1} were observed, developing at an

equilibrium pressure of $1 \cdot 10^{-2}$ mbar and $3 \cdot 10^{-2}$ mbar, respectively. In agreement with the literature (e.g. Fischer *et al.* [27,28]), we assign the band in the range 2206 – 2230 cm^{-1} to the asymmetric stretching vibration of isocyanate species –NCO. HNCO adsorbs dissociatively on metal oxides forming isocyanates bound to Lewis acid sites [29]. The counter ions proposed are five-coordinate Ti^{4+} ions (O^{2-} ions bridging two cations) in the (001) plane of anatase [23]. Zhan [13] also observed two shoulders during adsorption of HNCO on Al_2O_3 and assigned the one at higher wavenumber (at 2281 cm^{-1}, the main peak being at 2257 cm^{-1}) to weakly adsorbed HNCO due to its possible removal at mild conditions and the one at lower wavenumber (2238 cm^{-1}) to cyanamide species N-C≡N formed through the reaction of isocyanic acid with traces of ammonia. Another indication of the dissociative adsorption of HNCO is the appearance of two bands at 3511 and 3452 cm^{-1} (see Figure 5.7), which can be both assigned to perturbed OH groups resulting from the (hydrogen bonding) interaction with surface NCO^- groups [17,27]. Three further bands (3377, 3259 and 3162 cm^{-1}) result from NH stretching modes.

The bands at 1645, 1560 and 1500 cm^{-1} with additional smaller bands in the region 1750 – 1400 cm^{-1} deserve special attention. Piazzesi *et al.* [30], who adsorbed HNCO on anatase at 423 K, tentatively attributed these bands to cyanuric acid formed by a polymerization of HNCO and/or to s-triazine formed by a reaction of HNCO with traces of NH_3 adsorbed on the surface. In contrast Acke *et al.* [31] exposed γ-Al_2O_3 to HNCO and O_2 and assigned the bands at 1656, 1587 and 1500 cm^{-1} to surface coordinated ammonia and ammonium ions. Larrubia *et al.* [32] found bands at 1650, 1565 and 1490 cm^{-1} after adsorption of urea on Fe_2O_3-TiO_2 and V_2O_5-MoO_3-TiO_2 SCR catalysts and acetamide over Al_2O_3 and Fe_2O_3, respectively and assigned them to an anionic adsorbed species of the corresponding molecules. On the basis of these experiments we propose that the bands at 1645, 1560 and 1500 cm^{-1} are not due to only one intermediate species, but rather result from different species co-existing on the surface after HNCO adsorption following earlier work in our group [13] . In addition own LDA calculations of the vibrational frequencies of urea and acetamide indicate three characteristic vibrations in the region 1810–1429 cm^{-1} which are C=O stretching, NH_2 deformation and asymmetric C-N stretching modes (in the case of acetamide additional CH_3 "umbrella" deformation vibration) in descending wavenumber sequence. The observed band at 1645 cm^{-1} is therefore tentatively assigned to the carbonyl stretching vibration of either Ti-NCO and/or trimer-adsorbed HNCO - cyanuric acid, whereas the band at

1560 cm^{-1} (NH$_2$ deformation) can be assigned to either melamine or Ti-N=C(OH)(NH$_2$) which is formed by reaction of carbodiimide Ti-N=C=N-H with water. The band at 1500 cm^{-1} is tentatively assigned to asymmetric C-N stretching modes of cyanuric acid, melamine and/or adsorbed cyanamide Ti-NH-C≡N, the latter one being the isomer of carbodiimide and formed through reaction of HNCO with traces of NH$_3$ on the catalyst surface [13]. The sulfate groups (band at 1371 cm^{-1}) strongly interact with HNCO, which led to the disappearance of the band after increasing the equilibrium pressure from 6·10^{-3} to 1·10^{-2} mbar. Note that at the same time the intensity of the isocyanate band at 2206 cm^{-1} increased simultaneously. Two broad bands with low intensity at 1323 and 1155 cm^{-1} can be observed in spectra (c) and (d) in Figure 5.8. We tentatively assign the latter one to traces of NH$_3$ which is formed by hydrolysis of HNCO on the surface OH groups of titania.
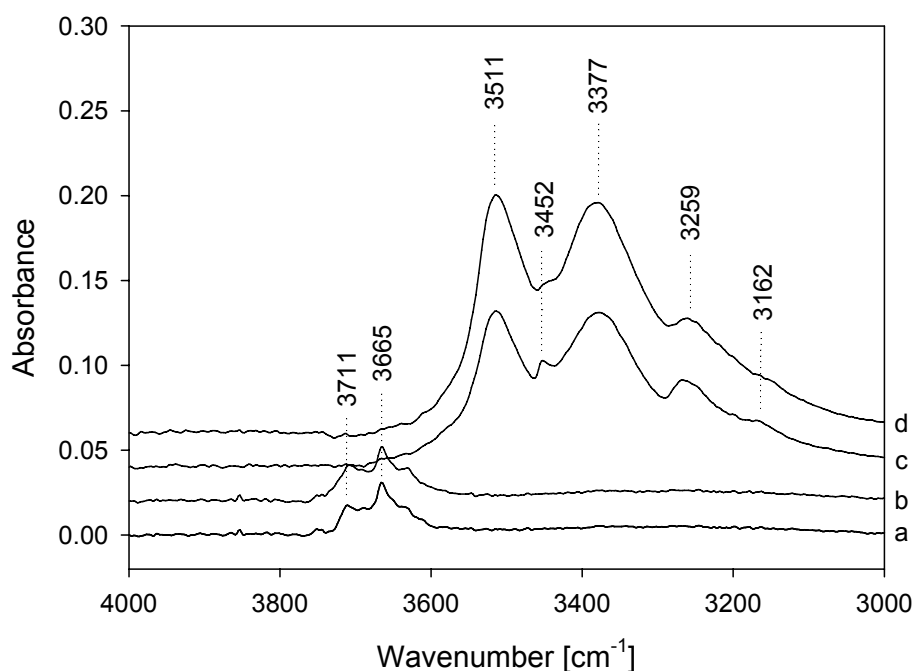

Figure 5.7 IR spectra of HNCO adsorption on TiO$_2$ anatase, T$_{Ads}$ = 393 K. (a) activated sample, after adsorption of (b) 1·10^{-3} mbar, (c) 1·10^{-2} mbar and (d) 1·10^{-1} mbar HNCO.
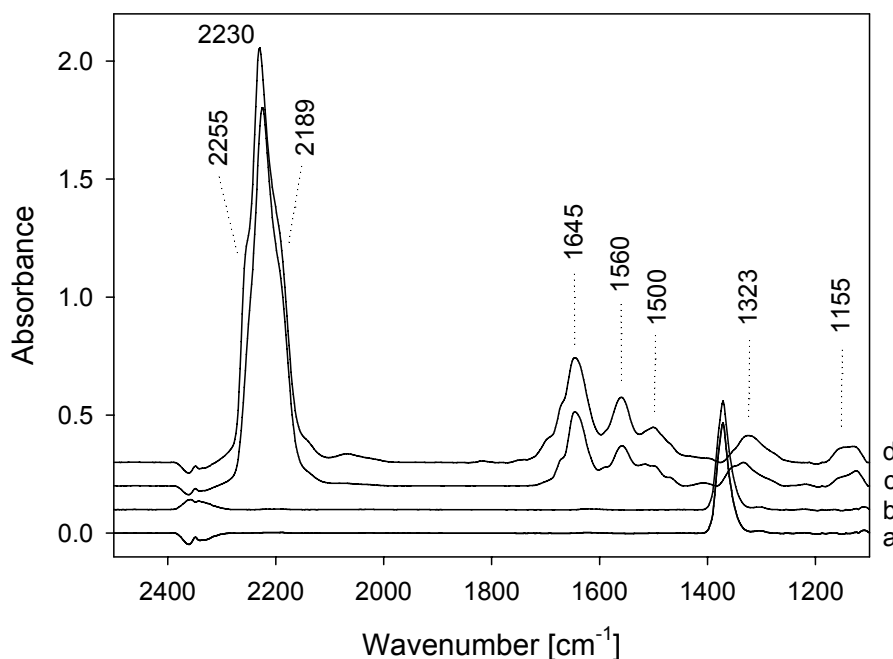
Figure 5.8 IR spectra of HNCO adsorption on TiO_2 anatase, T_{Ads} = 393 K. (a) activated sample, after adsorption of (b) $1 \cdot 10^{-3}$ mbar, (c) $1 \cdot 10^{-2}$ mbar and (d) $1 \cdot 10^{-1}$ mbar HNCO.

In order to further investigate the surface species of HNCO on TiO_2, the desorption was followed by *in situ* IR spectroscopy. After evacuation at 673 K, the band at 2230 cm^{-1}, attributed to isocyanate species, strongly decreased in intensity, and the bands in the region 1750 – 1400 cm^{-1} disappeared completely. In parallel, the intensity of the sulfate band at 1371 cm^{-1} was restored (Figure 5.9). This demonstrates the partially reversible character of the sorption/reaction processes. Solid cyanuric acid decomposes between 593 and 603 K [10], and the isocyanic acid released is not strongly adsorbed at 673 K. Simultaneously new bands were observed at 2030 and 2014 cm^{-1}. The band at 2072 cm^{-1}, which was already present during HNCO adsorption, increased in intensity. It is tentatively ascribed to carbodiimide species –N=C=NH formed in combination with carbon dioxide *via* disproportionation of isocyanic acid [12,33]. After evacuation in presence of 1 mbar O_2 at 673 K, almost all polymeric HNCO surface species were removed, except for one species represented by the band at 2030 cm^{-1} (see spectrum (c) in Figure 5.9).
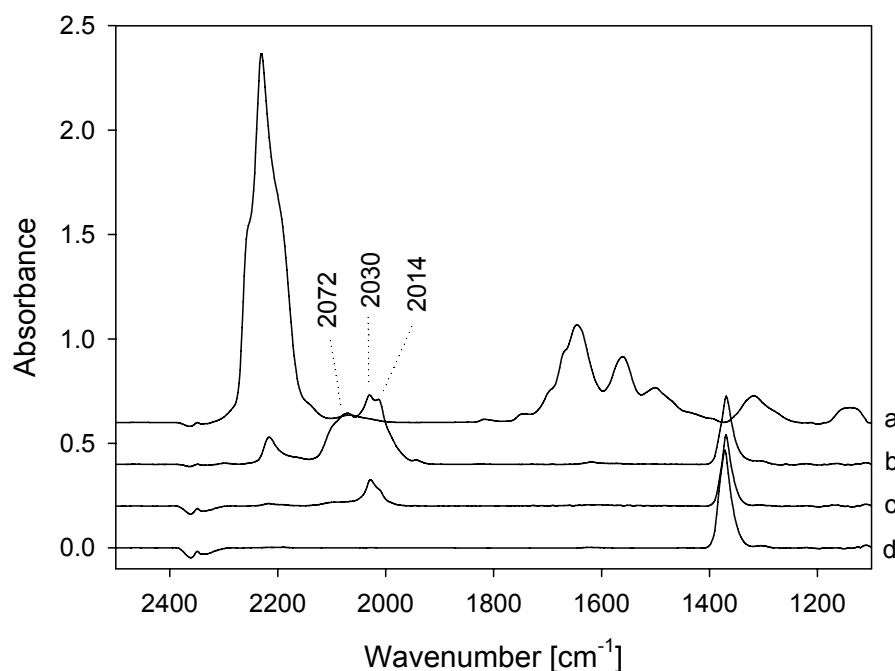
Figure 5.9 IR spectra of HNCO adsorption ($3 \cdot 10^{-1}$ mbar) on TiO_2 anatase, T_{Ads} = 393 K (a), followed by evacuation at 673 K (b) and after exposure to 1 mbar of O_2 at 673 K (c). For comparison activated sample before adsorption experiment (d).

To obtain the thermodynamic equilibrium constant for the HNCO adsorption, the intensity of the characteristic band in the range 2206 – 2230 cm^{-1} was used. It should be noted that this region includes isocyanate and possibly traces of cyanamide species. A peak deconvolution, however, was not performed as the cyanamide contribution to the peak area was below 5%. The sorption isotherm of HNCO over TiO_2 given in Figure 5.10 shows a sudden increase in the surface coverage of HNCO at an equilibrium pressure of $1 \cdot 10^{-2}$ mbar. At this equilibrium pressure all OH groups (3711, 3665 cm^{-1}) were covered, thus we defined this point as complete coverage. The IR spectra (Figure 5.8) indicated that HNCO undergoes a chemical reaction (most likely trimerization to cyanuric acid) on the titania surface in addition to the dissociative adsorption. For this reason the equilibrium constant could not be extracted from this experiment.
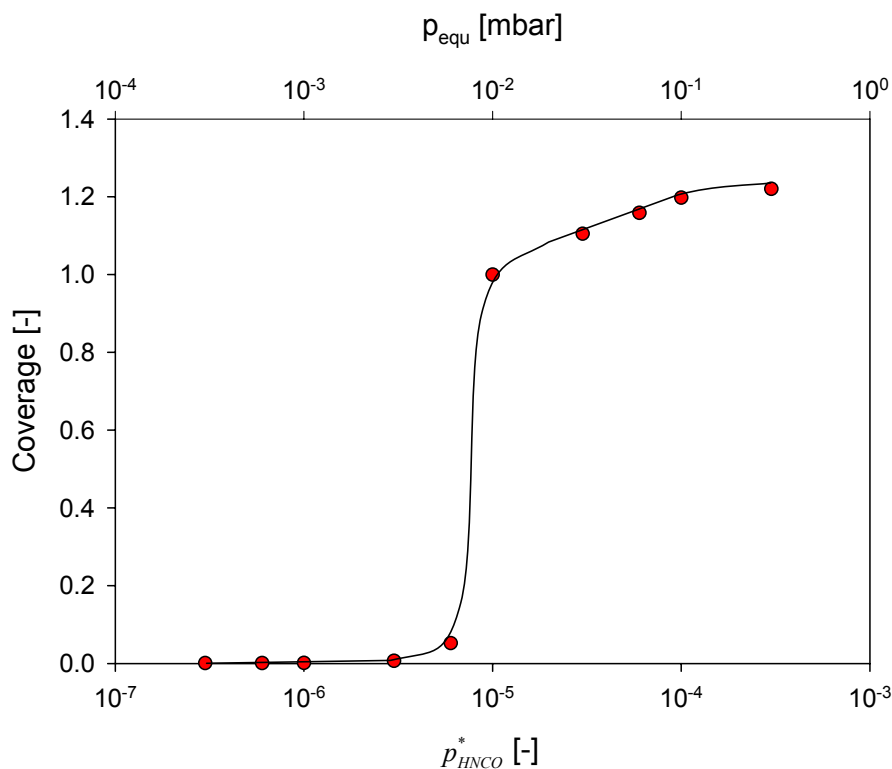
Figure 5.10 Adsorption isotherm of HNCO on TiO_2 anatase, $T_{Ads} = 393$ K.

During adsorption of CO_2 on TiO_2 at 393 K in the pressure range from $5 \cdot 10^{-4}$ to 1 mbar a significant surface concentration of adsorbed carbonates, which are typically observed at 1580 and 1320 cm^{-1} [23] was not detected. This is consistent with the kinetic experiments, which revealed a zero order dependence of the reaction rate of HNCO hydrolysis with respect to CO_2. This means that under the investigated conditions carbon dioxide does not interact noticeably with the titania surface, but shows inert behavior, and thus no effect in the kinetics is seen on variation of the CO_2 concentration.

5.4.2 H_2O adsorption isotherm by thermogravimetry

The monolayer sorption capacity for H_2O was additionally determined by thermogravimetry. Similar to the IR data, the BET isotherm expressed in Equation 5.4 was used to model the sorption isotherm. It should be noted at this point that the maximum partial pressure of H_2O achievable within the constraints of the experimental set-up was 16 mbar, which is of the same order of magnitude as the water content of a typical Diesel exhaust gas (4-5% according to ref. [34]).

V_{Mono} = 357 mm^3 (corresponds to m_{cat} = 21.31 mg) and c = 3306 were determined from the BET plot shown in Figure 5.11. Thus the area-related surface concentration of H_2O when the monolayer is predominant is calculated as $\hat{c}_{Mono}$ = 9.31·10^{-6} mol/m^2. The area-related surface concentration can be translated into the more suitable units [mol/l] regarding the rate of reaction by means of the following equation

$$c_{Mono} = (1-\varepsilon)\rho_a BET \hat{c}_{Mono},$$ Equation 5.6

in which ε denotes the porosity of the catalyst bed (estimated to be 0.5) and ρ_a the apparent density of the catalyst, which is estimated to be half of the real density (ρ_a = 1.94 g/cm^3). Thus c_{Mono} = 0.722 mol/l is obtained, which can be applied in the kinetic model.
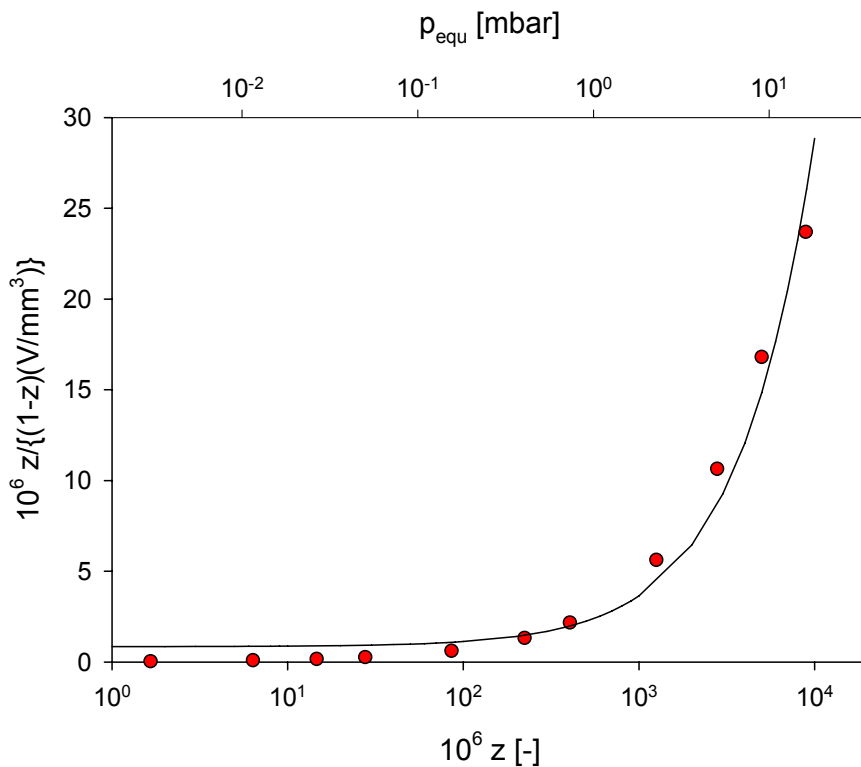

Figure 5.11 Adsorption isotherm of H_2O on TiO_2 anatase from thermogravimetry,
T_{Ads} = 393 K.

5.4.3 Rate expression

The overall reaction scheme compiled in Table 5.1 is proposed for the hydrolysis of isocyanic acid over TiO_2 anatase based on *in situ* IR studies reported previously [27]. In presence of 4 vol.% H_2O the main surface species observed during hydrolysis reaction were (i) molecularly adsorbed water, (ii) isocyanate (Ti-NCO) species bound to accessible Ti^{4+} cations and (iii) NH_3. Note that the same surface species were observed in additional studies on a sulfate free TiO_2 anatase catalyst, which was synthesized in-house by the hydrolysis of titanium tetraisopropanolate $Ti[OCH(CH_3)_2]_4$ [35].

Table 5.1 Reaction scheme proposed for the Langmuir-Hinshelwood mechanistic model.

Reaction

     Rate equation

1. Dissociative adsorption of isocyanic acid to yield surface isocyanates

   $HNCO + Ti^{4+} + Ti\text{-}OH \rightleftharpoons Ti\text{-}NCO + Ti\text{-}OH_2$

   $$r_1 = k_1 p_{HNCO} [Ti^{4+}][Ti-OH] - k_{-1}[Ti-NCO][Ti-OH_2]$$

2. Molecular adsorption of water

   $H_2O + Ti^{4+} \rightleftharpoons Ti\text{-}OH_2$

   $$r_2 = k_2 p_{H2O}[Ti^{4+}] - k_{-2}[Ti-OH_2]$$

3. Surface reaction according to Langmuir-Hinshelwood mechanism

   $Ti\text{-}NCO + Ti\text{-}OH_2 \rightleftharpoons Ti\text{-}NH_2 + Ti^{4+} + CO_2$

   $$r_{s1} = k_{s1}[Ti-NCO][Ti-OH_2] \text{ (only forward reaction)}$$

4. Formation of ammonia

   $Ti\text{-}NH_2 + Ti\text{-}OH_2 \rightleftharpoons Ti\text{-}NH_3 + Ti\text{-}OH$

   $$r_{s2} = k_{s2}[Ti-NH_2][Ti-OH_2] - k_{-s2}[Ti-NH_3][Ti-OH]$$

5. Desorption of ammonia and regeneration of active site

   $Ti\text{-}NH_3 \rightleftharpoons NH_3 + Ti^{4+}$

   $$r_3 = k_3 p_{NH3}[Ti^{4+}] - k_{-3}[Ti-NH_3]$$

On the TiO_2 anatase surface, polar hydroxyl groups Ti-OH are present as well as (coordinate) unsaturated Ti^{4+} and Ti^{3+} ions, which are strong Lewis acidic electron-pair-acceptor sites [17,24,36]. In the proposed reaction scheme Ti-OH$_2$ denotes molecularly (non-dissociative) adsorbed water on Ti^{4+} cations. We assume two different active sites

for H_2O molecule adsorption, i.e. Ti^{4+} ions having one or two coordinative unsaturations with respect to the octahedral overall coordination sphere of Ti^{4+} cations in the bulk.

Applying the concept of the rate determining step to the postulated reaction scheme, we start by assuming that the rate limiting elementary step is part of the convoluted surface reaction (Reaction (3) in Table 5.1), while all other reactions are quasi equilibrated, i.e. those rates are significantly faster and therefore the rate of the forward and backward reaction is the same. The resulting expression for the overall rate of reaction is therefore

$$r = k_s \cdot [Ti - NCO] \cdot [Ti - OH_2]$$ Equation 5.7

in which [Ti-NCO] and [Ti-OH$_2$] denote the reactant concentrations on the catalyst surface. The backward reaction is omitted, as a calculation of the thermodynamic equilibrium showed that the products are favored by eight orders of magnitude in the temperature range 393 to 773 K.

The kinetic data were collected over the TiO_2 anatase catalyst at T = 393 K under differential reaction conditions using the experimental setup described in ref. [27]. The low temperature was chosen in order to stay in the kinetically controlled regime, while at higher temperatures mass transfer processes additionally contribute to the reaction rate. In the temperature regime between 383 and 403 K the apparent activation energy of 73 kJ/mol was observed [27]. The concentrations of the reactants and products were varied systematically (see Table 5.2) to obtain a reliable set of data for the fitting of the kinetic parameters. The complete data set consists of 49 data points.

Table 5.2 Description of data sets used for fitting of rate expression.

Data set #	[HNCO]$_0$ in ppm	[H$_2$O]$_0$ in vol.%	[NH$_3$]$_0$ in ppm	Number data points
1	52 – 999	4^a	0^a	11
2	500^a	0.2 – 10	0^a	10
3	500^a	4^a	0 – 1311	8
4	97 – 1461	4^a	0^a	7
5	61 – 900	0.3 – 10	0^a	7
6	500^a	4^a	61 – 1324	6

^{a} standard reaction condition, kept constant,

gray shaded: variation of concentration.

To find an overall rate expression as a function of the individual reactant concentrations of the entire data set, we consider the variation of the water concentration first (data set number 2) as the adsorption isotherm could be expressed by the multilayer model (in contrast to the adsorption isotherm of isocyanic acid where no adsorption constant could be derived). In the kinetic experiments the water concentration was varied between 0.2 and 10 vol.%, which is equal to a dimensionless pressure p* between $2 \cdot 10^{-3}$ and $1 \cdot 10^{-1}$. According to Equation 5.4 the surface concentration of H$_2$O on the titania is

$$[Ti - OH_2] = [Ti - OH_2]_{Mono} \cdot \frac{K_2 \cdot p^*_{H2O}}{(1 - p^*_{H2O}) \cdot [1 - (1 - K_2)p^*_{H2O}]},$$

Equation 5.8

which can be substituted into the rate expression Equation 5.7

$$r = k_s \cdot [Ti - NCO] \cdot [Ti - OH_2]_{Mono} \cdot \frac{K_2 \cdot p^*_{H2O}}{(1 - p^*_{H2O}) \cdot [1 - (1 - K_2)p^*_{H2O}]} \cdot$$

Equation 5.9

In order to reduce the number of unknown variables, the rate constant k$_s$ and the isocyanate surface concentration can be combined to one constant k'_s yielding

$$r = k_s' \cdot \left[Ti - OH_2\right]_{Mono} \cdot \frac{K_2 \cdot p_{H2O}^*}{\left(1 - p_{H2O}^*\right) \cdot \left[1 - \left(1 - K_2\right) p_{H2O}^*\right]} \cdot \qquad \text{Equation 5.10}$$

This equation was used for a non-linear least mean squares (LMS) regression analysis performed by a Levenberg-Marquardt minimization algorithm [37,38] with [Ti-OH$_2$]$_{Mono}$ = 0.722 mol/l already determined from the thermogravimetric experiment (described in Section 5.4.2) to obtain the two variables k_s' and K$_2$. Figure 5.12 shows the fit of the experimental data using $k_s' = 0.037$ s^{-1} and K$_2$ = 105.
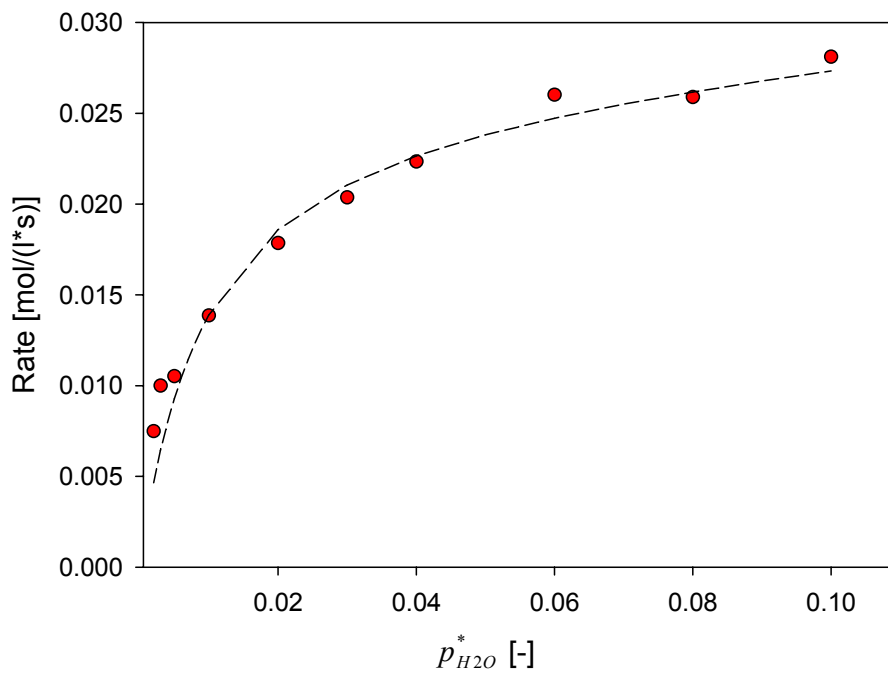
Figure 5.12 Preliminary Fit for data set number 2, (●) experimental data, (--) calculated rate.

In the following steps the simulation of the rate is stepwise expanded including the variation of H$_2$O, HNCO and NH$_3$, i.e. the whole experimental data at the end (data sets 1-6). In earlier kinetic studies, a decrease in hydrolysis activity in presence of NH$_3$ was observed which was ascribed to a product inhibition effect suppressing adsorption of HNCO [27]. Therefore, a competitive sorption of HNCO and NH$_3$ is assumed, and the surface concentration of isocyanate species can be described by:

$$\left[Ti - NCO\right] = \left[Ti - NCO\right]_{Mono} \cdot \frac{K_1 \cdot p_{HNCO}^*}{1 + K_1 \cdot p_{HNCO}^* + K_3 \cdot p_{NH_3}^*} \cdot \qquad \text{Equation 5.11}$$

By substitution of Equation 5.11 into the rate Equation 5.9 the extended rate expression can be obtained

$$r = k_s \cdot [Ti - NCO]_{Mono} \cdot \frac{K_1 \cdot p^*_{HNCO}}{1 + K_1 \cdot p^*_{HNCO} + K_3 \cdot p^*_{NH_3}} \cdot$$

$$[Ti - OH_2]_{Mono} \cdot \frac{K_2 \cdot p^*_{H2O}}{(1 - p^*_{H2O}) \cdot [1 - (1 - K_2)p^*_{H2O}]}$$

Equation 5.12

or, when combining $k_s \cdot [Ti - NCO]_{Mono}$ into k''_s,

$$r = k''_s \cdot \frac{K_1 \cdot p^*_{HNCO}}{1 + K_1 \cdot p^*_{HNCO} + K_3 \cdot p^*_{NH_3}} \cdot [Ti - OH_2]_{Mono} \cdot \frac{K_2 \cdot p^*_{H2O}}{(1 - p^*_{H2O}) \cdot [1 - (1 - K_2)p^*_{H2O}]} \cdot$$

Equation 5.13

In the next step, the variables k''_s and K_1 were determined using the values for [Ti-OH_2]$_{Mono}$ and K_2 already calculated. The parameters corresponding to rate expression 5.13 are summarized in Table 5.3, and the fit of the model to the variation of the HNCO, H_2O and NH_3 concentration is illustrated in Figure 5.13 - Figure 5.15.

Figure 5.13 Correlation between calculated rate (--) and experimental data (●) in case of variation of HNCO concentration (complete data set considered).

Figure 5.14 Correlation between calculated rate (--) and experimental data (●) in case of variation of H_2O concentration (complete data set considered).

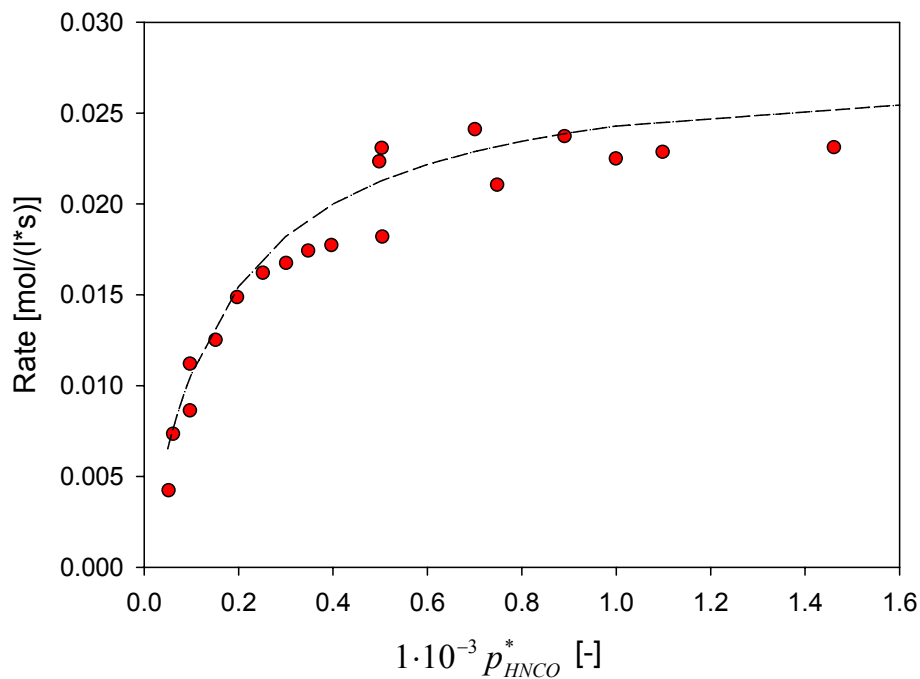**Figure 5.15** Correlation between calculated rate (--) and experimental data (●) in case of variation of NH_3 concentration (complete data set considered).

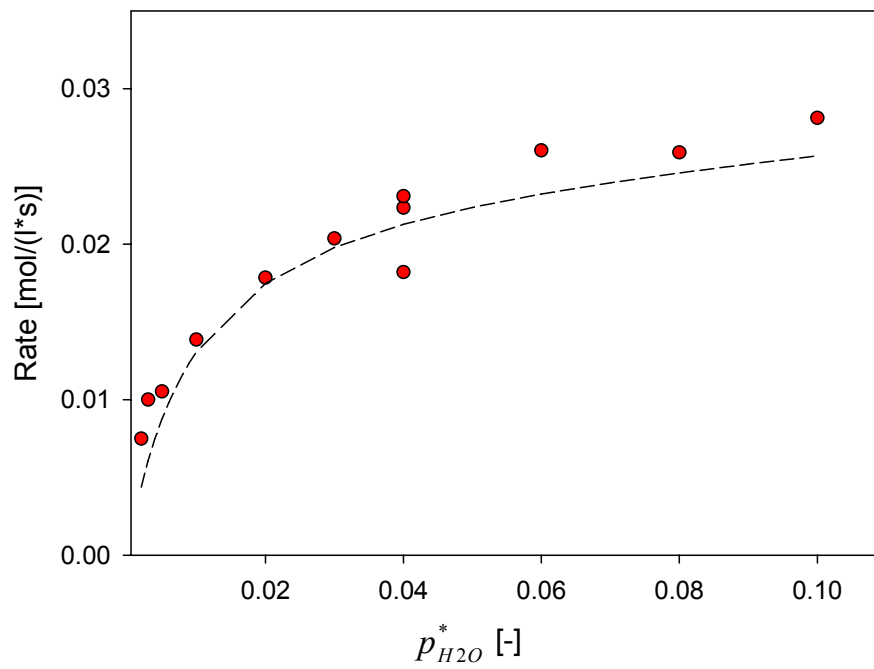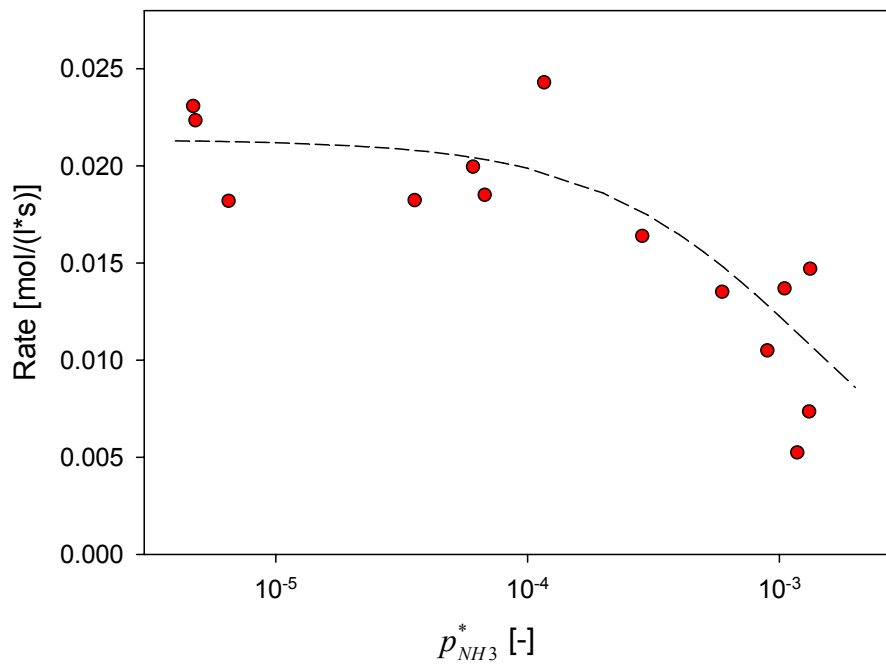It can be noted that the rates calculated for the variation of the HNCO concentration are marginally above the experimental data, while for the variation of the H_2O concentration the calculated values for the rate are slightly lower than the experimental data. It was found during carrying out the regression analysis that by varying the starting value of any parameter the two terms for the respective surface concentrations in Equation 5.13 could not be addressed independently. Figure 5.15 showing the dependence of the overall rate on the NH_3 concentration confirms the inhibiting effect of the hydrolysis product. The wider distribution at the high NH_3 partial pressures is attributed to the higher standard deviation of the measured NH_3 concentration there.

Table 5.3 Adsorption constants and combined rate constant (k_s'') estimated on the basis of Equation 5.13.

k_s'' [1/s]	K_1	K_2	K_3	[Ti-OH$_2$]$_{Mono}$ [mol/l]
$4.63 \cdot 10^{-2}$	6085	105	3000	0.722

The rate constant k_s can be estimated to be around $6.4 \cdot 10^{-2}$ l/(mol·s) assuming that $[Ti-NCO]_{Mono}$ is of the same order of magnitude as $[Ti-OH_2]_{Mono}$.

The observed and calculated rates using the model described are compared in the parity plot shown in Figure 5.16. The rate expression derived (Equation 5.12) describes the complete data set adequately and systematic deviations were not observed for the model.

Possible deviations from the diagonal are predominantly due to the following reasons:

The quantification method for determining the gas composition by IR spectroscopy was also used outside the specified concentration ranges of the calibration method. The applied catalysts were prepared as a (single) coated metal sheet of 10 mm length and a thickness of 110 μm. This configuration simulates a two channel monolithic structure with a cell density of 185 cpsi, but the mass of active material exposed to the gas stream was only about 1.75 mg. Although the size of the applied single sheet in the reactor was the same in all experiments (± 1% with respect to length), the layer thickness could have varied between the different samples.
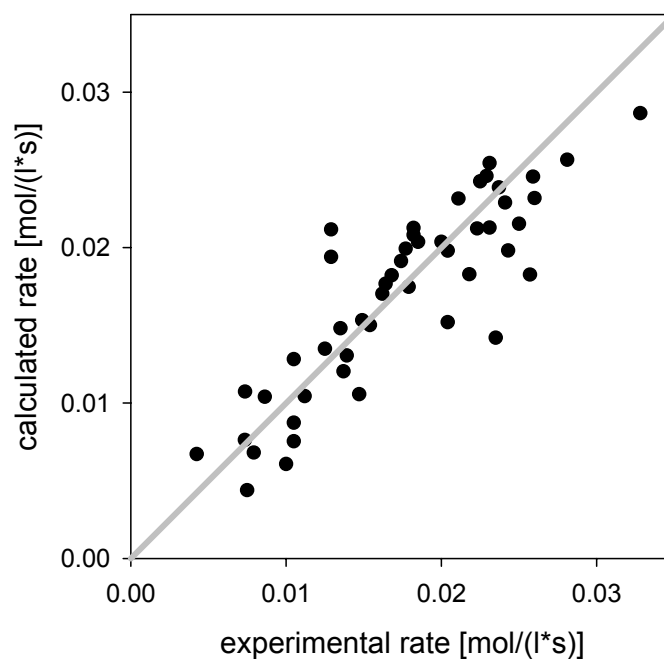
Figure 5.16 Parity plot using the complete data set.

5.5 *Conclusions*

Sorption isotherms of the reactants of the hydrolysis reaction of isocyanic acid on TiO_2 in anatase modification were determined by means of IR spectroscopy. The sorption isotherm of ammonia follows a Langmuir model while the sorption of water can be described best by the BET isotherm allowing for multilayer adsorption. Isocyanic acid adsorbs dissociatively on Ti^{4+} cations leading to surface coverage of reactive isocyanates Ti–NCO. The adsorption isotherm of isocyanic acid showed a sharp increase of the surface concentration in a narrow pressure range suggesting that a chemical reaction, most likely it is the autocatalytic trimerization of HNCO to cyanuric acid, takes place during sorption. During adsorption of CO_2 on TiO_2 anatase, characteristic carbonate bands were not observed.

The monolayer capacity as well as the equilibrium constants extracted from the sorption isotherms of H_2O and NH_3 were used for a stepwise determination of the other parameters contained in the kinetic model developed for the HNCO hydrolysis reaction. The kinetic model is based on the reaction scheme of elementary steps including the surface reaction of isocyanate with molecularly adsorbed water as the rate determining

step. The sorption and dissociation of HNCO as well as the desorption of NH_3 are significantly faster and do not contribute to the rate determining step. The model and the parameters derived are in good agreement to the experimental data for the rate and the yields.

5.6 Acknowledgements

5.7 References

[1]   H.P. Lenz, S. Prüller, Emissionen und Immissionen von Abgaskomponenten, Fortschritt-Berichte VDI, Reihe 12, Nr. 528, VDI-Verlag, Düsseldorf, 2003, 16.

[2]   P. Forzatti, Appl. Catal. A 222 (2001) 221.

[3]   H.L. Fang, H.F.M. DaCosta, Appl. Catal. B: Environmental 46 (2003) 18.

[4]   G. Busca, L. Lietti, G. Ramis, F. Berti, Appl. Catal. B: Environmental 18 (1998) 1.

[5]   M. Kleemann, M. Elsener, M. Koebel, A. Wokaun, Ind. Eng. Chem. Res. 39 (2000) 4120.

[6]   http://www.acea.be, Position Papers, 30/06/2003.

[7]   M. Koebel, M. Elsener, O. Kröcher, C. Schär, R. Röthlisberger, F. Jaussi, M. Mangold, Top. Catal. 30/31 (2004) 43.

[8]   M. Koebel, E.O. Strutz, Ind. Eng. Chem. Res. 42 (2003) 2093.

[9]   E. Jacob, A. Döring, From the SCR catalyst to the Controlled Diesel Catalyst (GD-KAT), Tagungsband VDA Technischer Kongress in Wolfsburg, April 2003, 163.

[10]   P.M. Schaber, J. Colson, S. Higgins, E. Dietz, D. Thielen, B. Anspach, J. Brauer, Am. Lab. 13 (1999) 13.

[11]   A.F. Hollemann, Lehrbuch der anorganischen Chemie / Hollemann-Wiberg, 101st ed., de Gruyter, Berlin, New York, 1995.

[12]   J.A. Lercher, Z. Zhan, Eur. Pat. Appl. 94113599 (1995).

[13]   Z. Zhan, Catalytic synthesis and conversion of melamine and its analogues, PhD Thesis, University of Twente, Netherlands (1995).

[14]   G. Mirth, F. Eder, J.A. Lercher, Appl. Spectrosc. 48 (1994) 194.

[15]   P.L.T. Gabrielsson, Top. Catal. 28 (2004) 177.

[16]   J.A. Lercher, Z. Phys. Chem. Neue Folge 118 (1979) 209.

[17]   A.A. Tsyganenko, V.N. Filimonov, Spectr. Lett. 5 (1972) 477.

[18]   G. Ramis, G. Busca, V. Lorenzelli, P. Forzatti, Appl. Catal. 64 (1990) 243.

[19]   G. Busca, H. Saussey, O. Saur, J.C. Lavalley, V. Lorenzelli, Appl. Catal. 14 (1985) 245.

[20]   G. Ramis, G. Busca, V. Lorenzelli, J. Chem. Soc. Faraday Trans. I 83 (1987) 1591.

[21]   M. Waqif, J. Bachelier, O. Saur, J.C. Lavalley, J. Mol. Catal. 72 (1992) 127.

[22]   O. Saur, M. Bensitel, A.B. Mohammed Saad, J.C. Lavalley, C.P. Tripp, B.A. Morrow, J. Catal. 99 (1986) 104.

[23]   H. Knözinger, Adv. Catal. 25 (1976) 209.

[24]   T. Bezrodna, G. Puchkovska, V. Shymanovska, J. Baran, H. Ratajczak, J. Mol. Struct. 700 (2004) 175.

[25]   P.W. Atkins, Physikalische Chemie, 3rd corrected ed., Wiley-VCH, Weinheim, 2001.

[26]   C.-T. Liu, W.T. Lindsay, Jr., J. Chem. Eng. Data 15 (1970) 510.

[27]   P. Hauck, A. Jentys, J.A. Lercher, Appl. Catal. B: Environmental 70 (2007) 91.

[28]   G. Fischer, J. Geith, T.M. Klapötke, B. Krumm, Z. Naturforsch. 57 b (2002) 19.

[29]   F. Solymosi, T. Bánsági, J. Phys. Chem. 83 (1979) 552.

[30]   G. Piazzesi, O. Kröcher, M. Elsener, A. Wokaum, Appl. Catal. B: Environmental 65 (2006) 55.

[31]   F. Acke, B. Westerberg, M. Skoglundh, J. Catal. 179 (1998) 528.

[32]   M.A. Larrubia, G. Ramis, G. Busca, Appl. Catal. B: Environmental 30 (2001) 101.

[33]   A. Schmidt, Monat. Chem. 99 (1968) 664.

[34]   R. Roudit, A. Baiker, F. Bettoni, J. Baldyga, A. Wokaun, AIChE J. 44 (12) (1998) 2731.

[35]   P.G. Mass, Oxidative Dehydrierung von Propan über getragenen Chromoxidkatalysatoren, PhD Thesis, Technische Universität München (1998).

[36]   T. Homann, T. Bredow, K. Jug, Surf. Sci. 555 (2004) 135.

[37]   K. Levenberg, Q. Appl. Math. 11 (1944) 164.

[38]   D.W. Marquardt, J. Soc. Ind. Appl. Math. 11 (1963) 431.

Chapter 6

6.1 Summary

More stringent NO_x and particulate emission limits for commercial vehicles have revived the so-called **selective catalytic reduction (SCR)** for application in mobile sources. The technology with urea as reducing agent constitutes the most promising strategy up to now and closest to start of production in order to reduce considerably the content of nitrogen oxides in Diesel exhaust gas. Urea has the vital advantage compared to other reducing agents that it is non-toxic and does not require sophisticated safety precautions for handling and storage. The conversion of urea into ammonia and carbon dioxide consists of two consecutive reactions, in which isocyanic acid is an intermediate that is hydrolyzed over TiO_2 anatase.

The main objective of the thesis was the investigation of the kinetics and the catalytic surface processes of the latter step of the urea decomposition, the catalyzed hydrolysis of HNCO into NH_3 and CO_2.

TiO_2 anatase is a very efficient catalyst for the hydrolysis of HNCO to NH_3 and CO_2. Over a broad temperature range, i.e., above 150°C, the hydrolysis of HNCO on TiO_2 is controlled by external mass-transfer under the experimental conditions used in this study. This is evidenced by the low temperature dependence expressed by the apparent activation energy of 10 ± 5 kJ/mol. However, at low temperatures, i.e., 110 – 130°C the evaluation of the surface reaction controlled kinetics was possible using a two channel monolithic structure at high areal velocities. The apparent energy of activation of 73 kJ/mol indicated a substantial barrier in the rate determining step. In the absence of water isocyanic acid adsorbs preferentially in dissociative form on Lewis acid sites generating OH groups or water and Ti-NCO groups. At longer time of exposure the formation of cyanuric acid occurs indicating that some of the isocyanic acid molecules do not dissociate and are able to be added to NCO^- groups. In the presence of water the hydrolysis dominates the surface chemistry so that only the more basic product, ammonia, and the reactant, water, are directly observed by IR spectroscopy.

In Chapter 3 the competitive adsorption of HNCO with NH_3, NO and NO_2 in the presence of H_2O was investigated at the model gas test rig (kinetic set-up) as well as by IR spectroscopy. In the presence of additional NO, NH_3 and NO_2 in the reactant gas stream the reaction rate decreases, when the catalyst is in the surface reaction rate controlled regime. While the overall impact increased in the sequence $NO < NH_3 < NO_2$,

the impact on the surface chemistry differs noticeably between the presence of the product ammonia and the nitrogen oxides. While ammonia had little impact on the surface concentrations measured during hydrolysis, the presence of NO and NO_2 led to the accumulation of NCO^- on TiO_2. Particularly with NO_2 the surface is quickly covered with nitrates, while the accumulation of NCO^- and the eventual formation of cyanuric acid are much slower. This suggests that nitrates block the sites catalytically active for hydrolysis and retard so the conversion of isocyanic acid. The existence of ammonium nitrate on the titania surface could not be confirmed by IR spectroscopy. The present data do not allow concluding whether or not HNCO is converted *via* an alternative reaction pathway under such conditions.

Chapter 4 focuses on the determination of the individual reaction orders with respect to the reactants and products. Furthermore, external and internal mass transport processes at a two-channel monolithic structure were addressed. The experiments were carried out in a novel type of flat bed reactor under differential reaction conditions. Educt as well as product partial pressures were varied individually in the feed gas mixture in order to determine the respective orders of reaction. Variation of the HNCO concentration confirmed a first order dependence while water showed an order of reaction of 0.33. NH_3 revealed a product inhibiting effect proven by the partial order of -0.70. Excess CO_2 in the feed gas up to 3 vol.% did not show any impact on the reaction rate. It has been demonstrated by standard reaction engineering experimentation that under the investigated conditions – i.e. at relatively high areal velocity and within the investigated temperature range - the hydrolysis of HNCO is *not* limited by external mass transport. In contrast, studies on the internal mass transport within the oxidic coating showed that in case of wash-coated metal substrates the coating thickness will be only rewarding up to a defined maximum value. If the coating thickness exceeds this threshold the enhanced adsorption capacity is not beneficial to activity anymore, but leads to a sub-optimal residence time of the isocyanic acid in the pore structure. The result is the formation of undesired polymeric species blocking the active sites for hydrolysis.

Chapter 5 introduces a simplified kinetic model for the overall rate of the HNCO hydrolysis on TiO_2 anatase based on the consolidated findings of Chapters 3 and 4. Values for the adsorption equilibrium constants of the reactants HNCO and water as well as of the products ammonia and carbon dioxide were determined experimentally from sorption isotherms (by IR spectroscopy and gravimetry) and implemented into the

macro-kinetic model. Thus, the sensitivity of the model was enhanced by reducing the number of unknown variables being determined. The sorption isotherm of ammonia follows a Langmuir model while the sorption of water can be described best by the BET isotherm Type II allowing for multilayer adsorption. Adsorption of isocyanic acid showed a sharp increase of the surface concentration in a narrow pressure range suggesting that a chemical reaction takes place during sorption. Most likely it is the autocatalytic trimerization of HNCO to cyanuric acid. During adsorption of CO_2 on TiO_2 anatase, characteristic carbonate bands were not observed. The monolayer capacity as well as the equilibrium constants extracted from the sorption isotherms of H_2O and NH_3 were used for a stepwise determination of the other parameters contained in the kinetic model developed for the HNCO hydrolysis reaction. The kinetic model is based on the reaction scheme of elementary steps including the surface reaction of isocyanate with water as the rate determining step. The adsorption of HNCO occurs competitively with the adsorption of NH_3, i.e. consideration of the product-inhibiting effect. The rate expression derived was used for a non-linear least mean squares (LMS) regression analysis performed by a Levenberg-Marquardt minimization algorithm. The model and the parameters derived are in good agreement to the experimental data for the rate and the yields.

6.2 Zusammenfassung

Strengere NO_x und Rußemissionsgrenzwerte für Nutzfahrzeuge haben dem Konzept "Selektive Katalytische Reduktion" (SCR) für die Anwendung in Fahrzeugen neues Leben eingehaucht. Die Technologie mit Harnstoff als Reduktionsmittel stellt bis zum heutigen Tag die aussichtsreichste und der Marktreife am nächsten stehende Strategie dar, um den Stickoxidgehalt in Dieselabgasen bedeutend zu verringern. Harnstoff hat den grundlegenden Vorteil im Vergleich zu anderen Reduktionsmitteln, dass er ungiftig ist und keine komplizierten Sicherheitsvorkehrungen bei Handhabung und Speicherung erfordert. Die Umsetzung von Harnstoff in Ammoniak und Kohlendioxid besteht aus zwei aufeinanderfolgenden Reaktionen, bei denen Isocyansäure als Intermediat auftritt, das über TiO_2 Anatas hydrolysiert wird.

Das Hauptziel dieser Arbeit war die Untersuchung der Kinetik und der Prozesse an der Katalysatoroberfläche des zweiten Schrittes der Harnstoffzersetzung, der katalytischen Hydrolyse von HNCO in NH_3 und CO_2.

TiO_2 Anatas ist ein äußerst effektiver Katalysator für die Hydrolyse von HNCO zu NH_3 und CO_2. Über einen breiten Temperaturbereich über 150°C, wird die Hydrolyse von HNCO über TiO_2 unter den, in dieser Studie verwendeten, experimentellen Bedingungen durch externen Stofftransport kontrolliert. Das wird durch die niedrige Temperaturabhängigkeit bewiesen, die durch die scheinbare Aktivierungsenergie von 10 ± 5 kJ/mol ausgedrückt wird. Bei niedrigen Temperaturen jedoch, d.h. zwischen 110 und 130°C, war die Evaluierung der intrinsischen Kinetik durch die Verwendung einer Zweikanal-Monolithstruktur bei hohen Flächengeschwindigkeiten möglich. Die scheinbare Aktivierungsenergie von 73 kJ/mol zeigte eine beträchtliche Barriere beim geschwindigkeitsbestimmenden Schritt an. Bei der Abwesenheit von Wasser adsorbiert Isocyansäure bevorzugt in dissoziativer Form an Lewissäure-Zentren, wobei OH-Gruppen oder Wasser und Ti-NCO-Gruppen gebildet werden. Bei längerer Verweilzeit tritt die Bildung von Cyanursäure ein, was zeigt, dass einige der Isocyansäure-Moleküle nicht dissoziieren, sondern fähig sind, an NCO^--Gruppen addiert zu werden. Bei Vorhandensein von Wasser dominiert die Hydrolyse die Oberflächenchemie, so dass nur das basischere Produkt Ammoniak und der Reaktant Wasser direkt mittels IR-Spektroskopie beobachtet werden.

In Kapitel 3 wurde die kompetitive Adsorption von HNCO mit NH_3, NO und NO_2 in der Gegenwart von H_2O sowohl am Modellgasprüfstand (kinetischer Prüfstand) als auch mittels IR-Spektroskopie untersucht. Bei Vorhandensein von zusätzlichem NO, NH_3 und NO_2 im Reaktantgasstrom nimmt die Reaktionsrate ab, wenn der Katalysator sich im durch die Oberflächenreaktionsrate kontrollierten Regime befindet. Während der Gesamteinfluss in der Reihenfolge NO < NH_3 < NO_2 zunahm, unterschied sich das Ergebnis deutlich bei Anwesenheit des Produkts Ammoniak im Gegensatz zur Anwesenheit von Stickoxiden. Während Ammoniak einen geringen Einfluss auf die, während der Hydrolyse gemessenen, Oberflächenkonzentrationen ausübte, führte die Anwesenheit von NO und NO_2 zur Anreicherung von NCO^- auf dem TiO_2 Katalysator. Besonders bei NO_2 ist die Oberfläche schnell mit Nitraten bedeckt, wohingegen die Akkumulation von NCO^- sowie die eventuelle Bildung von Cyanursäure bedeutend langsamer sind. Das deutet darauf hin, dass Nitrate die für die Hydrolyse katalytisch aktiven Zentren blockieren und so die Umsetzung von Isocyansäure verzögern. Das

Vorhandensein von Ammoniumnitrat auf der Titandioxid-Oberfläche konnte mittels IR-Spektroskopie nicht bestätigt werden. Die derzeitigen Daten erlauben keine Aussage darüber, ob HNCO unter solchen Bedingungen über einen alternativen Reaktionspfad umgesetzt wird oder nicht.

Kapitel 4 beschäftigt sich mit der Bestimmung der einzelnen Reaktionsordnungen bezüglich der Reaktanten und Produkte. Des Weiteren wurden externe und interne Stofftransportprozesse an einer Zweikanal-Monolithstruktur behandelt. Die Experimente wurden in einem neuartigen Flachbettreaktor unter differentiellen Reaktionsbedingungen durchgeführt. Sowohl Edukt- als auch Produkt-Partialdrücke wurden einzeln in der Feedgaszusammensetzung variiert, um die jeweiligen Reaktionsordnungen zu bestimmen. Variation der HNCO-Konzentration bestätigte eine Abhängigkeit Erster Ordnung, wohingegen Wasser eine Reaktionsordnung von 0,33 aufwies. NH_3 ließ einen produkthemmenden Effekt erkennen, der durch die Teilordnung von -0,77 belegt wurde. Überschüssiges CO_2 im Feedgas bis zu 3 Vol.% zeigte keine Auswirkung auf die Reaktionsrate. Es wurde mittels Standard-Reaktionstechnik-Experimenten demonstriert, dass die Hydrolyse von HNCO unter den gegebenen Bedingungen, d.h. bei relativ hoher Flächengeschwindigkeit und innerhalb des untersuchten Temperaturbereiches, *nicht* durch externen Stofftransport limitiert ist. Dagegen zeigten Untersuchungen zum internen Stofftransport innerhalb der oxidischen Beschichtung, dass die Beschichtungsdicke im Fall von mit Washcoat beschichteten Metallstrukturen nur bis zu einem bestimmten Maximalwert lohnend ist. Falls die Schichtdicke diesen Grenzwert überschreitet, fördert die erhöhte Adsorptionskapazität die Aktivität nicht mehr, sondern führt zu einer suboptimalen Verweilzeit der Isocyansäure in der Porenstruktur. Das Ergebnis ist die Bildung von unerwünschten Polymerspezies, welche die für die Hydrolyse aktiven Zentren blockieren.

Kapitel 5 stellt ein kinetisches Modell für die Gesamtrate der HNCO-Hydrolyse über TiO_2 Anatas vor, basierend auf den konsolidierten Ergebnissen von Kapiteln 3 und 4. Werte für die Adsorptionsgleichgewichtskonstanten der Reaktanten HNCO und Wasser sowie der Produkte Ammoniak und Kohlendioxid wurden experimentell aus Sorptionsisothermen (durch IR-Spektroskopie und gravimetrisch) bestimmt und in das makrokinetische Modell eingesetzt. Auf diese Weise, durch Verringerung der Anzahl der zu bestimmenden unbekannten Variablen, wurde die Empfindlichkeit des Modells verbessert. Während die Sorptionsisotherme von Ammoniak einem Langmuir-Modell folgt, kann die Sorption von Wasser am besten mit der BET-Isotherme Typ II

beschrieben werden, welche Mehrschichtenadsorption berücksichtigt. Die Adsorption von Isocyansäure zeigte einen steilen Anstieg der Oberflächenkonzentration in einem engen Druckbereich, was auf eine, während der Sorption stattfindende, chemische Reaktion hinweist. Am wahrscheinlichsten dafür ist die autokatalytische Trimerisation von HNCO zur Cyanursäure. Während Adsorption von CO_2 auf dem TiO_2 Anatas Katalysator wurden keine charakteristischen Carbonatbanden beobachtet. Sowohl die Monolagenkapazität als auch die Gleichgewichtskonstanten, die aus den Sorptionsisothermen von H_2O und NH_3 gewonnen wurden, wurden für die schrittweise Bestimmung der anderen, im kinetischen Modell enthaltenen Parameter verwendet. Das kinetische Modell, welches für die HNCO-Hydrolysereaktion erstellt wurde, basiert auf dem Reaktionsschema der Elementarschritte, einschließlich der Oberflächenreaktion von Isocyanat mit Wasser als dem geschwindigkeitsbestimmenden Schritt. Die Adsorption von HNCO tritt kompetitiv mit der Adsorption von NH_3 auf, d.h. Berücksichtigung des produkthemmenden Effekts. Der abgeleitete Ratenausdruck wurde für eine nicht-lineare Regressionsanalyse der kleinsten Fehlerquadrate verwendet, durchgeführt mittels eines Levenberg-Marquardt-Minimierungsalgorithmus. Das Modell und die erzielten Parameter stimmen gut mit den experimentellen Daten für die Rate und die Ausbeuten überein.

Chapter 7

7.1 Future prospects

The objective of this cooperative project was to advance the GD-KAT system for NO_x reduction in the exhaust gas of Diesel engines towards full applicability in vehicles. It was the overall objective to reduce the installed catalyst volume and the costs for the reducing agent by 40% each. The postulated volume reduction by 40% and a more dynamic response behavior with respect to NO_x conversion could be achieved by the substitution of extrudate catalysts with structured metal substrate SCR catalysts in the described V/H-RO system. A forward-looking concept is a two-part, advanced high-performance SCR system with increased volume-specific catalytic activity. This system is characterized by:

- "turbulent" catalyst with internal flow exchange, enabling increased mass transfer and optimizing the homogeneity of the chemical reactants inside the catalyst

- Assistant catalysts: urea-decomposition catalyst (hydrolysis catalyst) with system configuration in a slip-stream (so-called 1/H pre-reactor) or with parallel arranged H- and V-catalyst (pre-oxidation catalyst), so-called V/H pre-reactor, upstream of the SCR catalyst.

The required SCR catalyst volume in V/H-RO system configuration with assistant catalysts can be reduced by 40% when applying the "turbulent" LS/PE structure with internal flow distribution instead of the traditional laminar-flow standard catalyst structures, while maintaining the performance level of emission reduction [1]. These turbulent catalysts are already in production for three-way catalysts and diesel oxidation catalysts; their inherent advantage is the induction of turbulence in the flow due to their special geometry and thus significantly increase the mass transfer coefficient [2]. The setup and flow conditions of the LS/PE structure are shown in Figure 7.1. Other mixing structures are also available, all are particularly suitable for SCR technology because apart from generating turbulent flow they also promote the homgenization of the reducing agent in the exhaust gas due to their radial permeability [3,4]. Thus equalization of the concentrations and pressures can be realized.
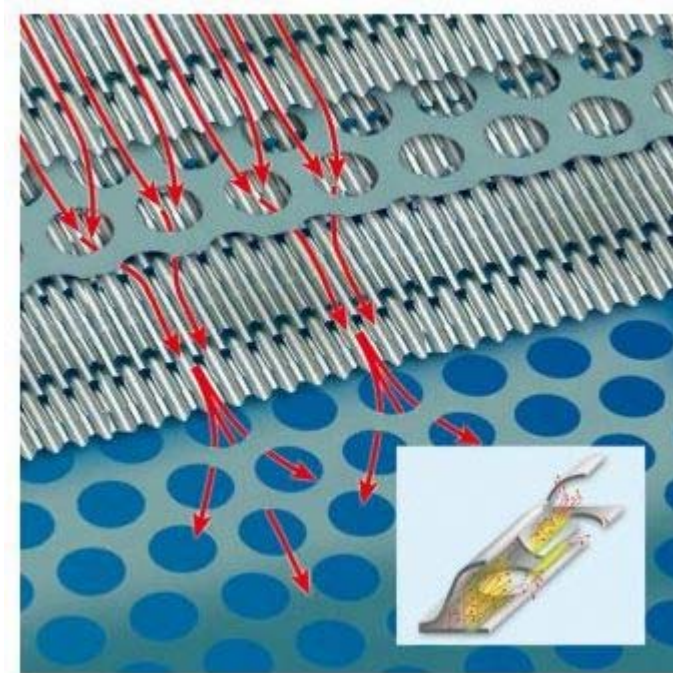
Figure 7.1 LS/PE structure [5].

For the compliance with Euro IV and Euro V emission standards for heavy trucks different strategies are currently pursued. The two major ones for NO_x emission minimization are exhaust gas recirculation (EGR) with particulate matter control in the exhaust and Selective Catalytic Reduction with PM-optimized engines [6]. Serial applications that meet the Euro V standard based on the latter strategy were introduced in commercial vehicles at the beginning of 2005. Experts state that neither of the two technologies can fulfill the legislation of the upcoming decade (Euro VI, US 2010, Japan 09) on its own, a reduction of the engine-out emissions seems to be insufficient. Therefore, future SCR technology for trucks is expected to orient more towards the approach that is currently taken with lean-running cars, following the implementation of inner-motor NO_x reduction through EGR and pre-oxidation catalyst/filters.

Mercedes-Benz has developed its so-called BlueTec® system. It comprises an enhanced, power-improved engine with a SCR catalyst and an AdBlue tank [7]. Development in the US promotes the technology tranfer onto the passenger Diesel car. Here the system consists of oxidation catalyst, Diesel particulate filter combined with an enhanced, particularly long-living NO_x storage catalyst as well as an additional SCR catalyst. First BlueTec model in the US was the E 320, which came into the market in October 2006.

Besides, further improvement of fuel quality will be a strong need in the future.

7.2 References

[1]   E. Jacob, R. Müller, A. Scheeder, T. Cartus, R. Dreisbach, H.-P. Mai, M. Paulus, J. Spengler, 27. Internationales Wiener Motorensymposium, H.P. Lenz (editor) Fortschritt-Berichte VDI, Reihe 12, Nr. 622, VDI-Verlag, Düsseldorf, 2006, 240.

[2]   W. Maus, R. Brück, Die Zukunft der heterogenen Katalyse im Automobil: „Turbulente" Katalysatoren für Otto- und Dieselanwendungen, 26. Internationales Wiener Motorensymposium, H.P. Lenz (editor) Fortschritt-Berichte VDI, Reihe 12, Nr. 595, VDI-Verlag, Düsseldorf, 2005, 297.

[3]   E. Jacob, Perspektiven der mobilen SCR-Technik, 15. Aachener Kolloquium Fahrzeug- und Motorentechnik, 2006.

[4]   S. Steinbach, J. Grünwald, U. Glückert, T. Sattelmayer, Characterization of structured hydrolysis catalysts for urea-SCR, 7. International Congress on Catalysis and Automotive Pollution Control (CAPoC7), Brussels, August 2006.

[5]   http://www.emitec.de.

[6]   A. Scheeder, R. Müller, M. Paulus, J. Spengler, „Downsizing" von zukünftigen Abgasnachbehandlungssystemen für Nutzfahrzeuge, 4. FAD Konferenz „Abgasnachbehandlung für Dieselmotoren", Dresden, November 2006.

[7]   http://www4.mercedes-benz.com/specials/scr/de/index_nocom_de.htm.

CURRICULUM VITAE

Philipp Christian Dino Patrick Hauck was born in Neuburg an der Donau, Germany, on 15th June 1976. After finishing high school in Neuburg in 1995 and subsequent mandatory military service, he started his chemical engineering course of studies at the Friedrich-Alexander-University Erlangen-Nuremberg in November 1996. He finished his studies in 2002 after writing his Diploma Thesis entitled "Preferred strategy for the development and scale-up of predictable heterogeneous catalytic hydrogenations", which was performed externally at the pharmaceutical company GlaxoSmithKline plc in Dartford, Kent, England under the academic supervision of Prof. G. Emig (Chair of Reaction engineering). He joined the Chair 2 of Chemical Technology (TC 2) of Prof. J.A. Lercher at the Technical University Munich in April 2003 to start research on aspects of the urea-based SCR technology for mobile Diesel engines.

LIST OF PUBLICATIONS

1. On the quantitative aspects of hydrolysis of isocyanic acid on TiO_2
   Catalysis Today, 2007, revised paper submitted
   Philipp Hauck, Andreas Jentys, Johannes A. Lercher

2. Kinetic aspects of the urea SCR technology for mobile diesel engines
   Proceedings zur Fifth Tokyo Conference on Advanced Catalytic Science and Technology (TOCAT 5), Tokyo, Juli 2006: Studies in Surface Science and Catalysis, 2007, accepted for publication
   Philipp Hauck, Andreas Jentys, Johannes A. Lercher

3. Surface chemistry and kinetics of the hydrolysis of isocyanic acid on anatase
   Applied Catalysis B: Environmental, Volume 70, Issues 1-4, 31 January 2007, Pages 91-99
   Philipp Hauck, Andreas Jentys, Johannes A. Lercher

4. Kinetik der Hydrolyse von Isocyansäure im Harnstoff-SCR Prozess
   Proceedings zur 3. FAD-Konferenz Herausforderung Abgasnachbehandlung für Dieselmotoren, Förderkreis Abgasnachbehandlungstechnologien für Dieselmotoren e.V., Dresden, Nov. 2005
   Philipp Hauck, Andreas Jentys, Johannes A. Lercher

ORAL AND POSTER PRESENTATIONS

1. XL. Jahrestreffen Deutscher Katalytiker, 14. – 16.03.2007 in Weimar
   P. Hauck, A. Jentys, J.A. Lercher, oral presentation

2. Seventh International Congress on Catalysis and Automotive Pollution Control (CAPoC 7), 30.08. – 01.09.2006 in Brussels, Belgium
   P. Hauck, A. Jentys, J.A. Lercher, poster

3. 5th Tokyo Conference on Advanced Catalytic Science and Technology, 23. – 28.07.2006 in Tokyo, Japan
   P. Hauck, A. Jentys, J.A. Lercher, oral presentation

4. XXXIX. Jahrestreffen Deutscher Katalytiker, 15. – 17.03.2006 in Weimar
   P. Hauck, A. Jentys, J.A. Lercher, poster

5. FAD-Konferenz (Förderkreis Abgasnachbehandlungstechnologien für Dieselmotoren e.V.), 09. – 10.11.2005 in Dresden
   P. Hauck, C. Gondaliya, A. Jentys, J.A. Lercher, oral presentation

6. 4th International Conference on Environmental Catalysis, 05. – 08.06.2005 in Heidelberg
   P. Hauck, C. Gondaliya, A. Jentys, J.A. Lercher, oral presentation

7. XXXVIII. Jahrestreffen Deutscher Katalytiker, 16. – 18.03.2005 in Weimar
   P. Hauck, A. Jentys, J.A. Lercher, poster

8. XXXVII. Jahrestreffen Deutscher Katalytiker, 17. – 19.03.2004 in Weimar
   P. Hauck, A. Jentys, J.A. Lercher, poster